MSc(Med) in Chemical Biology DISSERTATION

Photoimmunotheranostic targeting of CSPG4-positive melanoma cells using SNAP-tag technology

Zaria Malindi

Supervisor:
Prof. Dr. Dr. Stefan Barth

Co-supervisors:
Dr. Eden Padayachee
Fleury Augustin Nsole Biteghe

Medical Biotechnology and Immunotherapy Research Unit
Department of Integrative Biomedical Sciences
Institute of Infectious Diseases and Molecular Medicine
Faculty of Health Sciences
University of Cape Town

15 November 2018

PLAGIARISM DECLARATION

1. This thesis/dissertation has been submitted to the Turnitin module (or equivalent similarity and originality checking software) and I confirm that my supervisor has seen my report and any concerns revealed by such have been resolved with my supervisor.

2. I know that plagiarism is wrong. Plagiarism is using another's work and to pretend that it is one's own.

3. I have used the Vancouver Referencing Style as the convention for citation and referencing. Each significant contribution to, and quotation in, this thesis/dissertation from the work or works of other people has been attributed and has cited and referenced.

4. This thesis/dissertation is my own work.

5. I have not allowed, and will not allow, anyone to copy my work with the intention of passing it off as his or her own work.

6. I acknowledge that copying someone else's assignment or essay, or part of it, is wrong, and declare that this is my own work

Signed by candidate

SIGNATURE: _____

DATE: 14/11/2018

Acknowledgements

To Prof. Dr. Dr. Stefan Barth, I would like to thank you profusely for supervising this thesis. Thank you for giving me the chance to work with you on this research, for all your careful support and for being such a strong role model. It has been a true pleasure being at the MB&I Unit and I am proud to call myself a member.

To Dr. Eden Padayachee, thank you for co-supervising me and for all the encouragement over the years. You've always showed great belief in my abilities and I am appreciative of that.

To the MB&I post-docs and PhDs, Fleury, Krupa, Shivan, Alex, Trishana, Natasha and Sandra, thank you for all your assistance throughout this project and for training me.

To the whole MB&I team, thank you for being excellent labmates, for providing a great working environment and for always being willing to lend a hand.

To Ronnie in the Flow Cytometry Core Facility, thank you for your endless assistance with FACS.

To Susan Cooper and Dirk Lang in the Confocal Imaging Facility, thank you for all your help with microscopy.

To our neighbouring labs, Human Genetics, Sturrock, Blackburn and ICGEB, thank you for all your assistance and for being so generous with equipment.

To Matthias Peipp of Keil Univesity and Lester Davids of Univeristy of Pretoria, thank you for so generously providing the cell lines used in this thesis.

To the National Research Foundation, thank you for funding this research.

Lastly, to my examiners, Prof. Ben Loos and Dr. Mehmet Kemal Tur, thank you for your thourough evaluation of this thesis. Your comments and suggestions were invaluable in its final presentation.

Table of Contents

Abstract

Melanoma is one of the most aggressive and inherently resistant cancers and the most dangerous skin cancer. While it accounts for fewer than 5% of skin cancer cases, 80% of skin cancer related deaths are attributed to melanoma. While resection remains the gold standard for melanoma treatment, surgery is only effective in providing local control of the disease if the cancer is detected in the early stages. Once melanoma enters the later stages, and particularly in the metastatic phase, recurrence is probable, and no adequate treatment exists. Previous work in this group has shown that photodynamic therapy (PDT) presents an opportunity to induce cell death in melanoma cells through the production of ROS and singlet oxygen at doses high enough to overwhelm the resistance mechanisms of the cancer.

In this study, we investigated the use of recombinant SNAP-tag-based antibody fusion proteins as a means of delivering phototoxic molecules directly to cancer cells expressing the CSPG4 and PD-L1 cell surface receptors. SNAP-tag is an engineered version of the human DNA repair enzyme O^6-alkylguanine-DNA alkyltransferase. It reacts autocatalytically and in a strictly 1:1 coupling chemistry with substrates that have been modified with benzylguanine (BG). Through genetic fusion of this self-labelling protein with a tumour targeting antibody, we developed a recombinant immunoconjugate able to carry BG-modified photosensitizers to selectively target and eliminate malignant melanoma cells.

Conjugation of the SNAP-tag fusion protein with the fluorescent dye Alex Fluor 488 showed that anti-CSPG4-SNAP binds specifically to melanoma cells expressing the CSPG4 surface antigen. Binding was tested across a range of cell lines presenting melanoma in its radial and vertical growth phases, in the metastatic growth phase, in its chemoresistant form, and in both its pigmented and unpigmented forms. This binding data thus confirms CSPG4 as a suitable targeted for this treatment strategy. Conjugation of the fusion protein with the BG-modified photosensitizer IRDye 700DX (IR700) has produced no phototoxicity as of yet. In light of the convincing binding analysis, it is concluded that inefficient solubilization of the lyophilized product resulted in inadequate conjugation of BG-IR700 with SNAP-tag. Nonetheless, steps have been planned to resolve the problem in future ongoing work on this project, and we remain confident in the applicability of this technology. The results for the PD-L1 fusion protein were inconclusive.

In summary, SNAP-tag technology offers a simple and efficient method for immunofluorescent detection of cancerous cells. These fusions proteins are versatile as they 1) can contain any antibody targeting a tumour-associated or tumour-specific antigen of choice and 2) can be endowed with a wide variety of substrates, as long as the latter contains the BG moiety.

1. Literature Review

1.1 MELANOMA

1.1.1 Development, characteristics and prevalence

Melanocytes are the cells found in the epidermis of the skin that are responsible for the production of melanin; a pigment that carries photoprotective properties against harmful ultraviolet radiation (UVR) in its black/brown form, although it offers little photoprotection in its red/yellow form. Black/brown melanin is produced within the melanosomes and is able to scatter and absorb UVR, providing the cellular DNA with protection against UVR-induced damage.[1] Melanoma arises from the malignant transformation of melanocytes due to environmental changes, such as UVR over-exposure, and/or gene mutations, the most common occurring in $BRAF^{V600E}$ and N-RAS.[2] These mutations develop due to abnormal activation of the mitogen-activated protein kinase (MAP-K) pathway, which leads to increased cell proliferation and the formation of the nevi. Cells then undergo immortalisation, accompanied by further proliferation in the radial growth phase (RGP). Migration pathways are activated, and cells undergo invasion and epithelial-to-mesenchymal transition (EMT) in the vertical growth phase (VGP). Finally, metastasis and angiogenesis occur in the metastatic phase (Figure 1).[3]

Melanoma is one of the most aggressive and inherently resistant cancers, and the most dangerous skin cancer. While it accounts for fewer than 5% of skin cancer cases, 80% of skin cancer related deaths are attributed to melanoma.[1, 3, 4] Melanoma threatens a 1 in 266 lifetime risk in South Africa (CANSA National Cancer Registry, 2013), second only to that of Australia, where 1 in 17 people are estimated to be diagnosed with melanoma by the age of 85 (Cancer Australia, 2017). CANSA reports show that South Africa has around 20 000 new melanoma cases annually. While resection remains the gold standard for melanoma treatment, surgery is only effective in providing local control of the disease if the cancer is detected in the early stages. Once melanoma enters the later stages, and particularly the metastatic phase, recurrence is probable and no adequate treatment exists.[5]

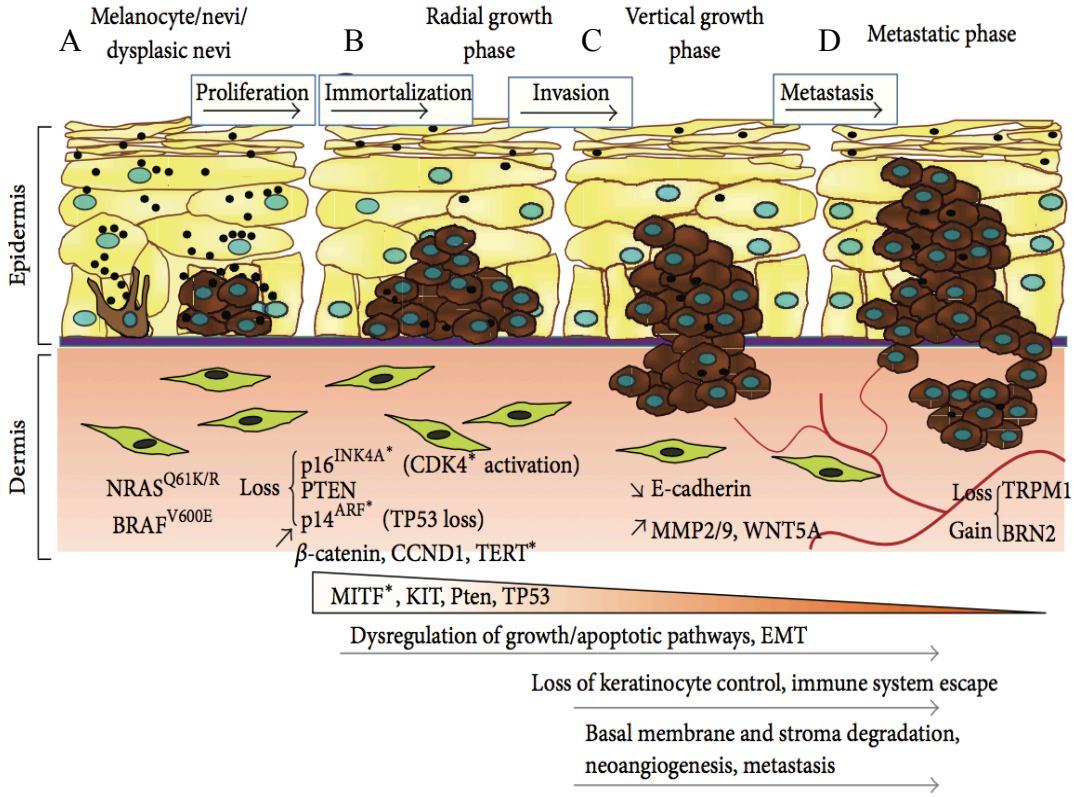

Figure 1: Progression of melanoma. A) Healthy melanocyte undergoes an activating *BRAF* mutation, resulting in proliferation to form a nevus. B) Subsequent gene dysregulation, immortalization of cells and entry into RGP. C) Cells begin invasion in VGP, as E-cadherin is lost, EMT occurs and cells move across the basal membrane into the dermis. D) Angiogenesis and metastasis occur in the metastatic phase.[1] EMT, epithelial-mesenchymal transition.

1.1.2 Chemoresistance

Recent years have seen tremendous advances in cancer research, which have vastly improved our understanding of the disease and brought about the development of new generations of immunotherapies and targeted therapies. Nevertheless, the majority of recent cancer clinical trials have not resulted in any drastic differences in treatment outcomes.[6, 7] Furthermore, the number of existing FDA-approved drugs, such as Vemurafenib and Ipilimumab,[8, 9] as well as the rate of new drug approval, is very low.[10] Despite progress in cancer research, our ability to reduce tumourigenicity and eradicate cancerous cells remains inadequate and most drugs exhibit non-specific cytotoxicity.[11] Therapeutic approaches ranging from chemotherapy to targeted molecule inhibition have not had the expected success,[12] as melanoma cells are highly successful at resisting treatment-induced apoptotic signals and are thus able to evade cell death.[13]

One mechanism through which melanoma cells are able to avoid chemo-induced cell death is through the expression of ATP-Binding Cassette (ABC) transporters. These proteins

facilitate resistance to classic chemotherapies by causing an efflux of cytotoxins from the cells thus preventing the accumulation of drugs intracellularly.[4, 14-18] The ABCB5 transporter has specifically been shown to mediate multi-drug resistance in melanoma.[18] Another survival mechanism of a transformed melanocyte is its antioxidant properties. Because cancer cells themselves produce reactive oxygen species (ROS) and are therefore inherently exposed to significant oxidative stress conditions, they have a highly developed antioxidant system. The antioxidant system of melanoma is particularly advanced as these cells naturally contain antioxidant substances, such as glutathione peroxidases, catalase, superoxide dismutases, tocopherol and glutathione, which offer defence additional against free radicals.[19] Melanoma has been shown to have higher antioxidant levels than other skin cancers, making it highly tolerant to oxidative stress. Melanin derivatives act as potent oxidants, putting melanocytes under continuous oxidative stress. In response to this danger, the melanocytes have developed the membrane-bound melanosomes to localize these substances and prevent cellular damage.[20] In contrast to it derivatives, melanin acts as a strong antioxidant and has the ability to scavenge free radicals. The melanosome thus functions to take up and store cytotoxic metabolites and waste products. It is thought that this property, although helpful in maintaining a toxin free intracellular environment in healthy skin cells, might act to sequester chemotherapeutic agents in melanoma cells, thus facilitating chemoresistance.[3]

These mechanisms enable melanoma to become therapeutically resistant, causing tumours to persist, metastasize, and recur with heightened tumorigenic power.[21] These facts are indicative of a need for new therapeutic techniques that can address currently unmet clinical requirements. Photodynamic therapy (PDT) has the potential to meet these needs.

1.2 PHOTODYNAMIC THERAPY

1.2.1 Principles of photodynamic therapy

PDT involves the irradiation of a photosensitizer (PS) in the presence of molecular oxygen to produce cytotoxic levels of ROS and singlet oxygen ($^1O_2$) that can overwhelm resistance mechanisms and induce cell death through apoptosis, necrosis or autophagy.[20, 22] While the PS is harmless in its natural ground state, light activation within its absorption spectrum causes its fluorescent and cytotoxic properties to become activated. The absorption of photons raises the PS to an excited singlet state, where it is unstable and subsequently decays,

returning to its ground state. In this event, fluorescence will be emitted, allowing for visualization of the PS. At the wavelength of peak absorption, the PS undergoes 'intersystem crossing', which results in an excited triplet state. The interaction between this excited PS and neighbouring molecules leads to the production of ROS through two mechanisms: 1) The Type I photo-oxidative pathway induces the transfer of electrons or hydrogen atoms from the PS to nearby biomolecules that then react with oxygen to produce superoxide ions, peroxides and hydroxyl radicals, which trigger free radical reactions. 2) In the Type II pathway, the energy released when the PS falls back to its ground state is transferred to ground state oxygen, creating $^1O_2$ (Figure 2). Oxygen is thus essential in the process, and it can be shown that the quantum yield of the ROS produced is proportional to the amount of oxygen available in the tissue, which directly affects the efficacy of the therapy.[23]

Although still emerging and not yet FDA approved, PDT has been approved for clinical trial; it has produced successful results for the treatment of several non-malignant skin diseases and malignant skin cancers[12, 22, 24]. While various mechanisms of cell death have been observed in PDT, the exact mechanisms of PDT-induced cell death remain to be fully characterised (Davids 2008).

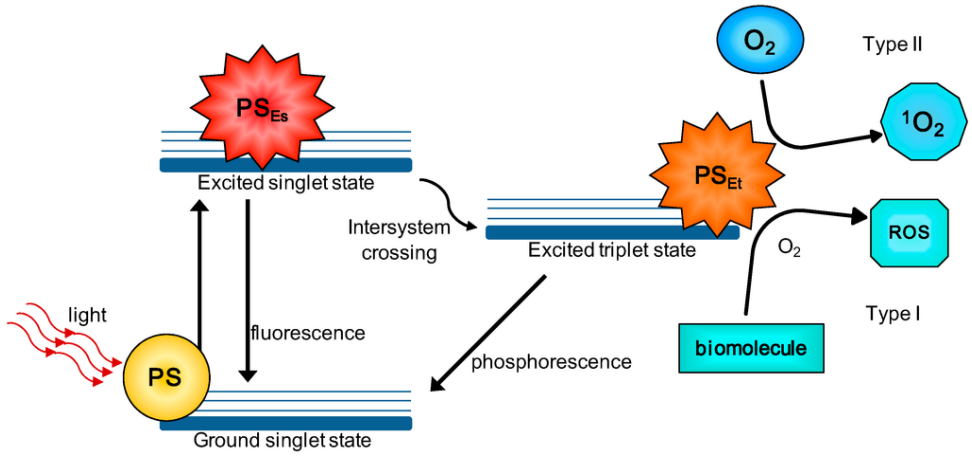

Figure 2: Energy levels diagram of PS excitation. The three components of PDT – PS, molecular oxygen and coherent light – result in production of ROS radicals and $^1O_2$.[25] PS: photosensitizer, Es: excited singlet, Et: excited triplet, O_2: dioxygen, $^1O_2$: singlet oxygen, ROS: reactive oxygen species.

1.2.2 Mechanisms of cell death

Several cell death mechanisms exist; the predominantly observed forms in PDT-induced cell death are apoptosis, necrosis and autophagy,[20] with immunogenic cell death (ICD) having been only recently identified.[26]

1.2.2.1 Autophagy

Under nutrient stress, cells undergo the self-degradative process of autophagy. In this process, autophagosomes engulf proteins and cytoplasm and then bind with lysosomes, where their content undergoes degradation.[27] There are three different mechanisms through which autophagy is activated: macroautophagy, microautophagy and chaperone-mediated autophagy.[27, 28] Several pathways control the autophagy process, including the PI3K/Atk/mTOR pathway. This pathway is often defective in melanoma cells; the phosphorylation of mTOR upstream causes a kinase cascade that ultimately leads to the inhibition of autophagy.[27]

1.2.2.2 Apoptosis

Apoptosis, currently the best understood mechanism of cell death, can be instigated by one of three pathways: the intrinsic, extrinsic, or granzyme pathway. The intrinsic (or mitochondrial) pathway can be activated through environmental pressures such as oxidative stress, nutrient starvation and UV exposure. Members of the pro- and anti-apoptotic Bcl-2 family regulate this process by increasing the permeability of the mitochondrial membrane, which causes cytochrome c to leak into the cytoplasm.[27, 29] Photodamage to the mitochondria or ER can also lead to destruction of the anti-apoptotic proteins, Bcl-2 and Bcl-xL.[30] Moreover, the effects of mitochondrial photodamage may be partially alleviated by autophagy,[31] but not if the target of PDT is the lysosomes.[32] The extrinsic pathway is dependent upon the binding of FasL to Fas and TNFα to TNFR, which leads to the activation of an intracellular death domain, whereas the granzyme pathway is activated by cytotoxic T cells. This elicits the release of granzyme, which results in the cleavage of caspases.[27]

However, it has been observed that melanoma cells are able avoid apoptosis through various mechanisms,[33] leading to an acquired apoptosis-resistance to many common cancer therapies.[27, 34] It is thus suggested that treatments that induce necrosis/necroptosis might be beneficial.

1.2.2.3 Necrosis

Necrosis commonly results from external cellular injury, e.g. photodamage, loss of membrane integrity and cell lysis.[30] Regulated necrosis, also referred to as necroptosis, is driven by kinases such as RIPK1 and RIPK3 and is not caspase-dependent.[27] The process occurs via the RIPK1/RIPK3/MLKL pathway and is negatively regulated by caspases, which cleave RIP1 and RIP3.[35] During this form of necrosis, the permeability of the plasma membrane increases, and it becomes damaged, leading to the release of damage-associated molecular patterns (DAMPs). However, low RIPK3 expression in melanoma cells can cause dysregulation of this process.

PDT has been shown to kill cells predominantly through necrotic cell death, unlike chemotherapy- and radiation-induced cell death, which triggers apoptosis by altering cell-cycle checkpoints.[20] During NIR PDT, cells are observed to swell due to rapid changes in membrane permeability that cause dramatic changes in osmotic pressure; thereafter, they rupture and release their intracellular contents.[36] Nevertheless, further research on the mechanisms on PDT-induced cell death are still necessary, as this process is not fully understood.

1.2.2.4 Immunogenic cell death

ICD occurs when damaged and dying cells release DAMPs. DAMPs are found endogenously and typically contribute to normal functions intracellularly; however, when they become exposed extracellularly, e.g. through cell rupture after NIR PDT, they gain immunogenic properties. After extracellular release or membrane exposure, these molecules alert the immune system to danger through interactions with pattern recognition receptors (PRRs). PRRs are expressed on various cells in the innate immune system, e.g. dendritic cells, monocytes and macrophages. Their interaction with DAMPS promotes the activation and maturation of the immune cells, which then present the TAA to the T cells, thus facilitating an adaptive anticancer immune response.[37, 38]

There are four know modes of ICD: 1) Necroptosis (not accidental necrosis), 2) Pathogen-driven ICD, 3) ICD due to certain chemotherapeutics that target essential cell compartments that induce cell death pathways, and 4) activation of ICD through physical cues, such as through hypericin PDT or irradiation.[37, 39, 40] Apoptosis has previously been thought not to

induce any immune effects, and necrosis has been thought to be the only cell death mechanism to produce an inflammatory response.[20] However, recent findings contradict this opinion; research on ICD has shown that apoptosis does in fact have some immunogenic abilities. ER stress, such as that caused through targeted PDT or in some chemotherapies, is thought to be essential to the occurrence of ICD.[37] Thus, a combination of both regulated necrotic cell death and apoptotic cell death might be favourable in cancer therapy. Moreover, given that it can elicit an enhanced immunologic effect, PDT may have important implications for the treatment of metastatic cancers.[41]

1.2.3 Photodynamic therapy and melanoma

A plant-derived PS called hypericin has shown some promise in melanoma treatment. Hypericin is a compound extracted from St John's Wort (*Hypericum perforatum L.)* that absorbs UVA (315-400nm, with peak absorbance at 351nm) and visible light (548-593nm, with peak absorption at 563nm) and emits at 594-642nm, with peak emission at 600nm, and has shown to be effective in eliminating cancerous skin cells *in vitro.*[3, 42] Hypericin PDT studies reveal that unpigmented melanoma cells die predominantly via apoptotic pathways, while pigmented melanoma cells die predominantly via necrotic pathways. The most plausible explanation for this is that the melanin provides photoprotection by absorbing UV light and preventing the production of ROS and inevitable apoptosis. Damage to the melanosomes membrane, however, results in leakage of cytotoxic melanin precursors into the cytoplasm, leading to necrosis. This is evidenced by the fact that localization of hypericin in the melanosomes is seen in pigmented melanoma.[20, 22, 43]

Despite successful *in vitro* outcomes, and although hypericin is a second-generation PS, designed to provide increased tumour accumulation and triple quantum yield, hypericin nonetheless suffers several limitations. Due to the aggressive VGP of the cancer, it is necessary that treatment penetrates deep into the skin, beyond its superficial layers. Visible and UV light fail to do so, which means that hypericin PDT in humans would fail in eliminating some population of cancerous cells, resulting in subcurative treatment. PDT performed within these absorption ranges would also be inefficient in highly pigmented melanomas due to the photoprotective properties of melanin.[44] In addition, the absorption spectrum of hypericin overlaps with that of haemoglobin, limiting the photoactivation of the PS.[45, 46] Furthermore,

prolonged treatment with UVA can lead to photo-aging and carcinogenesis. In addition to its suboptimal absorption spectrum, hypericin is hydrophobic, which means that it must permeate passively into the cells in order to produce intracellular ROS and has limited efficiency, because it must be internalised into the mitochondria and other organelle to produce its effects. Its hydrophobic nature also makes conjugation to antibodies more difficult as it compromises the immunoreactivity and *in vivo* accumulation.[20, 22]

There are many factors to be considered when selecting an appropriate PS with regards to the excitation and emission wavelengths and their properties. These factors can affect our ability to activate the PS and to detect its activity, heavily influencing the success of a PDT treatment. The use of near-infrared (NIR) dyes holds particular promise and offers various advantages over hypericin.

1.2.4 Near-infrared photosensitizers

NIR fluorescent dyes have several benefits over conventional fluorophores. The optical properties of NIR decrease light absorbance and scattering while increasing the depth of tissue penetration of the light up to several millimetres relative to visible light fluorescence (Figure 3). This is largely due to the fact that many biomolecules, such as oxyhemoglobin, deoxyhemoglobin and water, exhibit minimal absorption in the NIR range. As a result, NIR signals are more versatile and produce lower background, thus improving the tumour-to-background ratio (TBR) when accumulated in tumour tissue. Additionally, the extinction coefficient, which relates to how strongly a PS will absorb light, is up to 17-fold higher in NIR dyes compared to conventional PSs. Hypericin and the NIR PS IRDye 700DX (IR700), have extinction coefficients of 10 000 $M^{-1}cm^{-1}$ and 165 000 $M^{-1}cm^{-1}$, respectively. The low extinction coefficient of hypericin indicates that many more molecules of hypericin are

needed to elicit comparable effects to IR700. Overall, the phototoxicity per photon absorbed is more efficient in NIR agents than in conventional agents. [47-52]

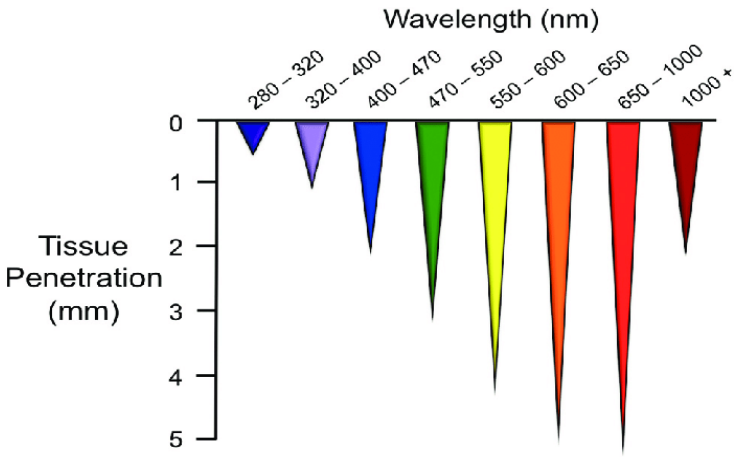

Figure 3: Image depicting the depth of tissue penetration from the UV to IR range. The bright red bar, 650-1000nm, includes the NIR range, where tissue penetration is maximal.[53]

IR700 is a dye of particular interest for NIR PDT. It absorbs light at 658-758nm, with peak absorption at 689nm (Figure 4).[54, 55] IR700 was originally developed for its fluorescent properties and its cytotoxic properties were only recently discovered. It has therefore become an incredibly useful theranostics agent, i.e. it is a single molecule that can be used as both a therapeutic and an imaging tool. It has previously been shown to be successful in eliminating the malignant cells of several cancers both *in vitro* and *in vivo* in xenograft mouse models.[26, 55-59] Furthermore, studies using this dye have shown that repeated light exposure with IR700 is not only safe but also facilitates complete eradication of the tumour. This is because, unlike in ionizing radiation therapies that use gamma rays or x-rays, there is no dose limitation for NIR light irradiation. NIR could therefore accommodate the long-term management of tumours.[48] Repeated exposure of the tumour to NIR irradiation also becomes vital when considering that subcurative PDT can lead to increased expression of vascular epithelial growth factor (VEGF), which is a lead player in angiogenesis.[60, 61] PDT creates hypoxia by consuming the available oxygen and damaging the vasculature, triggering a compensatory synthesis of VEGF. If repeated rounds of irradiation could not be performed, this would make patients vulnerable to increased angiogenesis and metastatic growth.[62, 63]

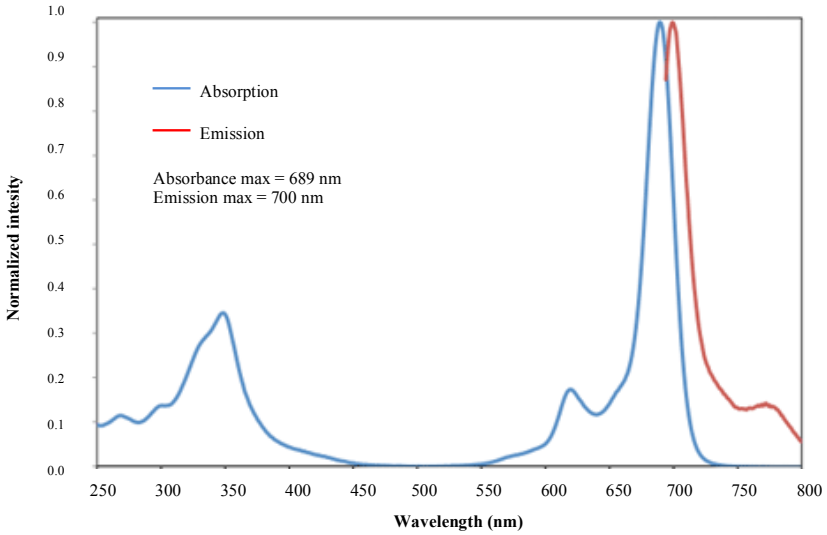

Figure 4: IR700 absorption and emission spectra (in water). Peak absorption at 689nm, peak emission at 700nm.[50]

Cell death appears to begin almost instantaneously with IR700 and persists for several days after light exposure. This immediate effect is indicative of the fact that NIR agents result in rapid necrotic cell death, as opposed to relying on the production of ROS and cell death through slower apoptotic pathways initiated by conventional PSs. This necrotic death is likely caused by physical injury, whereby membrane disruption occurs due to a local increase in heat upon light exposure, resulting in pressure waves.[48, 55] Research does show that there is some cell death due to ROS and apoptosis, although this effect accounts for only about 25% of the total cell death.[64]

Unlike hypericin and other conventional PSs, IR700 is hydrophilic. It is thus easily bound covalently to an antibody. Its lipophobic nature means that it does not freely enter cells and thus will not accumulate in tissue at random. It has been shown to have equal cell death effects when it is irradiated only once internalisation of the PS has occurred as with irradiation upon surface binding. Although, when internalised, monoclonal antibody (mAb)-IR700 conjugates show co-localisation with the endolysosomal compartment and damage to the membrane and lysosomes upon activation, internalisation is not necessary for efficient cytotoxic activity. Membrane binding, however, must occur in order to elicit targeted effects.[48, 64]

PDT is an underused therapy that has great potential, but also has much room for improvement. PDT depends on the passive accumulation of the PS compound in tumour

tissue. The technique thus lacks specificity and, while the effect is significantly less than that of traditional chemo- and radiotherapies, healthy tissue surrounding the tumour is damaged. This is referred to as the scattergun effect, and can lead to side effects, such as off-target necrosis and extensive photosensitivity.[65] Antibody technology enables us to greatly reduce systemic and dose limiting toxicity through the use of photoimmunotherapy (PIT).

1.3 ANTIBODY TECHNOLOGY

1.3.1 Monoclonal antibodies and antibody-drug conjugates

The discovery that malignant cells express tumour-associated antigens (TAAs) and altered receptor profiles has given rise to the potential for immunologically based diagnostic and therapeutic strategies in the form of mAbs. Cancer is a heterogeneous disease in which each subtype exhibits a distinct pattern of genetic dysregulation, resulting in a unique cell surface receptor expression profile.[66] Melanoma itself is a heterogeneous cancer with multiple causal pathways or aetiologies.[67] mAbs (such as trastuzumab, developed for the treatment of HER2-positive breast cancers[68, 69]) are capable of selective biorecognition and can thus target specific tumour cell receptors.[70] In melanoma, targets of interest include 1) the pro-angiogenic marker VEGF, 2) the negative T cell regulator, cytotoxic T-lymphocyte antigen-4 (CTLA4), expressed on T lymphocytes, 3) the migration promoting chondroitin sulphate proteoglycan 4 (CSPG4), 4) CD25 expressed on suppressive regulatory T cells (Tregs), and 5) the immune checkpoint programmed cell death-ligand 1 (PD-L1) expressed on antigen presenting cells and tumour cells.[71-74]

Upon antibody-antigen binding, cell death might occur through one of four ways: 1) inhibition of a signalling pathways results in desirable downstream effects, such as disruption of proliferation and survival pathways, 2) the antibody-dependent cellular cytotoxicity (ADCC) and immune response are activated via the fragment crystallizable (Fc) region, 3) the complement-dependent cytotoxicity (CDC) and cell lysis via the Fc region, or 4) drugs are delivered in the form of an antibody-drug conjugate (ADC) (Figure 5)[66, 75, 76]: this is what is referred to as immunotherapy, whereby antibodies are used to direct modulatory effects to a specific cellular target.[66] This ability to target selective cell surface markers unique to a specific disease modality enables us to overcome the problem of passive and off-target drug accumulation that is associated with PDT. Drugs can be delivered selectively to cells of our

choosing, eliminating systemic side effects. Several ADCs have been developed and approved for cancer immunotherapy.[77-80]

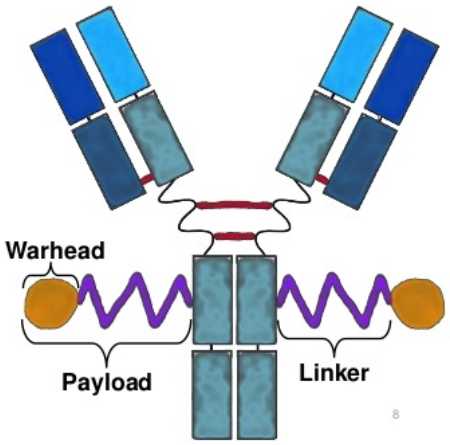

Figure 5: Diagram of an antibody-drug conjugate. A payload, i.e. the biologically active cytotoxic molecule comprised of a linker and a warhead responsible for cell death, conjugated to a monoclonal antibody.[81]

ADCs have gained popularity over naked mAbs because the latter are limited in their efficacy in so far as the inhibition of a particular receptor can facilitate cell death or elicit an immune response. It is also of benefit that the conjugation of a PS to a ligand increases its serum half-life, thus increasing its duration of blood circulation. This allows for unbound conjugate to redistribute and bind to more target cells.[55] Furthermore, because cancers can become resistant to directed mAbs, attaching a drug molecule to the mAb greatly increases the likelihood of successful treatment, as ADCs allow for directed and highly controlled drug release. The combination of selectivity and controllable release means that lower dosages of ADCs compared to mAbs can elicit comparable responses. Resistance to a particular ADC will therefore develop significantly later than that of the constitutive mAb alone, thus widening the therapeutic window.[82] Although immunotherapy has seen great progress in recent years, traditional ADCs have several limitations that make them suboptimal therapeutic agents.

1.3.2 Limitations of monoclonal antibodies and traditional ADCs

While ADCs are currently being used widely in cancer therapy[77-80], they have limitations. One limitation is the current lack of versatility and personalisation of these drugs, given the heterogeneity of the disease. Trastuzumab, for example, treats HER-positive breast cancers, which make up only about 25% of breast cancers. The remaining 75% of patients, in whom the HER2 antigen is absent, can see no benefits from the drug and, for patients with triple

negative breast cancer, no alternative mAb therapy exists.[83] As for melanoma, only three mAb treatments have been approved by the FDA. Nivolumab and pembrolizumab target programmed cell death protein 1 (PD-1) and ipilumimab targets CTLA4.[84-86] This narrow selection of targets means that non-responsive patients lack alternative options.

Moreover, the specificity and sensitivity of traditional ADCs is not optimal. ADCs are typically formed by cross-linking the cysteine or lysine amino acid side chains of an antibody with the drug. This leads to heterogeneous conjugates, as linking can happen across any of the twelve available residue side chains. Thus, not only does the configuration of each conjugate differ, but so does the number of drug molecules attached to each, i.e. the drug-to-antibody ratio (DAR) (Figure 6). As a result, the pharmacokinetic properties, efficacy and safety profile of each individual ADC differs. Moreover, when the DAR is too high (>4), the body might reject the conjugate as a damaged protein and rapidly clear it from the body. Drug load is therefore an imperative consideration in the design of ADCs.[11, 81, 87, 88]

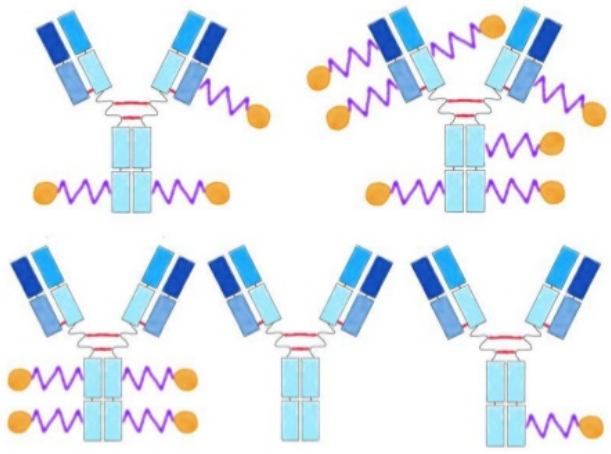

Figure 6: Traditional antibody-drug conjugates produce heterogeneous populations. Heterogeneous products have varied drug-to-antibody ratios.[81]

Another obstacle regarding ADCs is the preservation of the antibodies' structural integrity and biological functioning during and after the conjugation process. These properties are negatively impacted by factors such as the pH, toxicity and temperature of the environment in which the chemical reaction takes place. In addition, the drugs themselves can affect the properties of the antibodies. Any resulting changes to the antibody can in turn affect its binding properties and thus its targeting specificity[89]. Lastly, the first generation of mAbs and ADCs are not humanised, but rather derived from murine antibodies. This can lead to

immunogenicity whereby the human immune system is unable to bring about CDC and ADCC via the Fc, and human anti-mouse antibodies are produced to attack the foreign antibodies[76]. SNAP-tag is a unique antibody format technology that can overcome the above-mentioned limitations. The conjugation, targeting, cytotoxic efficiency and safety of ADCs can be greatly increased through the use of SNAP-tag technology.

1.4 SNAP-TAG TECHNOLOGY

1.4.1 Technical background

O^6-Alkylguanine-DNA alkyltransferase (hAGT) is the human DNA repair enzyme that removes DNA alkyl adducts from the O^6 position of guanine and transfers the alkyl group to one of its reactive cysteine residues (Cys145) to release guanine. Benzylguanine (BG) reacts readily as a substrate for hAGT. Exposure to BG results in the covalent bonding of the two molecules, causing the protein to become irreversibly inactivated.[90-92] SNAP-tag is an engineered version of this enzyme, which exploited this chemistry and can mimic it with any BG-modified substrate, creating a self-labelling fusion protein. Unlike traditional ADCs, which rely on additional conjugation steps that require chemical and enzymatic catalysts, this reaction is autocatalytic, which greatly simplifies the labelling process.[93] The reaction creates a covalent bond between SNAP-tag and any BG-modified molecule as the benzyl alkyl group is transferred to the SNAP-tag protein's reactive cysteine residue and guanine is released to produce a stable tioether (Figure 7). This coupling between SNAP-tag and BG occurs in a precisely 1:1 stoichiometry and at a distinct binding site,[90, 91, 94, 95] allowing for the production of a homogeneous product with a defined configuration and known DAR.[96]

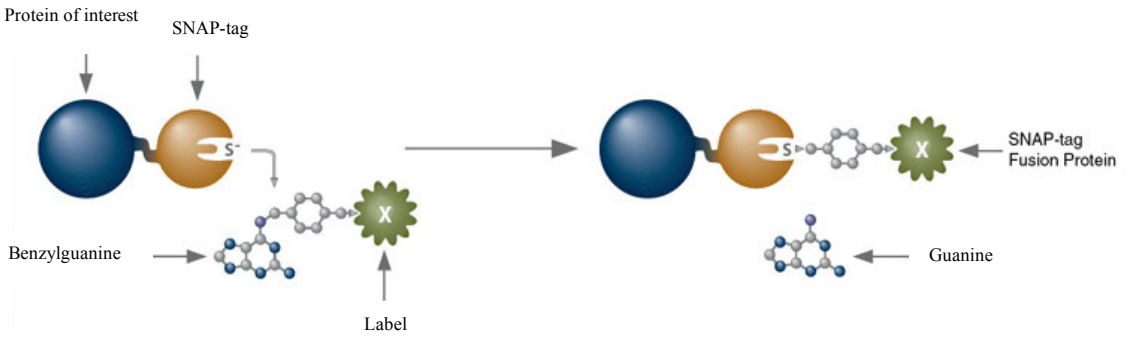

Figure 7: Depiction of SNAP-tags autocatalytic chemical reaction. An irreversible covalent bond is formed between SNAP-tag and BG derivatives as the benzyl alkyl group is transferred to the protein cysteine residue and guanine is released to produce a stable tioether[97]

Directed evolution of hAGT has decreased SNAP-tag's binding affinity for DNA and reduced its size, rendering a 182 amino acid mutant that is 50 times more reactive than the wild type.[91, 92, 98] Removal of unessential cysteine residues facilitates folding of the protein under oxidative conditions, and additional mutations have made SNAP-tag resistant to hAGT inhibitors.[99] Furthermore, because SNAP-tag is of human origin it does not require humanization to overcome the problem of immunogenicity and the risk of an induced immune response is minimized, making it a feasible agent for *in vivo* application in humans.[100]

SNAP-tag can be genetically fused to any ligand of choice, creating a fusion protein. Of interest in the current study is the scFv-SNAP construct, in which SNAP-tag is cloned with a single chain variable fragment (scFv) of the antibody of the cell surface receptor of interest fused at its N-terminus. A polypeptide linker is used to connect the variable heavy and light chains to form an scFv fragment (Figure 8). The scFv is the antigen-binding moiety of the antibody and is the smallest functional format in which the antibody's receptor-binding properties can be preserved.[101] Although removal of the Fc region means removal of the ADCC and CDC responses, such recombinant fragments are better suited than mAbs as ADCs because they allow for easy site-directed conjugation of the drugs to the antibody[76]. Nonetheless, these fragments do not typically withstand direct chemical modification, and the integrity and functionality of the protein, and sometimes the effector molecule, is therefore compromised in such procedures and it has been shown that there are detrimental effects when an antibody undergoes direct conjugation to a fluorophore.[89, 102] SNAP-tag addresses this problem by providing a proxy for chemical modification with no harmful effects on the ligand.[96, 103] Moreover, scFv-SNAP fusion proteins are ideal because of their relatively small size of about 50 kDa.

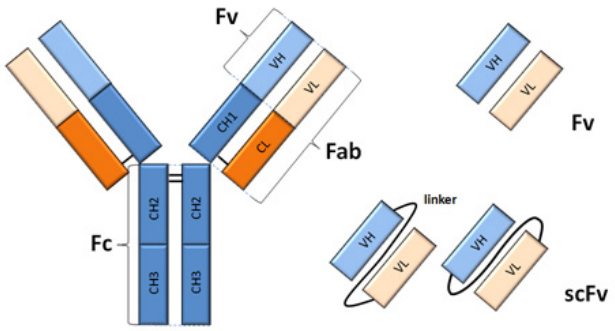

Figure 8: Examples of various antibody formats. Full-length antibody (left) with crystallizable (constant) region (Fc) and antigen-binding region (Fab), containing variable regions (Fv) of the heavy (V_H) and light chains (V_L) (top right). Single-chain variable fragment (scFv) comprised of V_H and V_L variable regions connected via a polypeptide linker (bottom right).[104] Fc:

fragment crystallizable, Fv: vairable fragment, VH: heavy chain, VL: light chain, Fab: antibody-binding fragment, scFv: single chain variable fragment.

1.4.2 Size, circulation and clearance

The size of the scFv-SNAP probe affects both its ability to penetrate tissue and the rate at which it is cleared from circulation.[105] Because deletions in the SNAP-tag gene sequence have reduced its size (20kDa) compared to that of the wild type AGT protein or endogenous fluorescent proteins, SNAP-tag has a much higher degree of penetrability than its larger counterparts. It is in fact largely unrestricted in its ability to access any cellular compartment.[92] In combination with an scFv, this protein has a total size of approximately 50 kDa. It has been shown that the reduced size of an scFv results in higher uptake of the probe into tumour tissue, resulting in a superior TBR, compared to that of the full-length mAb.[102] While full-length antibodies tend to exhibit superior tumour retention, their large hydrodynamic radius (∼5 nm) hinders their renal filtration.[105] The intermediate size of the scFv-SNAP construct facilitates rapid accumulation and efficacious tumour binding soon after injection together with rapid renal clearance. scFv-SNAP fusion proteins have been shown to accumulate in the kidneys shortly after administration, and subsequently in the bladder.[57, 92, 105-107] This further enhances the tumour signal as excess probe is rapidly cleared from the bloodstream, minimizing background interference during visualisation.

All of the above-mentioned attributes make SNAP-tag an attractive agent for application in cancer detection, subtype classification and diagnosis, and cell-specific drug delivery. It is a highly promising tool for precision medicine and, together with IR700, has great potential in PIT.

1.4.3 Photoimmunotherapy

PIT combines the cytotoxic power of photodynamic therapy with the targeting precision of immunotherapy to form an antibody-photoabsorber conjugate (APC). Thus, while PDT depends on the passive accumulation of drugs in the tumour tissue, PIT is an active targeting strategy.[56, 108] The adoption of SNAP-tag technology into PIT offers a simple solution to various issues associated with mAbs and ADCs. SNAP-tag protects the antibody from possible chemical alterations caused by conjugation, increasing the specificity and efficacy of the agent. It produces homogeneous conjugates, allowing for a defined DAR and thus measurable

kinetics and safety profiles. It eliminates off-target accumulation and prevents the damaging scattergun effect of PDT, reducing systemic toxicity. Proof of concept for SNAP-tag-based PIT was shown in 2011, when Hussain *et al.* used the anti-EGFR antibody fragment, scFv-425 to create scFv-425-SNAP fusion proteins conjugated to the chlorin e6 PS to target and kill EGFR-positive epithelial cancer cells.[109]

Because of the innate fluorescent properties of photosensitizing agents, the same molecule can be used to image a tumour, treat cancer, monitor accumulation of the PS and track treatment-induced changes (such as size, location and receptor expression). Tumours can be both assessed through real-time monitoring and treated non-invasively simply by changing the wavelength of the light to which the agent is exposed.[58, 109, 110] Conventionally, tumours have been evaluated by biopsy and morphological examination. However, these methods are invasive, and they fail to evaluate the tumour in its entirety. They rely on pathological changes that are typically late stage indicators of tumour progression, such as change in size and gross morphology.[111, 112] Ultimately, PIT is a theranostics approach, allowing for both diagnosis and treatment at an early stage.

Current diagnostic methods are invasive and are susceptible to both false-negatives and false-positives. This results in late stage detection, and consequentially poor prognosis, or patients with subclinical or benign cancers undergoing unnecessary harmful and expensive treatment[113]. Additionally, current methods of cancer treatment, such as chemotherapy and radiation, cause many unpleasant side effects and are not equally effective on all patients[114]. This is largely due to the heterogeneity of the disease and reiterates the need for targeted therapies using molecular techniques, subtype classification of individual cancers, and personalised and precision treatments.

The selectivity of PIT means not only that tumour cells can be targeted without harm to healthy cells but also that the individual can be screened for the particular receptor signature of their tumour, and the appropriate probe can then be administered, personalising the therapy. In the case of melanoma, programmed death-ligand 1 (PD-L1) is particularly interesting for diagnostic and prognostic purposes, while CSPG4 is an ideal target for diagnosis as well as the selective delivery of drugs to target cells.

1.5 PROGRAMMED DEATH-LIGAND 1

1.5.1 Tumour immune response

The discovery of TAAs has occurred fairly recently but has rapidly given way to an entirely new understanding of cancer. TAAs are generally self-antigens that are expressed unusually in the tumour, e.g. they might be mutated or over-expressed, but they could also be tumour-specific antigens (TSAs).[115] Though our knowledge in this area is still lacking, we now know that malignant cells express TAAs and that these, along with tumour infiltrating lymphocytes (TILs), in particular the TAA-specific $CD8^+$ cytotoxic T lymphocytes (CTLs), influence immune surveillance of the tumour microenvironment.[116] CTLs have been found within the tumour and its microenvironment, which indicates that cancer triggers the immune responses of its host. This response is mediated by the TAAs, which serve to discriminate between malignant and healthy cells.[117] The identification of these antigens has been of great value in the immunodiagnosis of several cancers, including hepatocellular carcinoma, ovarian cancer, breast cancer and osteosarcoma.[118-121] These studies used autoantibody detection panels to determine the presence of cancer. CTLs recognize TAAs that are presented by the MHC I receptors via the T cell receptors (TCRs).

1.5.2 PD-L1 expression and functional role

The PD-L1 ligand and its corresponding receptor, PD-1, are highly expressed on regulatory T cells (Treg cells). Tregs are essential for the regulation of peripheral tolerance.[122, 123] The PD-1/PD-L1 pathway is responsible for regulating the inhibitory and stimulatory signals that govern immunity; in particular, it modulates self-tolerance. When PD-1 is activated through binding with PD-L1, its expression is upregulated on T cells. Besides T cells, PD-L1 is also expressed on various non-haematopoietic cells, such as in the pancreatic islet cells, muscle, nerves and vascular endothelial cells, and in area that have immune privilege, such as the eyes and placenta.[124] The interaction between these proteins facilitates T cell tolerance at several checkpoint, thus mitigating self-reactive responses from the T cells when dendritic cells (DCs) present self-antigens.[125] PD-L1 also aids in inhibiting the function of self-reactive effector T cells[126] and in the development and function of the immune-suppressive induced Treg cells.[125]

PD-L1 has clear advantageous functions in healthy humans. However, in a cancerous person, the disadvantages of its expression are apparent. In these circumstances, the aberrant expression of PD-L1 becomes dangerous, as facilitates immunosuppression and self-tolerance of the tumour, leading to immune evasion.

1.5.3 PD-1/PD-L1 immune checkpoint

When PD-L1, which is often over-expressed on cancerous cells, binds PD-1 receptors on the TILs, it inhibits their functionality and proliferation, thus hindering immune responses by facilitating peripheral tolerance.[127] PD-1 becomes over-expressed on CTLs in caner patients, and coupling with PD-L1 causes their effector function and cytokine production to become impaired, leading to "T cell exhaustion". The PD-1/PD-L1 pathway facilitates immune tolerance of tumour cells, aiding the tumour's evasion of the immune system.[128] The anti-PD-L1 mAb inhibits the PD-1/PD-L1 pathway and re-establishes antigen-specific CTL function, thus counteracting the immunosuppressive tumour microenvironment.[70]

PD-L1 has been shown to be over-expressed in both its full-length form and in several splice variant forms in malignant melanoma cells, however; other studies have found little relevant PD-L1 expression on melanoma tissue. [129, 130] Nonetheless, two mAbs targeting this pathway, pembrolizumab and nivolumab, have been approved for clinical use and are showing improved survival in patients.[131, 132]

1.6 CHONDROITIN SULPHATE PROTEOGLYCAN 4

1.6.1 Characteristics and expression

CSPG4, also known as high molecular weight melanoma-associated antigen (HMW MAA) or melanoma-associated chondroitin-sulphate proteoglycan (MCSP), is the analogue of the rat brain progenitor marker, NG2. It is a cell surface antigen, first discovered on human melanoma cells and is often overexpressed in melanoma tumours.[133-135] It is a type I transmembrane chondroitin sulphate-modified glycoprotein-proteoglycan that is able to interact with cytoplasmic components as well as extracellular matrix components, thus mediating downstream signalling pathways. It is anchored to the actin filaments of the cytoskeleton (Figure 9), influencing actin polymerization, cell adhesion and motility.[136-138] It acts through the ERK and FAK pathways to influence tumour cell survival and proliferation, as

well as migration and invasion, thus contributing to melanoma's ability to grow and metastasize. CSPG4 plays a significant role in the regulation of various cell cycle pathways and in the promotion of EMT.[139-142]

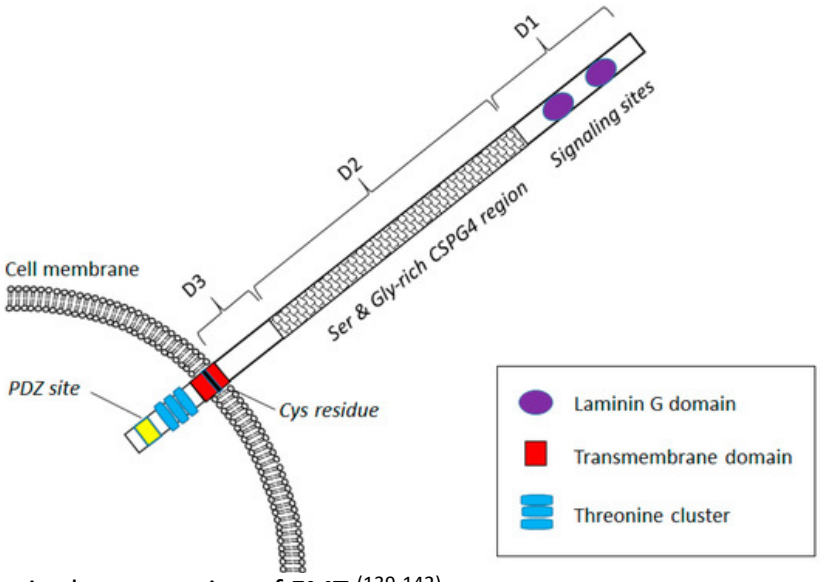

Figure 9: Schematic representation of the protein domain organization of CSPG4. Three extracellular domains (D1-3), transmembrane region (red) and short cytoplasmic domain.[137] PDZ: post-synaptic density protein 95 (PSD-95), drosophila disc large tumor suppressor (Dlg1), zona occludens 1 (ZO-1), D: domain, Cys: cysteine, Ser: serine, Gly: glycine, CSPG4: Chondroitin sulfate proteoglycan 4.

CSPG4 is expressed in various developing and immature tissues, as well as on a restricted number of adult tissues, including the gut and brain. However, it is post-translationally down-regulated in the terminally differentiated melanocytes of normal adult tissue.[134, 141-145] Over-expression of the antigen in malignant cells allows the cancer to evade normal regulatory signals, affects the cell-cell interactions that govern anchorage-dependant growth, and is a major player in the progression of melanoma into RGP and VGP.[146] CSPG4 is also expressed on some stem cells, including cancer stem cells (CSC). CSCs are highly regenerative, self-renewing (without diminishment of their capacity for proliferation), and have migratory and transformation capabilities.[147-149] These cells are highly resistant to therapy and serve as a good prognostic marker.[135, 150] These factors make CSPG4 a good target for immunotherapy.

1.6.2 CSPG4 as a therapeutic target

When choosing an appropriate therapeutic marker, one should be sure that the target antigen is differentially expressed on the target cell. It is also imperative that the target receptor undergoes minimal secretion into circulation, as the antibody could bind any

secreted receptors in the bloodstream, thus using up the probe and limiting exposure to the target cells.[151]

As stated above, CSPG4 has high expression on malignant melanoma cells, with relatively limited expression in normal, healthy skin tissue.[75] This target thus satisfies the first condition of differential expression on target cells. CSPG4 knockout has been shown to retard melanoma tumour growth and migration and promote necrosis and apoptosis of the tumour tissue. Furthermore, targeting the antigen with the anti-CSPG4 antibody, mAb9.2.27, interrupts tumour growth, while expression promotes anchorage-independent cell growth, EMT and survival.[142, 152-154] With regards to the second condition, CSPG4 is a transmembrane protein. As such, CSPG4 is permanently membrane-bound, limiting its secretion into circulation.[134, 155]

1.7 AIMS AND OBJECTIVES

1.7.1 Aims

Given the current limitations of both PDT and ADCs, there are two major changes we would implement in order to refine PIT. The first concerns the use of conventional PSs. The second concerns the use of mAb. Through the site-directed delivery of theranostics using SNAP-tag antibody technology, we aim to achieve photoimmunotheranostic targeting of the CSPG4 antigen via the anti-CSPG4 antibody, mAb9.2.27, and the photodiagnostic targeting of the CSPG4 and PD-L1 antigens.

mAb9.2.27(scFv)-SNAP-IR700 fusion proteins will be used to target and kill CSPG4-positive A375, UCT-Mel-1, UCT-Mel-1-DTIC, WM902, IG-R1, IG-R39 and SK-MEL-28 melanoma cells. We hypothesize that the conjugate will show selective binding to these cells and be equally effective in eliminating pigmented and unpigmented cell lines in all growth phases, as a) melanin absorbs UV light and thus shouldn't provide photoprotection to pigmented cells in the NIR range and b) CSPG4 is reportedly expressed in all growth phases, thus providing the suitable target throughout. Since IR700 is effective through membrane binding without internalisation, the mechanisms of cell death are expected to be the same in each case – rapid injury-induce necrotic cell death. Furthermore, the physical injury to the cell upon NIR light exposure is expected to be sufficient in eliminating the chemoresistant cell line, rendering its

resistance mechanisms useless, as the cells will not have the chance to internalise and sequester or efflux any toxins.

αPDL1(scFv)-SNAP-Alexa Fluor™ 594 (Alexa594) fusion proteins will be used target and visualize melanoma cells. It is hypothesized that the above cell lines will express PD-L1 and that the conjugate will show selective binding to these. αPDL1(scFv)-SNAP-Alexa594 in combination with mAb9.2.27(scFv)-SNAP-Alexa Fluor™ 488 (Alexa488) could then be used to establish a multiplex *ex vivo* diagnostic platform.

The diagnostic abilities and therapeutic efficacy of the combination of PDT and ADCs to target both CSPG4 and PD-L1 remains largely unknown. This project therefore aimed to:

1. Generate mAb9.2.27(scFv)-SNAP-Alexa488 and mAb9.2.27(scFv)-SNAP-IR700 to target CSPG4 receptors on the above-mentioned cell lines *in vitro* and determine the biological activity of the PIT agent.

2. Generate αPDL1(scFv)-SNAP-Alexa488 to target over-expressed PD-L1 receptors on melanoma cells for photodiagnosis.

1.7.2 Objectives

Aim (1) will be achieved by:

1. Developing recombinant mAb9.2.27(scFv)-SNAP fusion proteins, through cloning and expression of the pCB-CSPG4-SNAP plasmid in a eukaryotic expression vector co-expressing enhanced green fluorescent protein (eGFP).

2. Enrichment of secreted proteins by immobilized metal affinity chromatography (IMAC) and validation of functional protein by western blot.

3. Labelling proteins with BG-modified Alexa488 and IR700 and showing successful binding of proteins to target cells by flow cytometry and confocal microscopy.

4. Evaluating phototoxicity to CSPG4-positive cells via PIT through administration of mAb9.2.27(scFv)-SNAP-IR700 conjugates and subsequent application of NIR light.

Aim (2) will be achieved by:

1. Developing recombinant αPDL1(scFv)-SNAP fusion proteins, through cloning and expression of the pCB-PDL1-SNAP plasmid in a eukaryotic expression vector co-expressing eGFP.

2. Enrichment of secreted proteins by immobilized metal affinity chromatography (IMAC) and validation of functional protein by western blot.

3. Labelling proteins with BG-modified Alexa488 and showing successful binding of proteins to target cells by flow cytometry and confocal microscopy.

2. Methods and Materials

2.1 CELL CULTURE

2.1.1 HEK293T cell culture

Human embryonic kidney (HEK293T) cells were cultured in RPMI-1640 medium supplemented with 10% foetal bovine serum (FBS) and 100U/mL penicillin-streptomycin. Medium was changed every three to four days and cells were passaged when 90% confluent. Cells were incubated at 37^{o}C in 5% CO_2. All products were purchased from Gibco by Life Technologies (CA USA).

2.1.2 Transfection and protein expression in HEK293T cells

Two days before transfection, HEK293T cells were plated at 70% confluency. The XtremeGENE HP DNA Transfection Reagent Quick Protocol (Sigma-Aldrich, MO USA) was used, with some alterations. The 3:1 ratio of Transfection Reagent (µL) to DNA (µL) was used, with 5 ng DNA per transfection. 9 µL X-tremeGENE HP DNA Transfection Reagent and 190 µL DMEM were used. An untransfected cell condition was included as a negative control. 48 hours post-transfection, cells were observed on a ZOE Fluorescent Cell Imager (Bio Rad, CA USA) for detection of eGFP and transfection efficiency was determined through visual cell counting. All images were taken at 175x magnification. Cells were then treated with Zeocin to enrich the population expressing eGFP. These cells were expanded from T25 flasks to T150 flasks (SPL Life Sciences, Gyeonggi-do, Korea) for increased protein production. Cell culture supernatant (CCSN) was collected at every medium change, centrifuged at 2500 RPM for 3 min to remove cellular debris and the remaining cell-free supernatant was stored at 4^{o}C.

2.1.3 Mammalian cell line cell culture

CSPG4-negative MDA-MB-468 cells and CSPG4-positive SK-MEL-28 (lightly pigmented, RGP), HS578T (breast cancer), IGR-1 and IGR-39 (pigmentation and growth phase unknown), and CSPG4-negative MDA-MB-468 (breast cancer) were donated by Matthias Peipp of Keil University, Germany. CSPGP4-positive A375 (unpigmented, RGP), WM902 (pigmentation unknown, RGP), UCT-Mel1 (pigmented, MP) and UCT-Mel1-DTIC-R2 (pigmented, MP, chemoresistant) cells were donated by Lester Davids of the University of Pretoria. These cells were cultured in DMED medium supplemented with 10% FBS and 100U/mL penicillin-streptomycin. Medium was changed as required and cells were passaged when 90% confluent.

Cells were incubated at 37°C in 5% CO_2. All products were purchased from Gibco by Life Technologies.

2.2 *IN SILICO* CLONING

2.2.1 *In silico* vector design, plasmid constructs and cloning sites

SnapGene® software (GSL Biotech, Chicago, IL USA; available at www.snapgene.com) was used for *in silico* design of the mammalian vector system for transient expression of the SNAP-tag fusion protein. The pCB-H22-SNAP plasmid (8025 bp), previously developed in the MB&I lab and derivative of the pSecTag2 A plasmid, containing the sequences for H22(scFv) (747 bp) and SNAP-tag (534 bp) was used. H22(scFv), found between the *Sfi*I and *Not*I restriction sites, was removed and the scFv sequence of the mAb9.2.27 (750 bp) or the αPD-L1 antibody (720 bp), was inserted to produce the final pCB-CSPG4-SNAP (8026 bp) or pCB-PDL1-SNAP (7996 bp) construct. The open reading frame was translated into annotated base pair and amino acid sequences. These translations were used to order the pUC57$^{mAb9.2.27}$ and pUC57$^{\alpha PD\text{-}L1}$ production vectors containing the respective scFv inserts, including *Sfi*I and *Not*I restriction sites, from Genscript (NJ USA).

2.2.2 Sequence generation

To procure a new anti-PD-L1 antibody sequence, a literature search was performed to identify an ideal construct from publications and patents and obtain its amino acid sequence. Using the Gene Infinity Back Translation Tool (Gene Infinity LLC, San Diego, CA USA; available at http://www.geneinfinity.org/sms/sms_backtranslation.html), the amino acid sequence was used to translate the nucleotide sequence. IgBLAST (NCBI, Bethesda, MD USA; available at https://www.ncbi.nlm.nih.gov/igblast/) was used to analyse the nucleotide sequences of the heavy chain (V_H) and light chain (V_L) variable domains and identify the framework regions (FR) and complementarity determining regions (CDR) of each. Each FR and CDR was then translated into its corresponding amino acid sequence using the ExPASy Translate Tool (SIB, Lausanne, Switzerland; available at https://web.expasy.org/translate/) and CLC Genomic Workbench (Qiagen, Hilden, Germany; available at https://www.qiagenbioinformatics.com/products/clc-genomics-workbench/) was used to align each CDR with the original sequence.

2.3 MOLECULAR CLONING

2.3.1 Liquid transformation of competent cells

Plasmid DNA was incorporated into chemically competent DH5α *Escherichia coli* (*E. coli*) cells. Competent *E. coli* cells (NEB, MA United States) were thawed on ice for 10 minutes. Plasmid was diluted to obtain a final concentration of 100 ng/µL. 0.5 µL of plasmid was added to 50 µL of competent cells, mixed by gently flicking the tube and then placed on ice for 30 minutes. The cells were heat shocked in a water bath at 42°C for 60 seconds and subsequently placed on ice for 5 minutes. In order to increase the transformation efficiency, 950 µL of room temperature Super Optimal Broth with Catabolite repression (SOC) (NEB) was added to the mixture. The 1 mL mixture was inoculated into 50mL Luria Bertani Broth (LB) (Sigma-Aldrich) and placed at 37°C on a shaker overnight.

2.3.2 Midiprep (large-scale) DNA isolation

The NucleoBond Plasmid Purification Kit (Macherey-Nagel GmbH & Co, Düren, Germany) was used to purify DNA on a large scale (50 mL cultures). Minor alterations were made to the manufacturer's instructions. During the precipitation step the mixture was split into 8x 1mL aliquots in 1.5 mL microcentrifuge tubes. These were then centrifuged at 13 200 rpm at room temperature for 10 minutes. Each aliquot was then washed in 250 µL 70% ethanol, pellets were resuspended, and 4 aliquots were pooled into a tube and centrifuged for 10 minutes. Finally, pellets were dissolved in 30 µL sdH_2O pre-heated to 50°C to facilitate solubilisation of the DNA. The DNA concentration was then quantified using a NanoDrop ND-2000 (Thermo Fisher Scientific, DE USA).

2.3.3 Restriction enzyme digestion

All restriction enzyme (RE) digests were performed using the NEB Double Digest protocol and materials, with adjustments. To remove scFv fragments from between the *Sfi*I and *Not*I restriction sites in the vectors, the reaction was set up with 2 µg DNA, 5 µL CutSmart Buffer, 0.5 µL of *Sfi*I and made to a final volume of 49 µL with sdH_2O. The reaction was then incubated at 37°C for 4 hours, after which 1 µL of *Not*I-HF was added and the reaction was incubated at 50°C overnight.

2.3.4 Agarose gel electrophoresis

Agarose gel electrophoresis was performed to confirm digestion. A 1.2% (w/v) agarose gel (see Appendix 6.3.1) was placed in 1X TAE buffer (see Appendix 6.3.2). 4X Laemmli Load Dye

(see Appendix 6.3.2) was added to DNA samples in a 1:10 ratio before loading. Undigested template DNA was included as a control. The Quick-Load 1kB DNA Ladder and Generuler 100bp Plus DNA Ladder (New England BioLabs, MA USA) were used to evaluate the fragment sizes. DNA fragments were separated for 60 minutes at 100V using the Mini-Sub Cell system (Bio Rad) and then visualized and documented using the UVIpro Gold Gel Documentation System (UVItec, Cambridge, UK) under UV light.

2.3.5 Gel extraction

Agarose bands containing the DNA fragments of interest were excised using the QIAquick Gel Extraction Kit (QIAgen, Hilden, Germany), with some changes. Briefly, the gel was visualized using the Dark Reader Transilluminator (Clare Chemical Research, CO USA) and bands were cut out using a sharp, sterile scalpel. The excised bands were pooled and placed in 1.5 mL microcentrifuge tubes. The agarose gel was solubilized by adding enough Buffer QG to fully submerge the excised slices, this was considered as 'three volumes'. Tubes were incubated at 50°C for 10 minutes, ensuring that the gel was completely dissolved. Tubes were vortexed periodically to aid dissolution. One volume isopropanol was added. The solution was placed in a spin column inside a collection tube and centrifuged for 1 minute at 13 000 rpm. Flowthrough was discarded and the column was centrifuged once more. To wash the column, 0.75 mL Buffer PE was added and centrifuged for 1 minute. Columns were placed in clean microcentrifuge tubes and, to facilitate solubilisation of the DNA, 50 µL 50°C dsH_2O was added to the centre of the filter instead of Buffer EB. Tubes were incubated at 50°C for 5 minutes before centrifuging for 1 minute to elute DNA.

2.3.6 Ligation

Ligation of digested fragments was carried out using the NEB T4 Ligase kit and overnight protocol (NEB). 20 µL reactions were set up with 2 µL T4 DNA Ligase Buffer, 1 µL T4 DNA Ligase, 50 ng vector, and the required amount of insert (dependent upon fragment sizes), topped up to 20 µL with dsH_2O. Four ligations were performed using 1:1, 1:2, 1:3 and 1:0 (vector only control) vector-to-insert ratios. The online NEBioCalculator (available at https://nebiocalculator.neb.com/#!/ligation) was used to calculate the exact volumes of insert required at different vector-to-insert ratios. Transformation efficiency was calculated using the following formula: $TE = (\frac{colonies}{mL})/[DNA]$ (µg/mL)

2.3.7 Transformation with recombinant plasmids

Recombinant plasmid DNA was incorporated into chemically competent *E. coli* cells. The cells were thawed on ice for 10 minutes. Plasmid was diluted to obtain a final concentration of 100 ng/µL. 0.5 µL of plasmid was added to 50 µL of competent cells, mixed by gently flicking the tube and then placed on ice for 30 minutes. The cells were heat shocked in a water bath at 42^{o}C for 60 seconds and subsequently placed on ice for 5 minutes. In order to increase the transformation efficiency, 950 µL of room temperature SOC was added to the mixture, which was then placed in an incubator at 37^{o}C for 60 minutes. Cells were mixed thoroughly by gently flicking and inverting the tube. 50 µL of mixture was spread on a LB agar plate supplemented with 200 ng/µL AMP (see Appendix 6.3.3) and left at 37^{o}C overnight. Vector only and bacteria only controls were included. Six single colonies were picked, and each placed in 2 mL LB in separate 10 mL conical tubes. The cultures were left on a shaker (220 rpm) at 37^{o}C overnight.

2.3.8 Miniprep (Small-Scale) DNA isolation

Recombinant plasmids were purified from the *E. coli* on a small-scale (10 mL cultures) using the Zyppy Plasmid Miniprep Kit (Zymo Research, CA USA), according to the manufacturer's instructions, with minor alterations. Briefly, in order to increase the number of bacterial cells and thus the final DNA concentration, 1.2 mL culture was placed in a 1.5 mL microcentrifuge tube and centrifuged at 16 000 rpm for 1 minute. Thereafter, 600 µL of the supernatant was discarded, the pellet was resuspended, and the protocol was continued with the remaining 600 µL of starter culture. Furthermore, to prevent interference in downstream applications, elution was achieved with 30 µL of sterile deionized water (sdH_2O), pre-warmed to 50^{o}C, instead of Zyppy Elution Buffer. Lastly, rather than standing at room temperature for 1 minute, the columns were incubated at 50^{o}C for 5 minutes to facilitate solubilisation of the DNA. The eluted DNA concentration was then quantified using a NanoDrop ND-2000. Note, the remaining 800 µL of each 2 mL culture was stored at 4^{o}C for potential downstream application after confirmation of ligation and sequencing.

2.3.9 Restriction mapping

Single enzyme digest simulations were performed on SnapGene to predicate the cutting patterns of HindIII-HF and BamHI-HF for pCB-H22-SNAP against pCB-CSPG4-SNAP and pCB-PDL1-SNAP, respectively. The expected band fragments were as follows. HindIII-HF digest of

pCB-H22-SNAP: three bands at 6964 bp, 360 bp and 348 bp. HindIII-HF digest of pCB-CSPG4-SNAP: four bands at 5868 bp, 1450 bp, 360 bp and 348 bp. BamHI-HF digest of pCB-H22-SNAP: two bands at 6183 bp and 1840 bp. BamHI-HF digest of pCB-PDL1-SNAP: one band at 7996 bp. 10 µL reactions were then set up with 2 µg DNA, 1 µL CutSmart Buffer and 0.5 µL enzyme, topped up to 10 µL with dsH_2O. Samples were incubated at 37^oC for 4 hours. Agarose gel electrophoresis was performed as described above. Gels were analysed to confirm correct ligation of recombinant plasmids, as predicted by the simulation.

2.3.10 DNA sequencing

Recombinant clones that were confirmed by restriction mapping were bulk prepped and purified using the NucleoBond Plasmid Purification midiprep protocol, as described above. Samples were sent to Inqaba Biotechnology, as a pay-for-service, in order to confirm the accuracy of the open reading frame (ORF) sequence. The universal T7 primer was used, in addition to an internal primer with the sequence GCTGATCTATGACGCTAG. Sequencing was done with the ABI V3.1 Big dye kit according to manufacturer's instructions. The labelled products were cleaned with the Zymo Seq Clean-Up kit and cleaned products were injected on the ABI3500XL.

2.4 PROTEIN PURIFICATION

2.4.1 Immobilized metal affinity chromatography

CCSN containing the secreted his_6-tagged fusion proteins was first centrifuged in order to rid the medium of residual cellular material, as per section 2.1.2. The remaining cell-free supernatant (CFSN) was then filtered using the Nalgene vacuum filtration system (Sigma Aldrich) with a 0.45 µm Durapore membrane filter (Millipore, MA USA) to exclude remaining debris before enrichment by Immobilized Metal ion Affinity Chromatography (IMAC). IMAC was performed on an ÄKTA FLPC system (GE Healthcare Europe GmbH, Freiburg, Germany). Briefly, a Ni^{2+}-NTA Superflow cartridge column was equilibrated with equilibration buffer (see Appendix 6.4.4). CFSN was loaded directly onto the column at a flow rate of 2 mL/min and his_6-tagged proteins were captured by Ni^{2+}-NTA. The column was washed with equilibration buffer. Bound his_6-tagged protein was eluted with elution buffer containing 250 µM imidazole (see Appendix 6.4.4). Elution buffer was applied at an increasing gradient of 0-30% to separate elution peaks. Thereafter a 100% gradient was applied to removal all remaining bound protein. 5 mL fractions were collected throughout.

2.4.2 Protein concentration

Amicon Ultra-15 Centrifugal Filter Units (Merck Milipore, MA USA) were used to further concentrate purified protein, as well as to remove imidazole. Fractions associated with each peak on the ÄKTA chromatogram were pooled in separate Amicon filter tubes, to a maximum volume of 15 ml per tube. Tubes were centrifuged at 4000 xg for 25 min, at 4°C. Flowthrough was discarded and imidazole-free concentrate was recovered and placed at 4°C.

2.5 PROTEIN ANALYSIS

2.5.1 Quantification of purified protein

The concentration of purified mAb9.2.27(scFv)-SNAP and αPDL1(scFv)-SNAP protein was determined using a NanoDrop ND-2000 (Thermo Fisher Scientific).

2.5.2 Sodium dodecylsulphate polyacrylamide gel electrophoresis (SDS-PAGE)

Protein samples were separated by size by SDS-PAGE in order to detect protein in each fraction and determine its weigh. 1 µg protein was diluted to a final volume of 20 µL. 5 µL NEB 4X protein-loading buffer was added to each sample and samples were heated to 95°C for 5 min before loading. Proteins were separated electrophoretically at 100V for 75 min on the Mini-Sub Cell system (Bio Rad). Protein bands were visualised by soaking the gel in Coomassie Staining Solution for 30 min. GelAnalyzer software (available at: http://www.gelanalyzer.com) was used to determine the size (kDa) of all bands. Briefly, images were uploaded onto the program and all intensity peaks were gated, including those of the ladder. The band sizes of the ladder were inserted in order to calibrate band molecular weight. Additionally, the volume of each band was provided, allowing for the yield of SNAP-tag protein to be estimated. Purification fractions corresponding to bands of the appropriate size for mAb9.2.27(scFv)-SNAP or αPDL1(scFv)-SNAP were pooled for downstream application.

2.5.3 Western blot

Western blotting was used for the detection of functional his_6-tag protein. A gel was run as describe in section 2.4.2, with 2 µg of protein. Protein bands were transferred from the gel to a nitrocellulose membrane using the electro-tank blotting method at 100V for 75 min. Blocking was achieved using 2% milk and PBS for 1 hour at room temperature. A 1:1000 dilution of anti-His_6-tag rabbit primary antibody and a 1:5000 dilution of goat anti-rabbit IgG

horse radish peroxidase (HRP)-conjugated secondary antibody (Bio Rad) were used to detect proteins. A Gel Doc™ XR Gel Documentation System (Bio Rad) was used to visualize protein.

2.6 PROTEIN LABELLING

2.6.1 Protein labelling with SNAP-Surface® Alexa Fluor® 488 and SNAP-Surface® 549

The NEB Protein Labelling *in vitro* protocol was used to label purified mAb9.2.27(scFv)-SNAP and αPDL1(scFv)-SNAP with BG-modified substrates, SNAP-Surface® Alexa Fluor®488 and SNAP-Surface® 549, respectively, according to the manufacturers' instructions. Briefly, a 50 µL reaction was set up with 42 µL Phosphate Buffered Saline (PBS), 1 µL DTT (50 mM), 5 µL SNAP-tag purified protein (50 µM) and 2 µL SNAP-tag substrate (250 µM) and incubated in the dark for 30 min at 37°C. Unbound substrate was then removed according to the Zeba Spin Desalting Columns 7K MWCO protocol. The final constructs were named mAb9.2.27(scFv)-SNAP-Alexa488 and αPDL1(scFv)-SNAP-549.

2.6.2 Protein labelling with BG-IR700

Lyophilized BG-IR700 was solubilised in 50% DMSO. Purified mAb9.2.27(scFv)-SNAP was incubated with a two-fold molecular excess of BG-IR700 at room temperature in the dark for 2 hours. After labelling, unbound dye was removed according to the Zeba Spin Desalting Columns 7K MWCO protocol. The final construct was named mAb9.2.27(scFv)-SNAP-IR700.

2.7 IMMUNOASSAYS

2.7.1. Validation of binding by flow cytometry

The binding of mAb9.2.27(scFv)-SNAP-Alexa488 to CSPG4-positive cells and αPDL1(scFv)-SNAP-549 to PD-L1-positive cells was monitored by flow cytometry using a FACSCalibur system and FlowJo software for analysis (Becton & Dickinson, Heidelberg, Germany). The CSPG4-negative MDA-MB-468 cell line was used as a negative control for mAb9.2.27(scFv)-SNAP-Alexa488. HS578T was used as a positive control for both probes. In each experiment, approximately $1x10^6$ cells were incubated with 5 µL labelled proteins on ice in the dark for 30min. Cell were fixed for 20 minutes in 4% paraformaldehyde (PFA) and were washed three times with PBS before detection.

2.7.2 Validation of surface binding by confocal microscopy

Targeted protein binding was visualized by confocal microscopy. $2.5x10^4$ to $1x10^5$ cells were seeded on a cover slip in a 35mm dish and incubated in medium at 37°C in 5% CO_2 overnight. Cells were incubated with 15 μg mAb9.2.27(scFv)-SNAP-Alexa488 or αPDL1(scFv)-SNAP-549 in 100 μL serum free medium and 200μL 1:5000 Hoechst counter stain. Excess dye was removed by washing cells three times with medium before fixing for 20 minutes with 4% PFA. Cells were washed three times with PBS and the cover slip was mounted on a slide. After sitting at room temperature for 24 hours, images were captured on the Ziess LSM880 Airyscan (Oberkochen, Germany) on the 40X air objective.

2.8 EVALUATION OF PHOTOTOXICITY

2.8.1 Cell viability assay

Cells were treated with increasing concentrations of unconjugated mAb9.2.27(scFv)-SNAP (negative control), mAb9.2.27(scFv)-SNAP-IR700 or Zeocin (positive control). 3 hour later, cells were irradiated with 690 nm light at 1.5 W for 90 seconds. Following treatment, the XTT Cell Proliferation Kit (Roche, Basel, Switzerland) was used, according to the manufacturers' instructions, to determine cell viability. Briefly, 20 hours after irradiation, cells were incubated with XXT solution for 4 hours. The cleavage of the yellow tetrazolium salt by metabolically active cells to form orange formazan crystals, which absorb light at 450 nm, was measured by spectrophotometry using softMax pro4.3.1 software. The measured absorbance was normalized to the untreated control (vehicle). All graphs were created using GraphPad Prism software (available at: https://www.graphpad.com/scientific-software/prism/)

3. Results

3.1 mAb9.2.27(scFv)-SNAP-IR700 FOR CSPG4-TARGETED THERAPY

3.1.1 Molecular cloning

3.1.1.1 *In silico* vector design

The pCB-H22-SNAP plasmid contains SNAP-tag between the *Not*I and *Blp*I restriction sites and H22(scFv) between *Sfi*I and *Not*I. This plasmid was used as the backbone for the current study. H22(scFv) was removed and replaced with mAb9.2.27(scFv) to create the pCB-CSPG4-SNAP plasmid. Figure 10A represents the structure of the ORF. Figure 10B is the plasmid map, generated on SnapGene. Annotated nucleotide and amino acid sequences were generated and used for ordering of the production vector containing the mAb9.2.27(scFv) sequence, as well as for alignment (Figure 10C). The alignment confirms that cloning between the *Sfi*I and *Not*I restriction sights will produce an in-frame sequence with no stop codon interference. Table 1.1 summarises the components of the pCB-CSPG4-SNAP vector, while Table 1.2 summarises the plasmids used in this project.

A

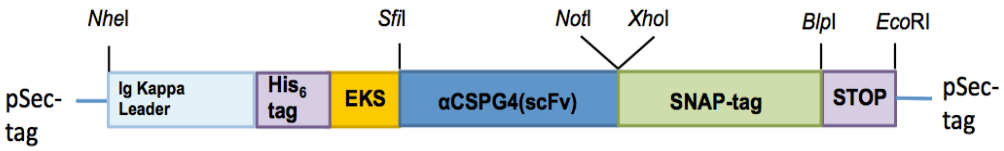

B

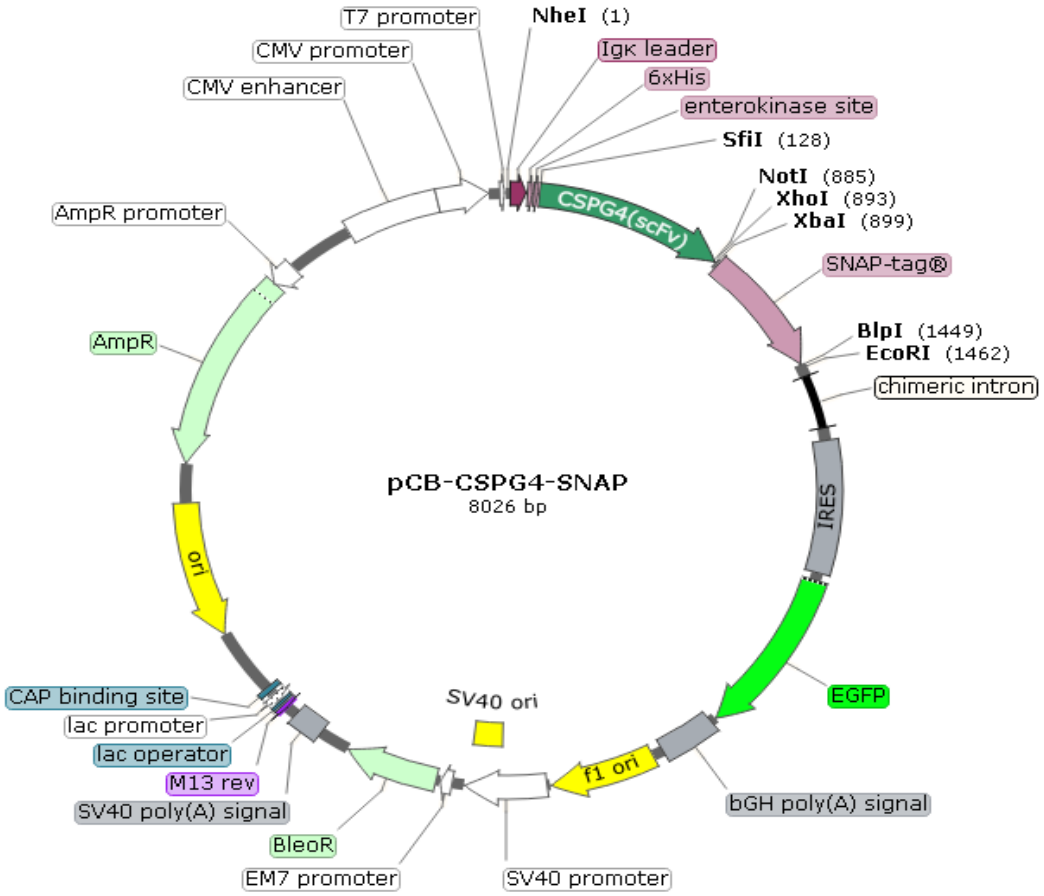

C

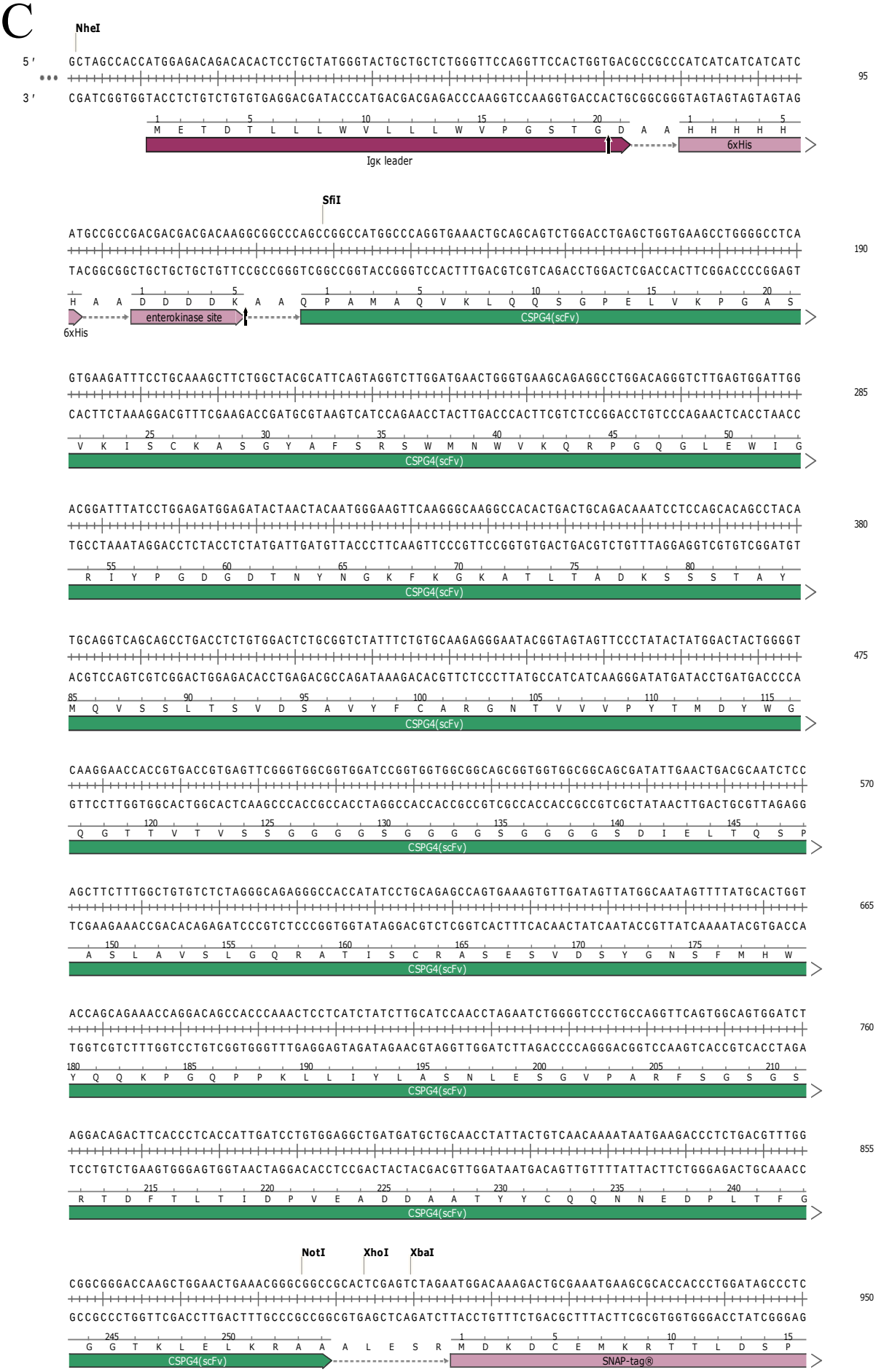
NheI
5′ GCTAGCCACCATGGAGACAGACACACTCCTGCTATGGGTACTGCTGCTCTGGGTTCCAGGTTCCACTGGTGACGCCGCCCATCATCATCATCATC
3′ CGATCGGTGGTACCTCTGTCTGTGTGAGGACGATACCCATGACGACGAGACCCAAGGTCCAAGGTGACCACTGCGGCGGGTAGTAGTAGTAGTAG
95
M E T D T L L L W V L L L W V P G S T G D A A H H H H H H
Igκ leader
6xHis
SfiI
ATGCCGCCGACGACGACGACAAGGCGGCCCAGCCGGCCATGGCCCAGGTGAAACTGCAGCAGTCTGGACCTGAGCTGGTGAAGCCTGGGGCCTCA
TACGGCGGCTGCTGCTGCTGTTCCGCCGGGTCGGCCGGTACCGGGTCCACTTTGACGTCGTCAGACCTGGACTCGACCACTTCGGACCCCGGAGT
190
H A A D D D D K A A Q P A M A Q V K L Q Q S G P E L V K P G A S
enterokinase site
CSPG4(scFv)
6xHis
GTGAAGATTTCCTGCAAAGCTTCTGGCTACGCATTCAGTAGGTCTTGGATGAACTGGGTGAAGCAGAGGCCTGGACAGGGTCTTGAGTGGATTGG
CACTTCTAAAGGACGTTTCGAAGACCGATGCGTAAGTCATCCAGAACCTACTTGACCCACTTCGTCTCCGGACCTGTCCCAGAACTCACCTAACC
285
V K I S C K A S G Y A F S R S W M N W V K Q R P G Q G L E W I G
CSPG4(scFv)
ACGGATTTATCCTGGAGATGGAGATACTAACTACAATGGGAAGTTCAAGGGCAAGGCCACACTGACTGCAGACAAATCCTCCAGCACAGCCTACA
TGCCTAAATAGGACCTCTACCTCTATGATTGATGTTACCCTTCAAGTTCCCGTTCCGGTGTGACTGACGTCTGTTTAGGAGGTCGTGTCGGATGT
380
R I Y P G D G D T N Y N G K F K G K A T L T A D K S S S T A Y
CSPG4(scFv)
TGCAGGTCAGCAGCCTGACCTCTGTGGACTCTGCGGTCTATTTCTGTGCAAGAGGGAATACGGTAGTAGTTCCCTATACTATGGACTACTGGGGT
ACGTCCAGTCGTCGGACTGGAGACACCTGAGACGCCAGATAAAGACACGTTCTCCCTTATGCCATCATCAAGGGATATGATACCTGATGACCCCA
475
M Q V S S L T S V D S A V Y F C A R G N T V V V P Y T M D Y W G
CSPG4(scFv)
CAAGGAACCACCGTGACCGTGAGTTCGGGTGGCGGTGGATCCGGTGGTGGCGGCAGCGGTGGTGGCGGCAGCGATATTGAACTGACGCAATCTCC
GTTCCTTGGTGGCACTGGCACTCAAGCCCACCGCCACCTAGGCCACCACCGCCGTCGCCACCACCGCCGTCGCTATAACTTGACTGCGTTAGAGG
570
Q G T T V T V S S G G G G S G G G G S G G G G S D I E L T Q S P
CSPG4(scFv)
AGCTTCTTTGGCTGTGTCTCTAGGGCAGAGGGCCACCATATCCTGCAGAGCCAGTGAAAGTGTTGATAGTTATGGCAATAGTTTTATGCACTGGT
TCGAAGAAACCGACACAGAGATCCCGTCTCCCGGTGGTATAGGACGTCTCGGTCACTTTCACAACTATCAATACCGTTATCAAAATACGTGACCA
665
A S L A V S L G Q R A T I S C R A S E S V D S Y G N S F M H W
CSPG4(scFv)
ACCAGCAGAAACCAGGACAGCCACCCAAACTCCTCATCTATCTTGCATCCAACCTAGAATCTGGGGTCCCTGCCAGGTTCAGTGGCAGTGGATCT
TGGTCGTCTTTGGTCCTGTCGGTGGGTTTGAGGAGTAGATAGAACGTAGGTTGGATCTTAGACCCCAGGGACGGTCCAAGTCACCGTCACCTAGA
760
Y Q Q K P G Q P P K L L I Y L A S N L E S G V P A R F S G S G S
CSPG4(scFv)
AGGACAGACTTCACCCTCACCATTGATCCTGTGGAGGCTGATGATGCTGCAACCTATTACTGTCAACAAAATAATGAAGACCCTCTGACGTTTGG
TCCTGTCTGAAGTGGGAGTGGTAACTAGGACACCTCCGACTACTACGACGTTGGATAATGACAGTTGTTTTATTACTTCTGGGAGACTGCAAACC
855
R T D F T L T I D P V E A D D A A T Y Y C Q Q N N E D P L T F G
CSPG4(scFv)
NotI
XhoI
XbaI
CGGCGGGACCAAGCTGGAACTGAAACGGGCGGCCGCACTCGAGTCTAGAATGGACAAAGACTGCGAAATGAAGCGCACCACCCTGGATAGCCCTC
GCCGCCCTGGTTCGACCTTGACTTTGCCCGCCGGCGTGAGCTCAGATCTTACCTGTTTCTGACGCTTTACTTCGCGTGGTGGGACCTATCGGGAG
950
G G T K L E L K R A A A L E S R M D K D C E M K R T T L D S P
CSPG4(scFv)
SNAP-tag®

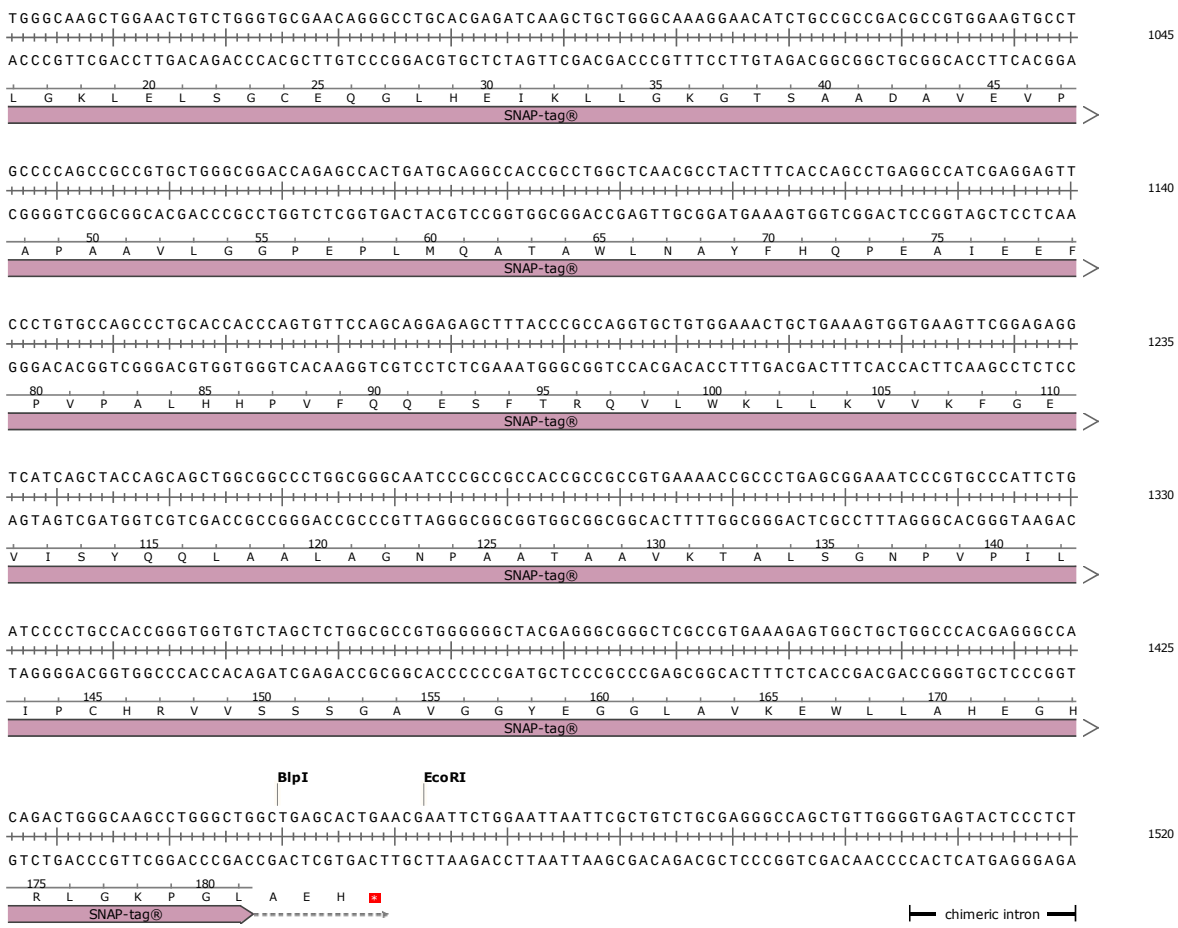

Figure 10: *In silico* design of pCB-CSPG4-SNAP expression vector, containing mAb9.2.27(scFv) and SNAP-tag. A) Diagrammatic representation of the structure of the ORF. B) pCB-CSPG4-SNAP plasmid map. D) Annotated protein sequence of ORF. EKS: enterokinase site, CSPG4: chondroitin sulfate proteoglycan 4, scFv: single chain variable fragment, CMV:, AmpR: ampicilin resistance, IRES: internal ribosome entry site, SV40: simian virus 40, EGFP: enhanced green fluorescent protein, bGH: bovine growth hormone, CAP: catabolite activator protein.

Table 1.1: Summary of plasmids

Plasmid	Description	Reference
pCB-H22-SNAP	Fusion protein expression vector derived from the pSecTag2 A plasmid, containing H22. Also used as a dummy construct for restriction mapping.	Previous work by MBI https://www.thermofisher.com/order/catalog/product/V90020
pUC57$^{mAb9.2.27(scFv)}$	Production vector containing mAb9.2.27(scFv) insert.	http://www.genscript.com/vector/SD1176-pUC57_plasmid_DNA.html
pUC57$^{\alpha PD\text{-}L1\ (scFv)}$	Production vector containing αPD-L1(scFv) insert.	http://www.genscript.com/vector/SD1176-pUC57_plasmid_DNA.html
pCB-CSPG4-SNAP	Expression vector containing mAb9.2.27(scFv) (*Sfi*I/*Not*I) and SNAP-tag (*Not*I/*Blp*I).	Current study
pCB-PDL1-SNAP	Expression vector containing αPD-L1(scFv) (*Sfi*I/*Not*I) and SNAP-tag (*Not*I/*Blp*I).	Current study

Table 1.2: pCB-CSPG4-SNAP plasmid components

Component	Description
Igκ leader	Secretory sequence, facilitates secretion of fusion protein into the cell culture supernatant[66]
His_6-tag	High affinity binding to Ni^{2+}-chelating resin for purification . In addition, allows detection of fusion proteins with anti-His_6-tag antibody[70]
Enterokinase site	DDDDK cleavage site
scFv	N-terminal single-chain variable fragment
SNAP-tag®	C-terminal self-labelling SNAP-tag protein
Chimeric intron	Rapid and efficient mRNA export out of the nucleus, significantly increase transgene expression
IRES	Allows the initiation of translation from any position within an mRNA immediately downstream from where the IRES is located (here, eGFP).[156]
eGFP	Allows for detection of translated protein in HEK293T cells
bGH Poly(A) signal	Ensures efficient transcription termination and polyadenylation of mRNA[77]
F1 origin	Facilitates rescue of single-stranded DNA
SV40 promoter	Facilitates high-level expression of the Hygromycin resistance gene and episomal replication in cells expressing the SV40 large T antigen.[156]
SV40 ORI	Origin of replication
EM7 promoter	Drives expression of the blasticidin resistance gene to allow for selection in mammalian cells
bleO	Bleomycin (zeocin) resistance protein for selection in HEK293T cells
SV40 Poly(A) signal	Efficient transcription termination and polyadenylation of mRNA.[156]
M13 rev	Single-stranded oligonucleotide possessing 5'-hydroxyl and 3'-hydroxyl ends and a selection of four fluorescent lables for use in polymerase chain reaction (PCR) protocols. Synonym: **5'-CAG GAA ACA GCT ATG ACC-3'.**[157]
lac operator	Short region of DNA that lies partially within the promoter and that interacts with a regulatory protein that controls the transcription of the operon.[158]
lac promoter	Controls transcription of lac operon genes
CAP binding site	Binding site for catabolite activator protein (CAP), which interacts with cAMP and RNAP to activate transcription.[159]
ORI	Origin of replication
Amp^R	Ampicillin resistance gene for selection in E. coli
Amp^R promoter	Efficient expression of the Ampicillin resistance gene
CMV enhancer	Aids efficient and high-level expression of recombinant protein[78, 79, 88]
CMV promoter	Aids efficient and high-level expression of recombinant protein[78, 79, 88]

T7 promoter	Allows for *in vitro* transcription in the sense orientation and sequencing through the insert.[156]

3.1.1.2 Midiprep DNA isolation

pCB-H22-SNAP and PUC57$^{mAb9.2.27(scFv)}$ plasmids were bulk prepped to amplify the DNA. After successful transformation into and growth of competent *E. coli* cells, plasmid DNA was extracted and purified. Table 2.1 and Table 2.2 show the protein concentration, the 260/280 ratio and the 260/230 ratio. 260/280 represents the nucleic acid to protein absorbance ratio and should sit at ~1.8 when DNA is pure and uncontaminated with protein or reagents that absorb at 280nm, such as phenol. 260/230 indicates the presence of contaminants that absorb at 230nm, such as EDTA, and should sit at ~2.0-2.2 when nucleic acids are not contaminated.[160] The purified plasmid samples were all within the acceptable ranges and were thus confirmed for downstream application.

Table 2.1: Quantification of pCB-H22-SNAP plasmid, following large-scale purification

Sample	Yield (ng/µL)	260/280	260/230
1	449.9	1.90	2.21
2	778.1	1.90	2.21
3	590.3	1.89	2.19
4	857.7	1.89	2.22

Table 2.2: Quantification of pUC57$^{mAb9.2.27(scFv)}$ plasmid, following large-scale purification

Sample	Yield (ng/µL)	260/280	260/230
1	4330.1	1.78	2.08
2	138.3	1.82	2.00

3.1.1.3 Restriction enzyme digestion and agarose gel electrophoresis

Digestion of both the production vector and the expression vector was successful (Figure 11). In the pCB-H22-SNAP expression vector digestion, the large backbone (or vector) fragment can be seen at approximately 7000 bp (with the expected size being 7365 bp) and the small fragment, relating to the removed H22 sequence, can be seen at approximately 700 bp. Although the undigested control appears to weigh less than the digested backbone, this is not a true representation of their relative sizes but rather the result of too much DNA being loaded in the this well, as can be seen by the high intensity of the band. The pUC57$^{mAb9.2.27(scFv)}$ production vector was also successfully digested, with a small band, representing the

mAb9.2.27 scFv insert fragment, seen at approximately 700 bp. Both the backbone and the insert were digested with *SfiI* and *NotI* and can thus be ligated in frame.

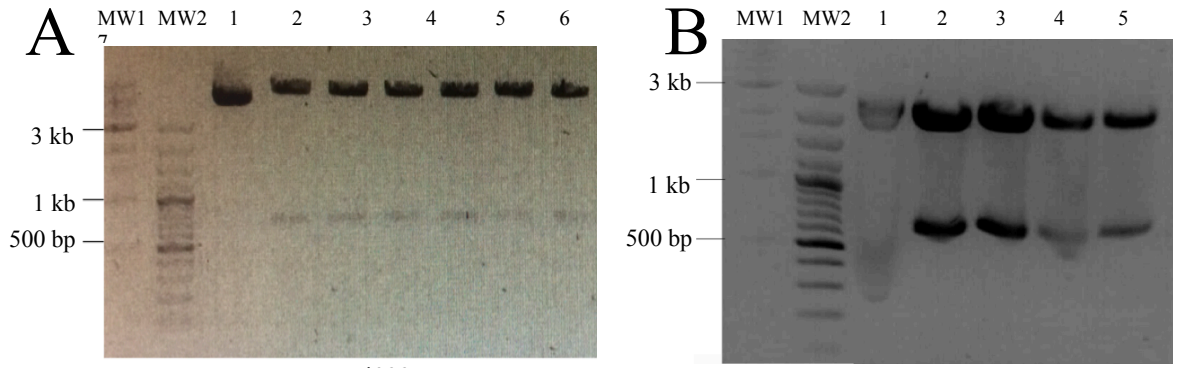

Figure 11: pCB-H22-SNAP and pUC57$^{mAb9.2.27}$ RE digests. Fragment sizes were evaluated using a 1kB DNA ladder (MW1) and a 100bp+ ladder (MW2). A) pCB-H22-SNAP. An undigested control was used for comparison (lane 1) and six samples were digested with *Sfi*I and *Not*I (lanes 2-7). B) pUC57$^{mAb9.2.27(scFv)}$. An undigested control was used for comparison (lane 1) and four samples were digested with *Sfi*I and *Not*I (lanes 2-5).

3.1.1.4 Gel extraction and ligation

Vector and insert bands were extracted from the gel and purified. The samples with the highest concentrations were subsequently used for ligation, i.e. sample 2 of the vector (51.5 ng/µL; Table 3.1), and sample 1 of the insert (16.5 ng/µL; Table 3.2). During ligation, three vector:insert ratios (1:1, 1:2 and 1:3) were used (Figure 12), due to the fact that a new kit was used and a standard protocol had not yet been established. Although a 1:3 ratio is recommended for this kit, the 1:1 plate showed the best transformation efficiency ($1.8x10^4$). The vector-only control shows minimal colony formation of autoligated clones, indicating that there was some partial digestion in the previous step. The bacteria only control shows no colony formation, confirming that all colonies present contain the pCB-SNAP vector. Table 3.3 contains information regarding the colony formation of each plate.

Table 3.1: Quantification of vector purified from agarose gel

Sample	Yield (ng/µL)
1	45.1
2	51.5
3	6.0
4	7.8
5	12.7
6	18.0
7	15.7

Table 3.2: Quantification of insert purified from agarose gel

Sample	Yield (ng/µL)
1	16.5
2	14.2
3	10.2

Table 3.3: Colony formation data

Sample (vector:insert)	Number of colonies	Transformation efficiency	Autoligated clone (%)
1:1	904	2.2×10^6	1.22
1:2	112	1.4×10^5	9.82
1:3	208	1.7×10^5	5.29
1:0 (vector only)	11	n/a	100
0:0 (bacteria only)	0	n/a	n/a

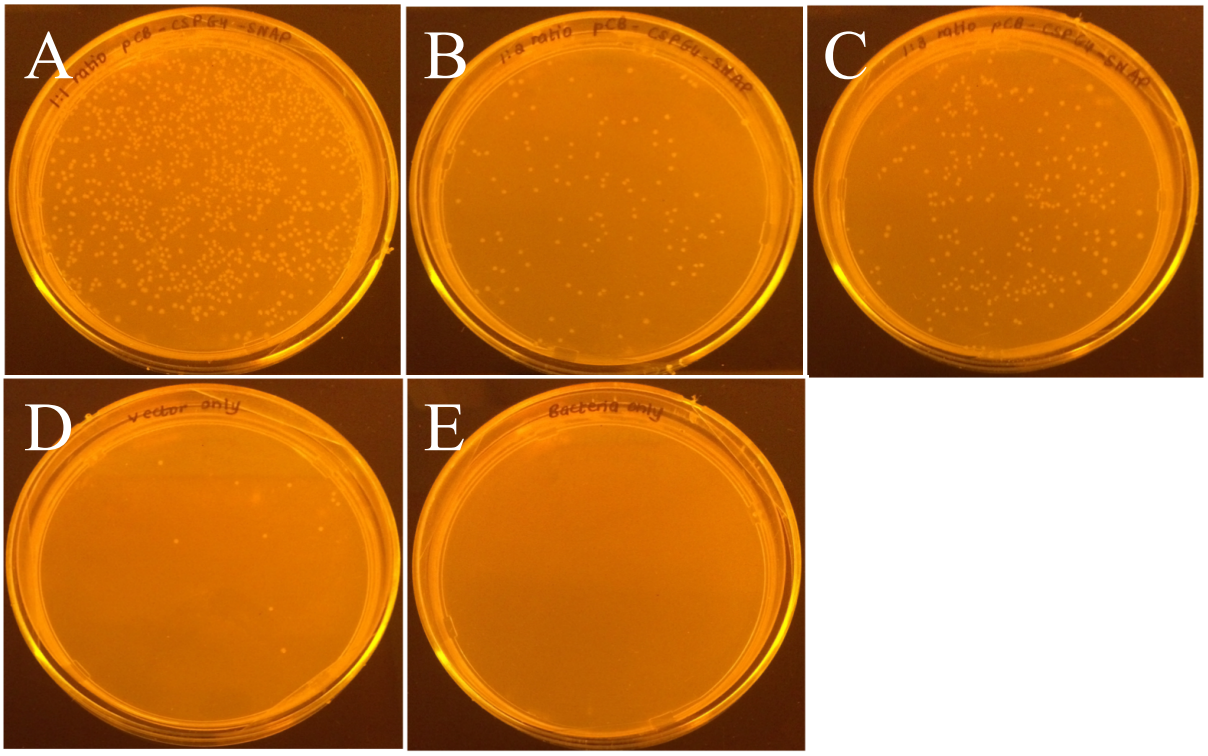

Figure 12: Ligation of mAb9.2.27 insert and pCB-SNAP backbone to create final recombinant plasmid, pCB-CSPG4-SNAP. A) 1:1 vector:insert ligation ratio. B) 1:2 vector:insert ligation ratio. C) 1:3 vector:insert ligation ratio. D) Vector only control (1:0 ligation ratio). E) Bacteria only control.

3.1.1.5 Restriction mapping

Restriction mapping, using the HindIII restriction enzyme, was used to confirm the successful ligation of the mAb9.2.27(scFv) insert into the pCB-SNAP backbone. A virtual simulation was first performed on SnapGene in order to determine which enzyme would produce differential fragmentation of the original pCB-H22-SNAP plasmid compared to the novel pCB-CSPG4-SNAP plasmid (Figure 13A). The *in vitro* mapping confirms that fragmentation has occurred as expected (Figure 13B). This gives

confirmation that the correct fragments have been ligated and that autoligated clones have not been selected.

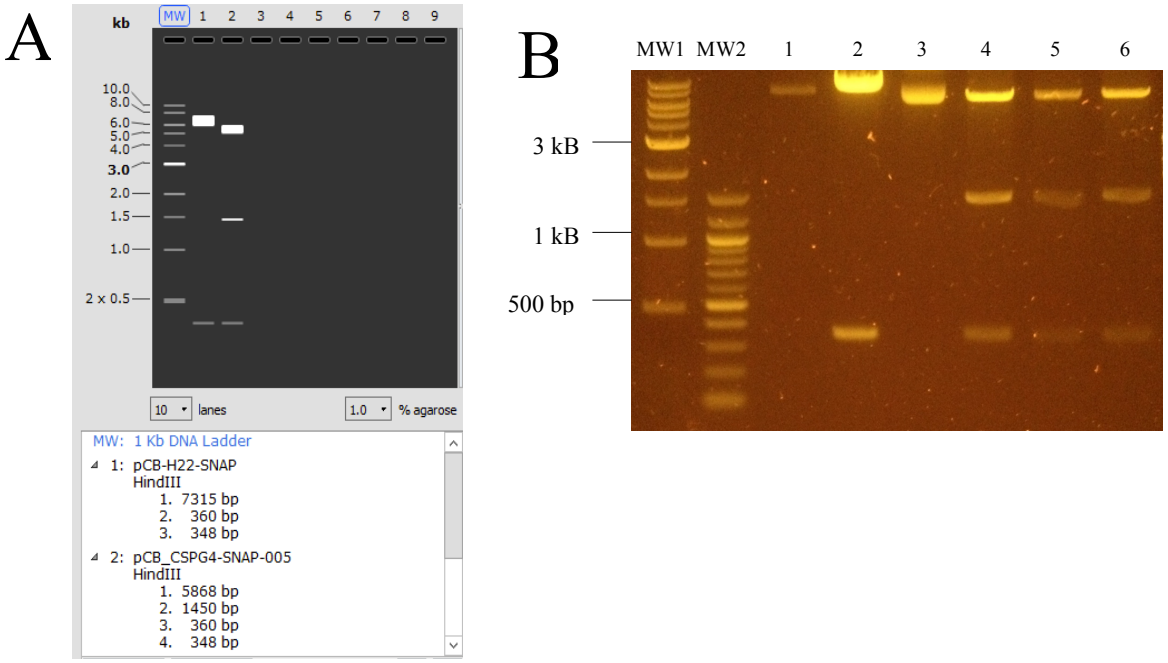

Figure 13: Restriction mapping to confirm ligation of mAb9.2.27(scFv) insert into pCB-SNAP vector. A) *In Silico* agarose gel simulation using SnapGene™. A 1Kb DNA ladder (MW) was used to evaluate fragment sizes of pCB-H22-SNAP (lane 1) and pCB-CSPG4-SNAP (lane 2) when cut with HindIII. B) *In vitro* restriction mapping of pCB-H22-SNAP and pCB-CSPG4-SNAP with HindIII. A 1Kb DNA ladder and a 100 bp+ DNA ladder were used to evaluate fragment sizes (MW1 and MW2) of undigested pCB-H22-SNAP (lane 1), digested pCB-H22-SNAP (lane 2), undigested pCB-CSPG4-SNAP (lane 3) and digested pCB-CSPG4-SNAP (lanes 4-6). MW: molecular weight.

3.1.1.6 DNA sequencing

Of the clones that were confirmed through restriction mapping, two were bulk prepped (Table 4.1), diluted to 20ng/µL in 30 µL, and sent for sequencing. The sequences of both clones were confirmed (see Appendix 6.2.1).

Table 4.1: Quantification of pCB-CSPG4-SNAP recombinant clones, following large scale purification

Clone	Yield (ng/uL)	260/280	260/230
1	1728.4	1.92	2.26
2	1817.0	1.83	2.02

3.1.2 Transfection and protein expression

Upon confirmation of its ORF sequence, the pCB-CSPG4-SNAP plasmid was introduced into a HEK293T mammalian vector expression system, co-expressing eGFP. Successful transfection

and expression of the mAb9.2.27(scFv)-SNAP fusion protein was determined via visualization of eGFP reporter gene expression and zeocin was subsequently used to select for positively transfected cells, enriching this population (Figure 14). Transfection efficiency was evaluated visually by taking the average of multiple cell counts and was determined to be approximately 63.3%. The cell culture supernatant (CCSN) containing secreted fusion protein was collected every 3-4 days over four weeks as described in section 2.1.2.

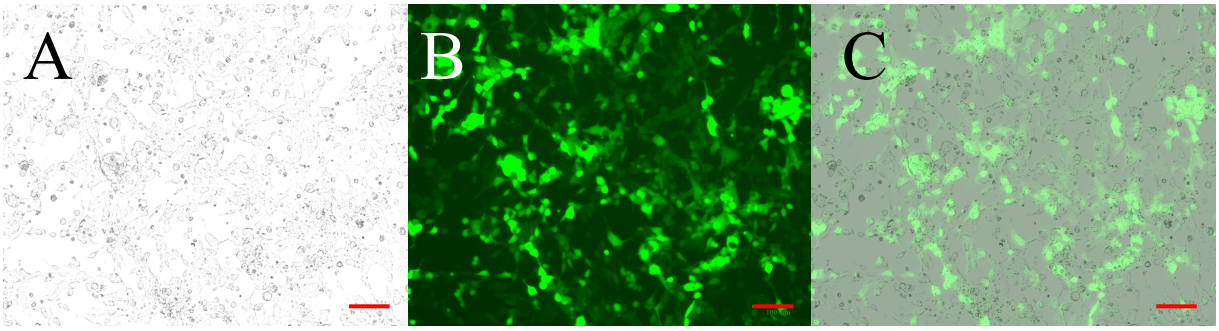

Figure 14: Enhanced green fluorescent protein expression in HEK293T cells transfected with pCB-CSPG4-SNAP. A) Brightfield, B) green channel C) merge image. **Scale bar: 100 µm**

3.1.3 Protein purification and analysis

3.1.3.1 Protein purification

mAb9.2.27(scFv)-SNAP fusion proteins were purified through a single-step purification using column immobilized nickel ions to which hexa-histidine-tag of mAb9.2.27(scFv)-SNAP had a strong affinity. Hence, elution of the recombinant protein was performed through competitive binding affinity between hexa-histidine-tag of mAb9.2.27(scFv)-SNAP and increased concentration of imidazole to Ni^{2+} on the column. Collection of the eluted fractions was monitored at wavelength 280 nm (Figure 15). The fractions (5mL) which corresponded to each individual peak on the chromatogram were then concentrated down to a volume of 200 µL, using 10kDa Amicon Ultra-Filtration devices. The concentrated fractions were transferred onto a nitrocellulose membrane for immunodetection using an anti-His primary and HRP-conjugated secondary antibody and confirming expression of full-length protein. The first and largest peak, prior to the increase in the gradient of the elution buffer contains BSA flow through. The second peak, seen immediately after the imidazole gradient and spanning fractions 4-12, has several shoulders and was predicted to contain mAb9.2.27(scFv)-SNAP contaminated with BSA that bound non-specifically to the column and was eluted at the initiation of the elution buffer gradient. The third peak, spanning fractions 14-18, shows major irregularities in the absorbance reading. This was due to air bubbles entering the system.

However, these fractions were tested for the presence of mAb9.2.27(scFv)-SNAP. The fourth peak, spanning fractions 23-25, was also suspected to contain mAb9.2.27(scFv)-SNAP.

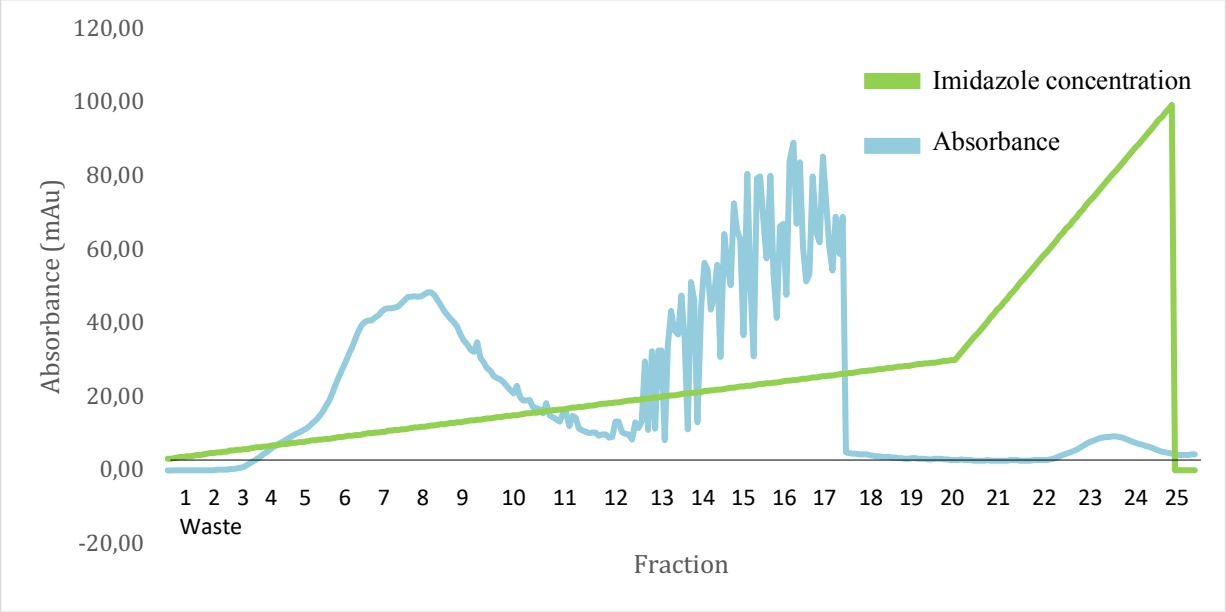

Figure 15: Chromatograph from IMAC purification of His_6-tagged mAb9.2.27(scFv)-SNAP fusion proteins.

3.1.3.2 Protein validation and quantification

Following IMAC, fractions corresponding to the peaks above were run on an SDS-PAGE gel to identify the presence of protein corresponding to the weight of mAb9.2.27(scFv)-SNAP (53.13 kDa) and determine which fractions should thus be pooled (Figure 16). Fractions 5-11 showed multiple bands, indicating the presence of mAb9.2.27(scFv)-SNAP and BSA contaminant. Fractions 12, 16, 17, 23-25 showed a single band each of an appropriate weight. These were thus pooled (pool 1) during protein concentration. Fractions 6-11 (pool 2) were pooled and concentrated, with fraction 5 (pool 3) concentrated separately due to volume limitations. Based on the data generated on GelAnalyzer using raw volume values, the protein yield was estimated to be 27,59%.

The concentration of the protein was then determined by measuring absorbance on a NanoDrop ND-2000, and these values were used to measure the volume of protein required for Western blot. The 260/280 ratio is 0.57 when protein is 100% pure and 1.06 when protein is 95% pure. All four samples are will within this range (Table 5.1).

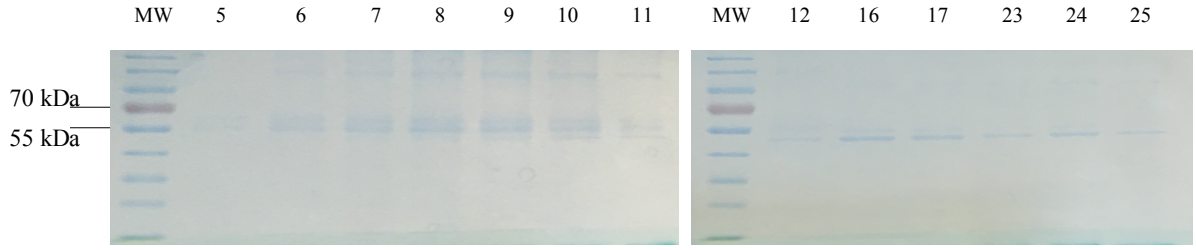

Figure 16: SDS-PAGE with coomassie blue stain to detect presence of protein. A protein ladder (MW) was used to evaluate the molecular weight of the protein in each band. The numbers correspond to the fraction represented in the chromatogram. This was used to determine the contents of each fraction in order to determine appropriate fraction pools.

Table 5.1: Quantification of purified mAb9.2.27(scFv)-SNAP

Pool	Fractions	Conc. (mg/mL)	260/280	Vol. loaded (µL)
1	12,16,17,23-25	1.5645	0.68	1.278
2	8-11	2.2120	0.57	0.904
3	5	2.3295	0.61	0.859

3.1.3.3 Protein confirmation

Following quantification, functional His_6-tag protein was detected by Western blot (Figure 17). An Anti-His_6-tag antibody conjugated to HRP was used for the chemiluminescent detection of functional His_6-tag protein. As predicted, pool 1 contain high quantities of mAb9.2.27(scFv)-SNAP. Some functional protein was seen in pool 2, but none was detected in pool 3. Pool 1 was thus used for downstream experiments.

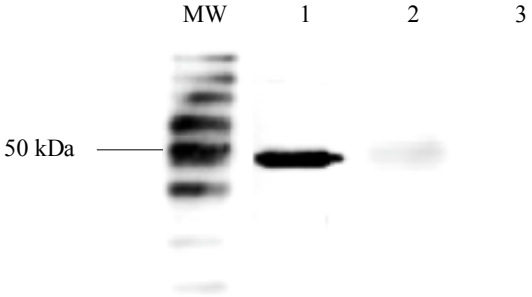

Figure 17: Visualization functional His_6-tag protein. A protein ladder (MW) was used to evaluate the molecular weight of the protein in each band. The numbers correspond to pools 1, 2 and 3.

3.1.4 Immunoassays

3.1.4.1 Flow cytometry

Selective binding of mAb9.2.27(scFv)-SNAP-Alexa488 conjugates to CSPG4-positive melanoma cell lines was confirmed by flow cytometry. MDA-MB-468 was used as a negative control and SK-MEL-28 as a positive control. All additional cell lines, except for IGR-1, showed

significant binding relative to unlabelled control cells (Figure 18B-F), while the MDA-MB-468 cells did not (Figure 18A). This is indicative of specific binding of the conjugate to cells expressing CSPG4. Furthermore, these results confirm that CSPG4 is over-expressed in melanoma cells in all growth stages, with and without pigmentation, and in it chemoresistant form. CSPG4 is thus been conclusively identified as a suitable target for melanoma in this and future PIT strategies. Table 7.1 shows the quantification of mean fluorescent intensity (MFI), here represented as the geometric mean (gMFI), for all cell lines when cells are unlabelled (background autofluorescence) compared to when they are labelled (signal). As is show, the gMFI of the control cell line remains unchanged, while the signal-to-background ratio of the CSPG4-positive cell lines is increased up to 14:1.

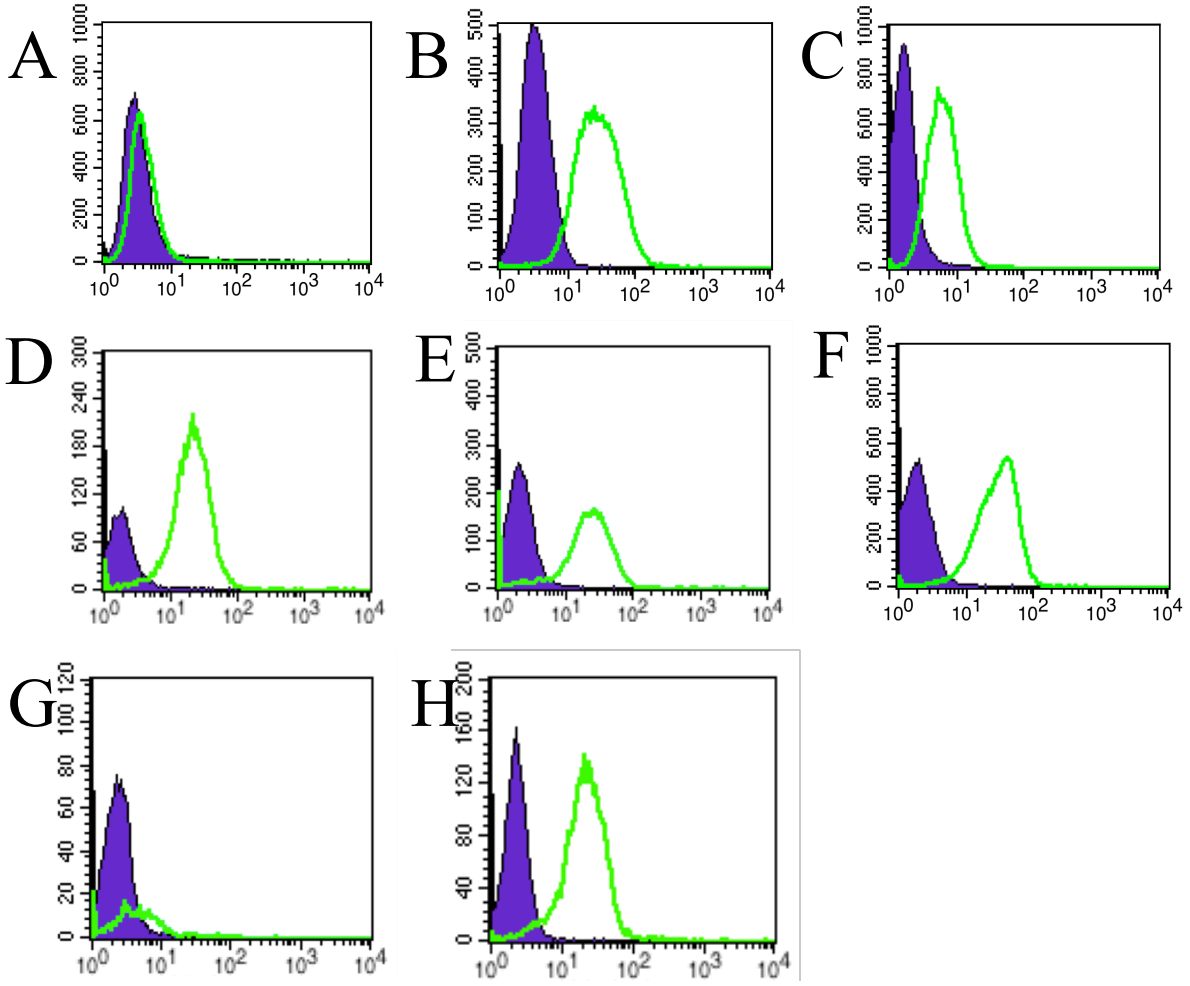

Figure 18: Validation of binding of mAb9.2.27(scFv)-SNAP to CSPG4-positive melanoma cells by flow cytometry, where the x-axis represents the gMFI and the y-axis represents the number of events. A) MDA-MB-468 negative control. B) SK-MEL-28 positive control. C) A375. D) WM902. E) UCT-Mel1. F) UCT-Mel1-DTIC. G) IGR-1. H) IGR-39

Table 6.1: Quantification of geometric mean fluorescence

Cell line	Unlabelled	Labelled
MDA-MB-468	2.67	2.71
SK-MEL-28	3.34	25.73
A375	1.68	5.83
WM902	1.52	19.06
UCT-Mel1	1.93	19.63
UCT-Mel1-DTIC	1.86	25.98
IGR-1	2.23	4.38
IGR-39	2.21	19.26

3.1.4.2 Confocal microscopy

Confocal microscopy was performed to further validate binding of mAb9.2.27(scFv)-SNAP to the surface of the melanoma cells. As seen above, CSPG4-positive cell lines exposed to the conjugate all showed significant surface binding (Figure 19B-F), while the CSPG4-negative control did not (Figure 19A). It should be noted that the intensity of the signals does not correlate with the flow cytometry gMFI data above. This suggests that the cell lifting in flow cytometry affects the surface receptor expression of adherent cells. Nonetheless, these results confirm that mAb9.2.27(scFv)-SNAP is suitable for diagnostic imaging.

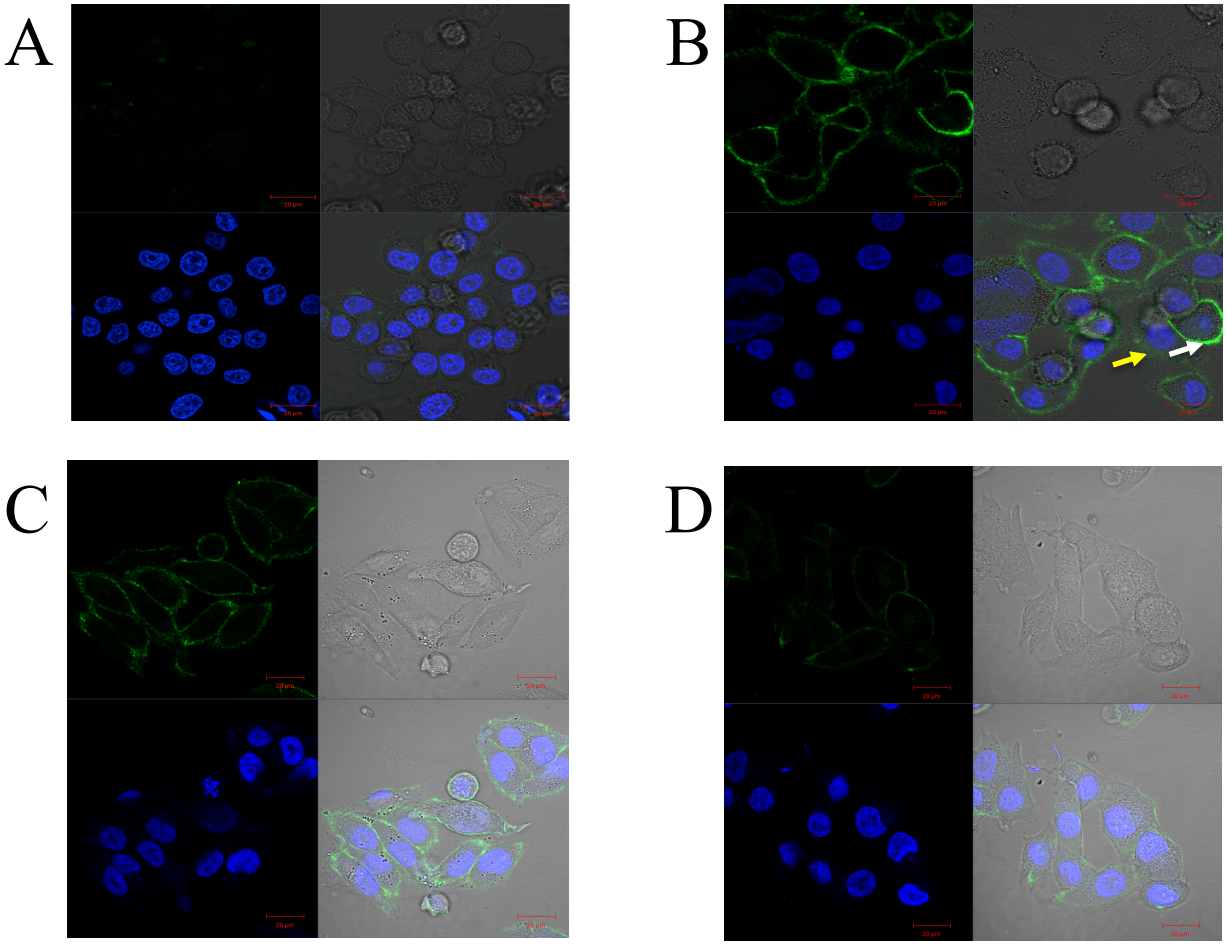

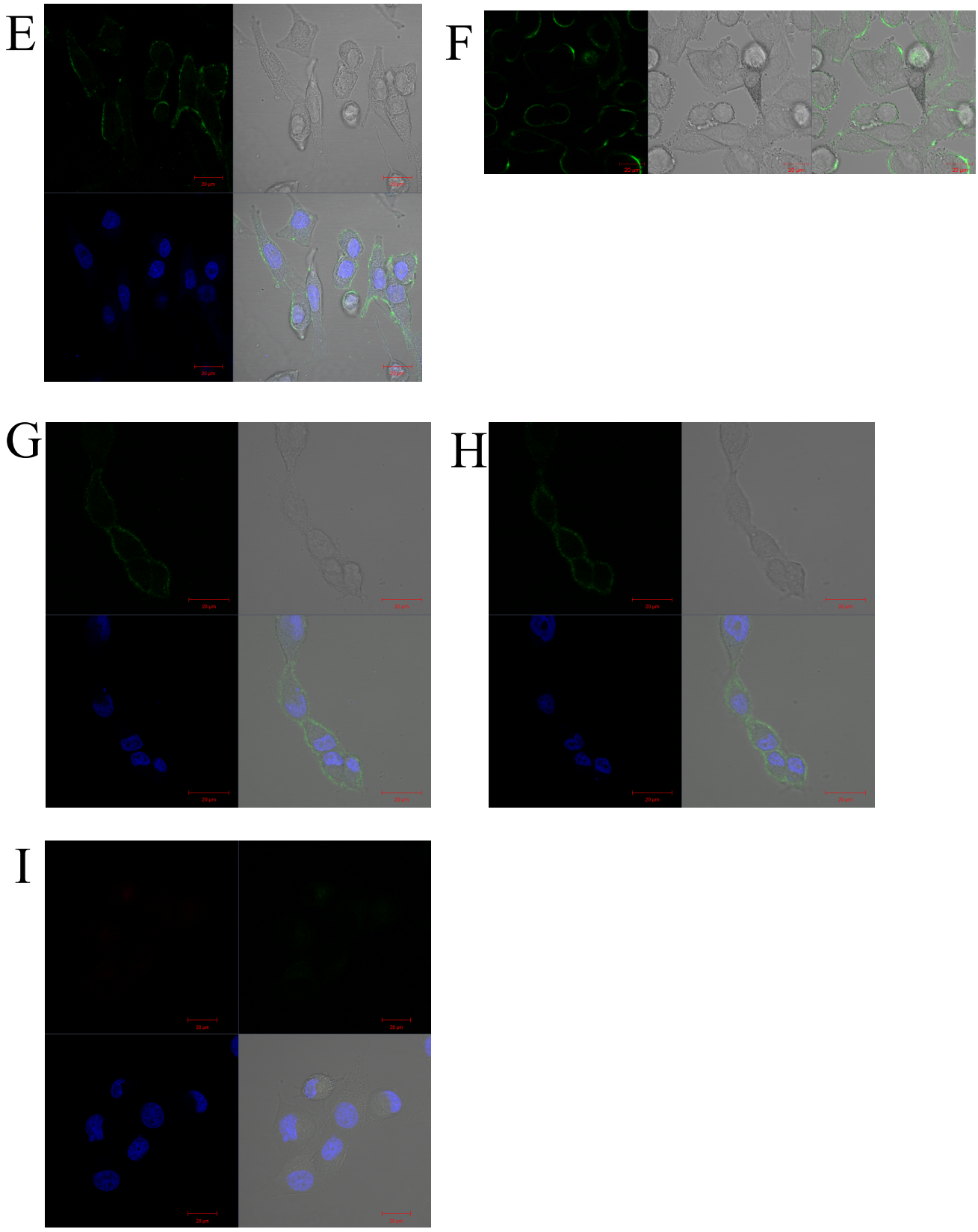

Figure 19: Confirmation of surface binding of mAb2.9.27(scFv)-SNAP to CSPG4-positive melanoma cells by confocal microscopy. A) MDA-MB-468 negative control. B) SK-MEL-28 positive control. White arrow: membrane signal; yellow arrow: cytoplasmic signal. C) A375. D) WM902. E) UCT-Mel1. F) UCT-Mel1-DTIC. G) IGR-1. H) IGR-39. I) Autofluorescence unstained control

3.1.5 Cell viability

The XTT cell viability assay is dependent upon the cleavage of yellow tetrazolium salt by metabolically active cells to form orange formazan crystals, which absorb light at 450 nm. After administration of mAb9.2.27(scFv)-SNAP-IR700 and irradiation with 689 nm light, cells received 50 μL of XTT solution 1 and 1 μL of XTT solution 2. After 4 hours, absorbance was measured in order to determine the percentage of viable cells. Across all technical and biological repeats, no cytotoxicity was seen in any cell lines, i.e. no dose-dependent change in the absorbance reading. Figure 20 shows absorbance as a function of mAb9.2.27(scFv)-SNAP-IR700 concentration for the negative and positive control cell lines, MDA-MB-468 and SK-MEL-28, respectively. Similar results were seen for other CSPG4-positive cell lines. Due to the absence of a dose-dependent response, IC_{50} curves were not generated. Given the convincing binding data, as illustrated through both flow cytometry and confocal microscopy, which furthermore confirms the preservation of the autocatalytic self-labelling reaction of SNAP-tag and its substrates, it can be concluded that the method used for solubilization of the lyophilized BG-IR700 was inefficient and lead to inadequate conjugation.

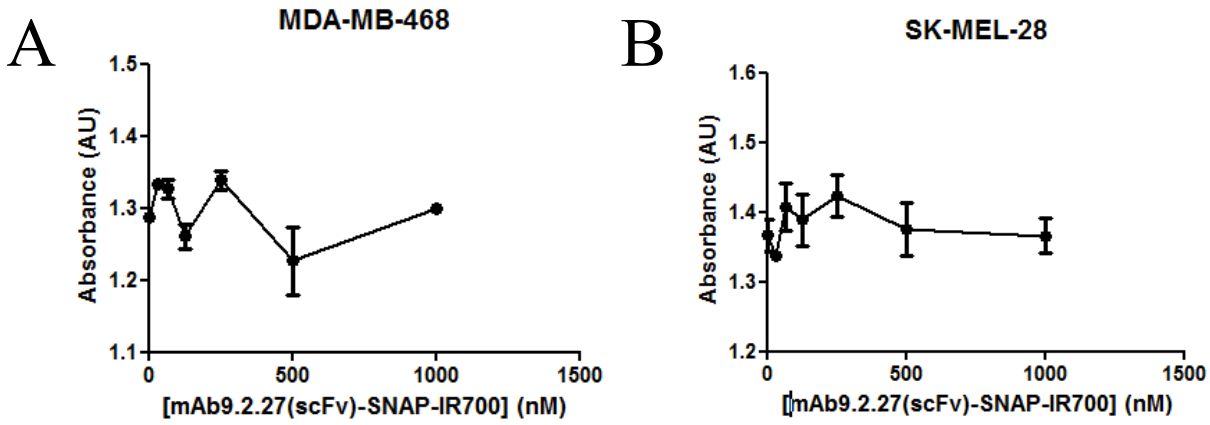

Figure 20: XTT cell viability assay. Absorbance vs dose concentration curves showing activity of mAb9.2.27(scFv)-SNAP-IR700 on SK-MEL-28 (positive control), MDA-MB-468 (negative control). Doses range from 0 to 1000 nM.

3.2 αPDL1(scFv)-SNAP-ALEXA488 FOR PD-L1 IMMUNODETECTION

3.2.1 *in silico* cloning

3.2.1.1 *In* silico vector design

As per section 3.1.1.1, H22(scFv) was removed from the pCB-H22-SNAP backbone vector and replaced with the αPD-L1 scFv to create the pCB-PDL1-SNAP plasmid (Figure 21).

A

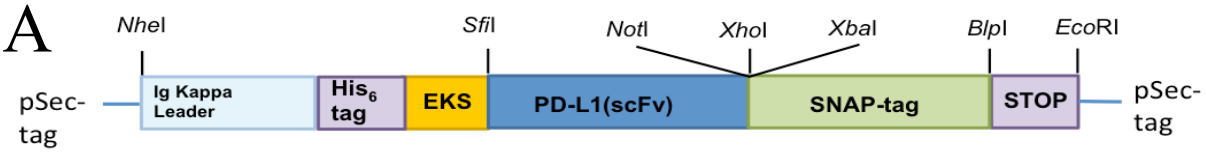

B

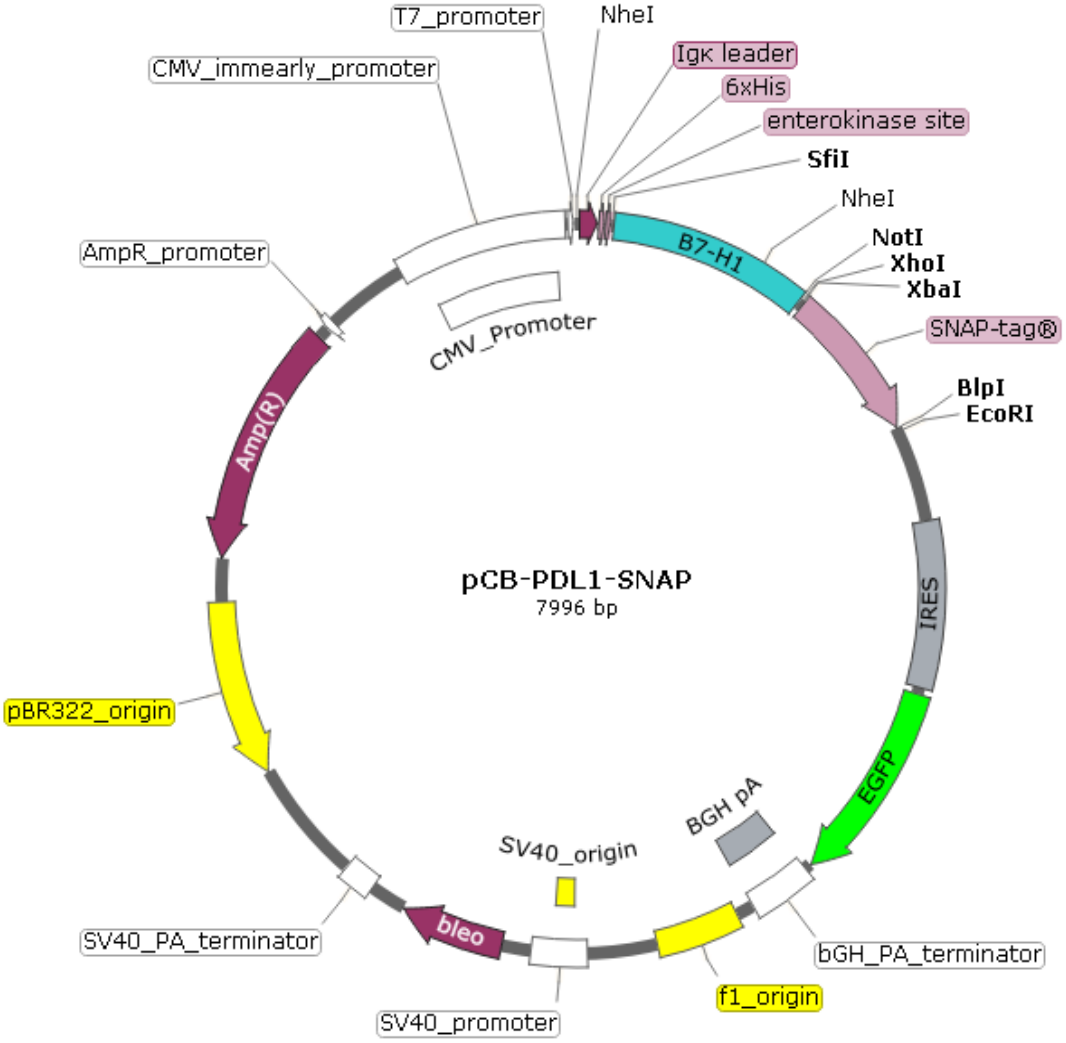

C

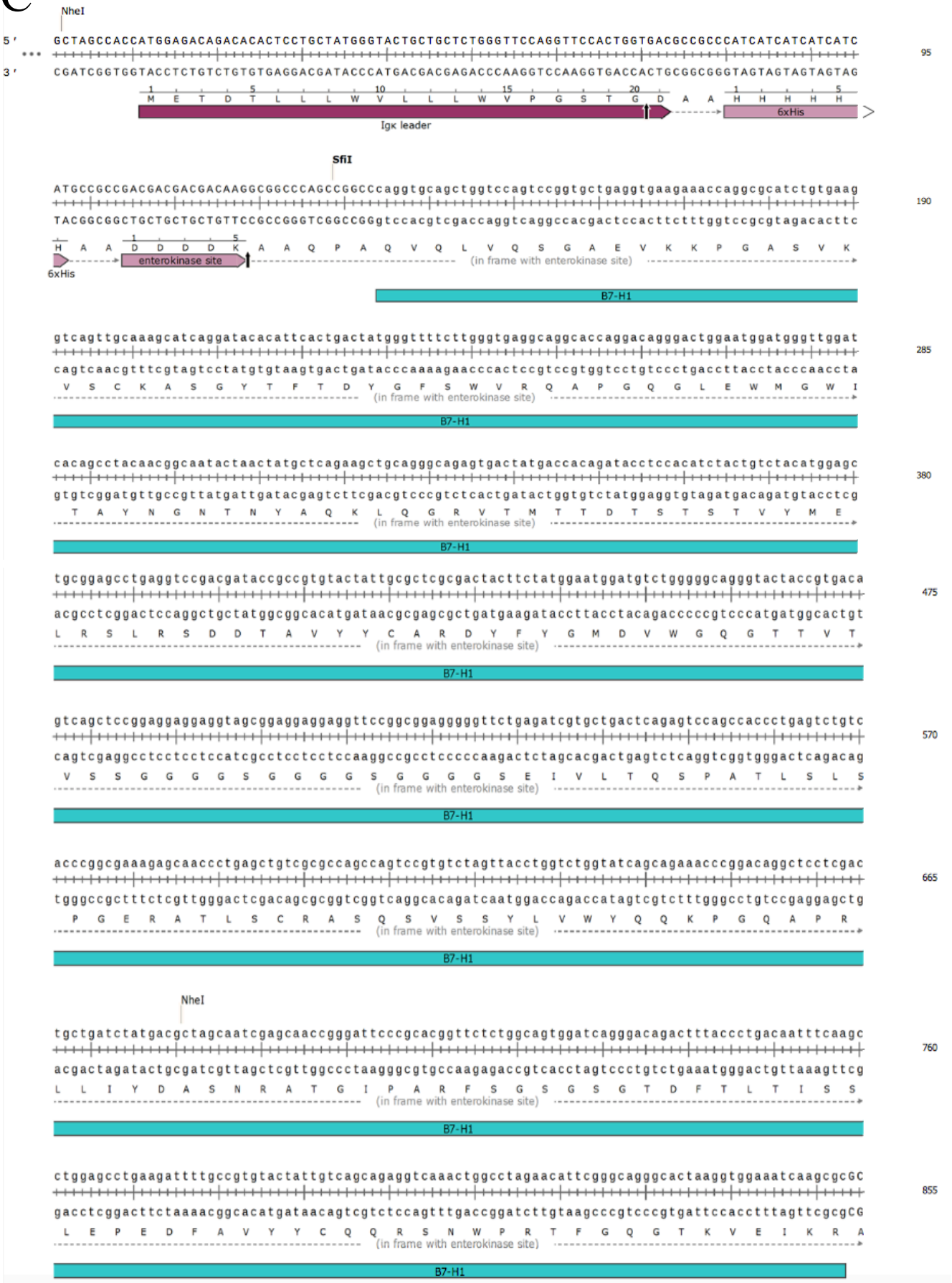
NheI
5′ GCTAGCCACCATGGAGACAGACACACTCCTGCTATGGGTACTGCTGCTCTGGGTTCCAGGTTCCACTGGTGACGCCGCCCATCATCATCATCATC 95
3′ CGATCGGTGGTACCTCTGTCTGTGTGAGGACGATACCCATGACGACGAGACCCAAGGTCCAAGGTGACCACTGCGGCGGGTAGTAGTAGTAGTAG
M E T D T L L L W V L L L W V P G S T G D A A H H H H H H
Igκ leader
6xHis
SfiI
ATGCCGCCGACGACGACGACAAGGCGGCCCAGCCGGCCcaggtgcagctggtccagtccggtgctgaggtgaagaaaccaggcgcatctgtgaag 190
TACGGCGGCTGCTGCTGCTGTTCCGCCGGGTCGGCCGGgtccacgtcgaccaggtcaggccacgactccacttctttggtccgcgtagacacttc
H A A D D D D K A A Q P A Q V Q L V Q S G A E V K K P G A S V K
6xHis
enterokinase site
(in frame with enterokinase site)
B7-H1
gtcagttgcaaagcatcaggatacacattcactgactatgggttttcttgggtgaggcaggcaccaggacagggactggaatggatgggttggat 285
cagtcaacgtttcgtagtcctatgtgtaagtgactgatacccaaaagaacccactccgtccgtggtcctgtccctgaccttacctacccaaccta
V S C K A S G Y T F T D Y G F S W V R Q A P G Q G L E W M G W I
(in frame with enterokinase site)
B7-H1
cacagcctacaacggcaatactaactatgctcagaagctgcagggcagagtgactatgaccacagatacctccacatctactgtctacatggagc 380
gtgtcggatgttgccgttatgattgatacgagtcttcgacgtcccgtctcactgatactggtgtctatggaggtgtagatgacagatgtacctcg
T A Y N G N T N Y A Q K L Q G R V T M T T D T S T S T V Y M E
(in frame with enterokinase site)
B7-H1
tgcggagcctgaggtccgacgataccgccgtgtactattgcgctcgcgactacttctatggaatggatgtctgggggcagggtactaccgtgaca 475
acgcctcggactccaggctgctatggcggcacatgataacgcgagcgctgatgaagataccttacctacagacccccgtcccatgatggcactgt
L R S L R S D D T A V Y Y C A R D Y F Y G M D V W G Q G T T V T
(in frame with enterokinase site)
B7-H1
gtcagctccggaggaggaggtagcggaggaggaggttccggcggaggggggttctgagatcgtgctgactcagagtccagccaccctgagtctgtc 570
cagtcgaggcctcctcctccatcgcctcctcctccaaggccgcctccccccaagactctagcacgactgagtctcaggtcggtgggactcagacag
V S S G G G G S G G G G S G G G G S E I V L T Q S P A T L S L S
(in frame with enterokinase site)
B7-H1
acccggcgaaagagcaaccctgagctgtcgcgccagccagtccgtgtctagttacctggtctggtatcagcagaaacccggacaggctcctcgac 665
tgggccgctttctcgttgggactcgacagcgcggtcggtcaggcacagatcaatggaccagaccatagtcgtctttgggcctgtccgaggagctg
P G E R A T L S C R A S Q S V S S Y L V W Y Q Q K P G Q A P R
(in frame with enterokinase site)
B7-H1
NheI
tgctgatctatgacgctagcaatcgagcaaccgggattcccgcacggttctctggcagtggatcagggacagactttaccctgacaatttcaagc 760
acgactagatactgcgatcgttagctcgttggccctaagggcgtgccaagagaccgtcacctagtccctgtctgaaatgggactgttaaagttcg
L L I Y D A S N R A T G I P A R F S G S G S G T D F T L T I S S
(in frame with enterokinase site)
B7-H1
ctggagcctgaagattttgccgtgtactattgtcagcagaggtcaaactggcctagaacattcgggcagggcactaaggtggaaatcaagcgcGC 855
gacctcggacttctaaaacggcacatgataacagtcgtctccagtttgaccggatcttgtaagcccgtcccgtgattccacctttagttcgcgCG
L E P E D F A V Y Y C Q Q R S N W P R T F G Q G T K V E I K R A
(in frame with enterokinase site)
B7-H1

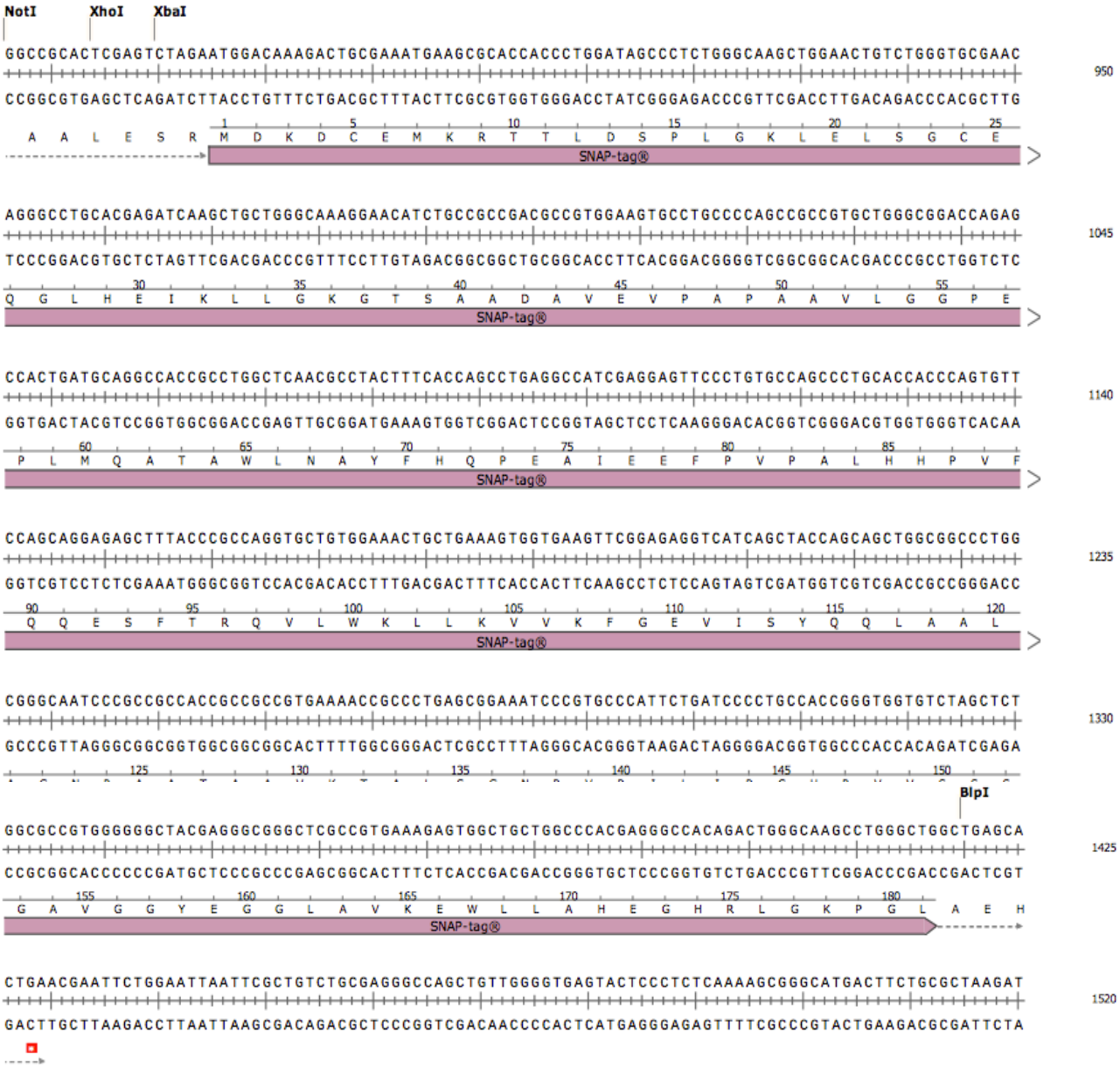

Figure 21: ***In silico*** **design of pCB-PDL1-SNAP expression vector, containing αPD-L1(scFv) and SNAP-tag**. A) Diagrammatic representation of the structure of the ORF. B) pCB-PDL1-SNAP plasmid map. D) Annotated protein sequence of ORF.

3.2.1.2 Midiprep DNA isolation

PUC57$^{\alpha PD\text{-}L1(scFv)}$ plasmid was bulk prepped, transformed and purified, as per section 3.1.1.2 (Table 7.1). The purified plasmid samples were all within the acceptable purity range and are thus confirmed for downstream application.

Table 7.1: Quantification of pUC57$^{\alpha PD\text{-}L1(scFv)}$ plasmid, following large-scale purification

Sample	Yield (µg/µL)	260/280	260/230
1	1797.0	1.96	2.26
2	465.1	1.83	2.02

3.2.1.3 Restriction enzyme digestion and agarose gel electrophoresis

Digestion of the pUC57$^{\alpha PD\text{-}L1scFv)}$ production vector was successful, with a small band seen at approximately 720 bp (Figure 22).

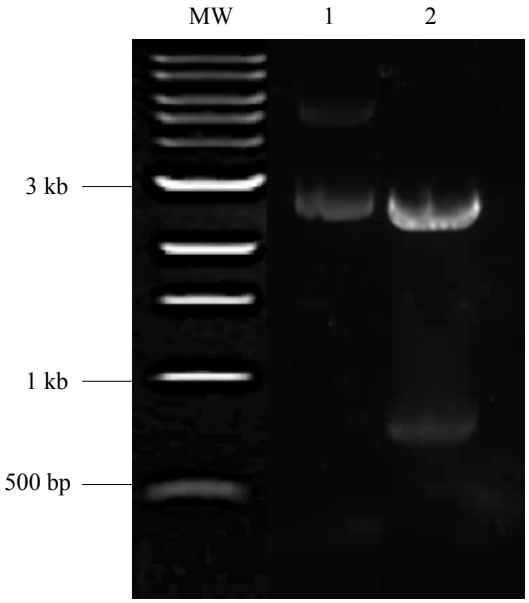

Figure 22: RE digest of pUC57$^{\alpha PD\text{-}L1(scFv)}$. Fragment sizes were evaluated using a 1kB DNA ladder (MW). An undigested control was used for comparison (lane 1) and pUC57$^{\alpha PD\text{-}L1(scFv)}$ was digested with *Sfi*I and *Not*I (lane 2).

3.2.1.4 Gel extraction and ligation

Insert bands were extracted from the gel and purified. Sample 2 of the vector, 51.5 ng/µL (Table 3.1) was ligated with the insert (42.6 ng/µL; Table 8.1).

During ligation, three vector:insert ratios (1:2, 1:3 and 1:5) were used (Figure 23). The 1:3 plate shows the highest transformation efficiency. Although transformation efficiency was low, the vector only control shows no colony formation of autoligated clones, thus selection of such a clone would be very unlikely. The bacteria only control has no colony formation, confirming that all colonies present contain the pCB-SNAP vector. Table 8.2 contains information regarding the colony formation of each plate.

Table 8.1: Quantification of insert purified from agarose gel

Sample	Yield (ng/µL)
1	42.6
2	16.4

Table 8.2: Colony formation data

Sample (vector:insert)	Number of colonies	Transformation efficiency	Autoligated clone (%)
1:2	0	0	n/a
1:3	68	2.1×10^4	0
1:5	0	0	n/a
1:0 (vector only)	0	n/a	n/a
0:0 (bacteria only)	0	n/a	n/a

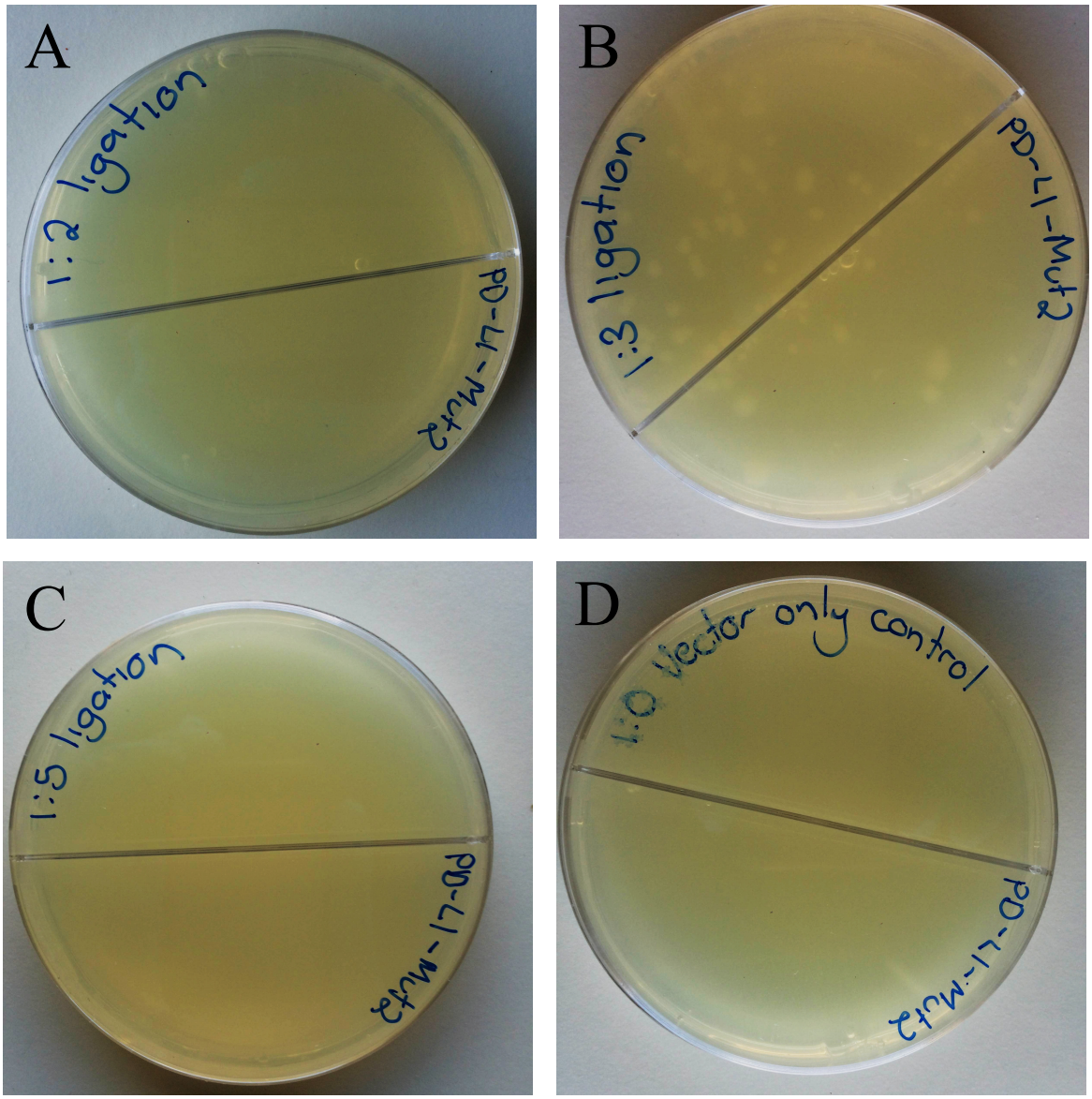

Figure 23: Ligation of αPD-L1 insert into pCB-SNAP backbone to create final recombinant plasmid, pCB-PDL1-SNAP, and subsequent transformation of pCB-PD-L1-SNAP into *E. coli*. A) 1:2 vector:insert ligation ratio. B) 1:3 vector:insert ligation ratio. C) 1:5 vector:insert ligation ratio. D) Vector only control (1:0 ligation ratio).

3.2.1.5 Restriction mapping

Restriction mapping, using the BamHI restriction enzyme, was used to confirm the successful ligation of the αPD-L1(scFv) insert into the pCB-SNAP backbone. A virtual simulation was first performed as per section 3.1.1.5 (Figure 24A). The *in vitro* mapping shows the expected fragmentation, confirming correct ligation (Figure 24B).

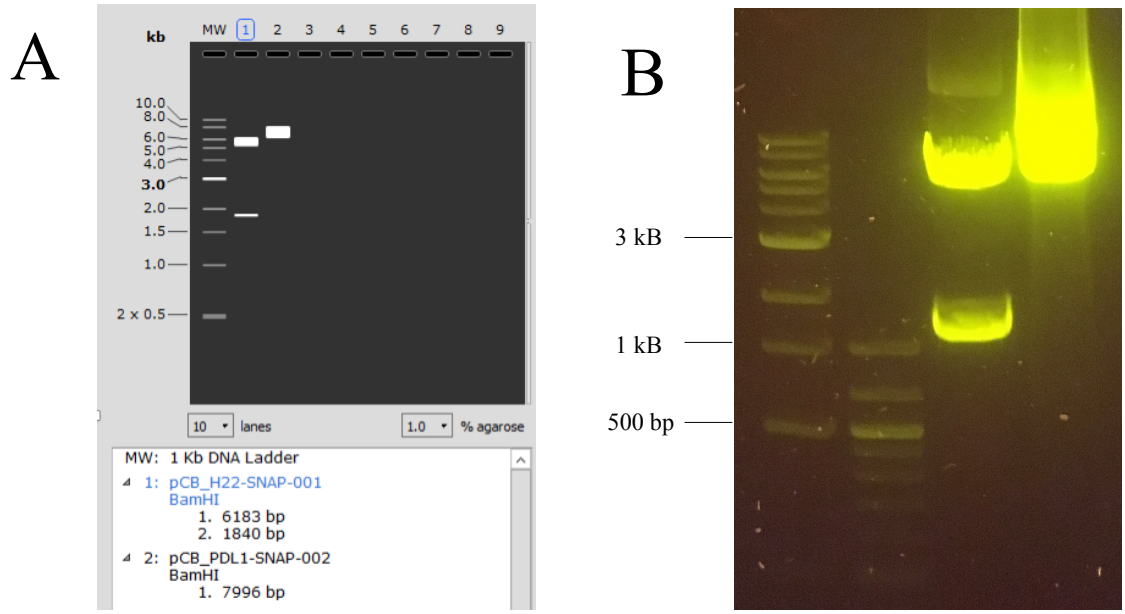

Figure 24: Restriction mapping to confirm correct ligation of αPD-L1(scFv) insert into pCB-SNAP vector. A) *In Silico* agarose gel simulation using SnapGene™. A 1Kb DNA ladder (MW) was used to evaluate fragment sizes of pCB-H22-SNAP (lane 1) and pCB-PDL1-SNAP (lane 2) when cut with BamHI. B) *In vitro* restriction mapping of pCB-H22-SNAP and pCB-PDL1-SNAP with BamHI. A 1Kb DNA ladder and a 100 bp+ DNA ladder were used to evaluate fragment sizes (MW1 and MW2) of digested pCB-H22-SNAP (lane 1) and digested pCB-PDL1-SNAP (lanes 2).

3.2.1.6 DNA sequencing

Of the clones that were confirmed through restriction mapping, two were bulk prepped (Table 10.1), diluted to 20ng/µL in 30 µL, and sent for sequencing. The sequences of both clones were confirmed (see Appendix 6.2.2)

Table 9.1: Quantification of pCB-PDL1-SNAP recombinant clones, following large scale purification

Clone	Yield (ng/uL)	260/280	260/230
1	1438.9	1.90	2.13
2	959.8	1.92	2.14

3.2.2 Transfection and protein expression

Upon confirmation of its ORF sequence, the pCB-PDL1-SNAP plasmid was introduced into a HEK293T mammalian vector expression system, co-expressing eGFP. Successful transfection

and expression of the αPDL1(scFv)-SNAP fusion was determined via visualization of eGFP reporter gene expression and zeocin was used to select for positively transfected cells, enriching this population (Figure 25). Transfection efficiency was evaluated visually by taking the average of multiple cell counts and was determined to be approximately 52.3%. The cell culture supernatant (CCSN) containing secreted fusion protein was collected every 3-4 days over 4 weeks.

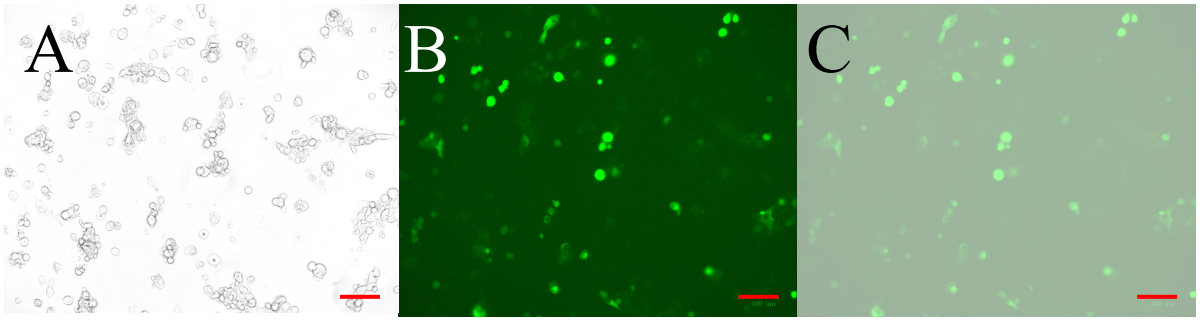

Figure 25: eGFP expression in HEK293T cells transfected with pCB-PDL1-SNAP. A) Brightfield, B) green channel C) merge image. **Scale bar: 100 µm**

3.2.3 Protein purification and analysis

3.2.3.1 Protein purification

CCSN harvests were enriched as per section 3.1.3.1. Figure 26 shows the resultant chromatograph. The first and largest peak has several shoulders. It was predicted that fractions 3-7 would contain mostly BSA that bound non-specifically to the column and was eluted at the initiation of the imidazole gradient. Fractions 8-18 were expected to contain αPDL1(scFv)-SNAP. The third peak, at fraction 23, was also suspected to contain αPDL1 (scFv)-SNAP.

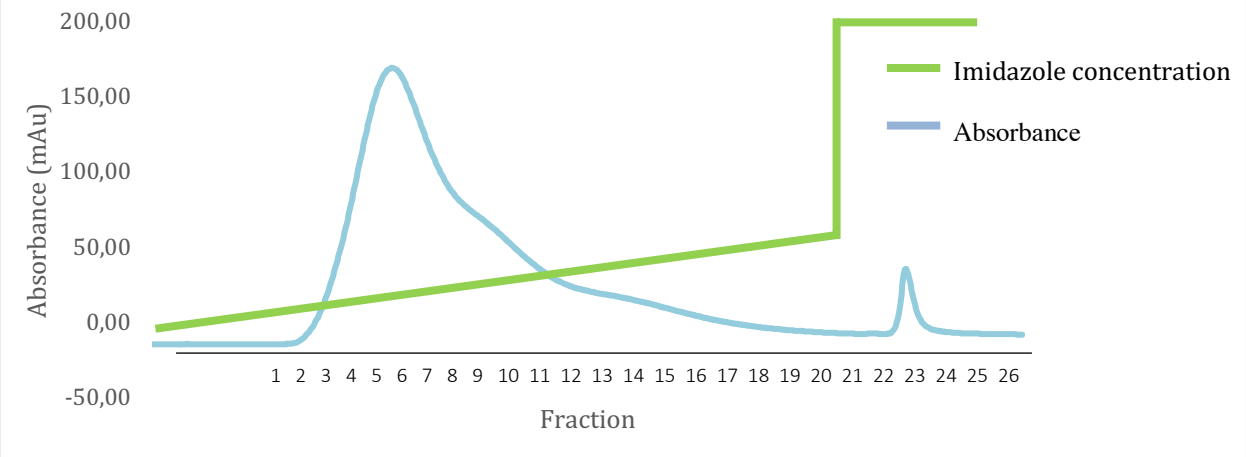

Figure 26: Chromatograph from IMAC purification of His_6-tagged αPDL1(scFv)-SNAP fusion proteins.

3.2.3.2 Protein validation and quantification

Following IMAC, fractions corresponding to the peaks above were run on an SDS-PAGE gel to identify protein corresponding to the weight of αPDL1(scFv)-SNAP (52.03 kDa) and determine which fractions should be pooled (Figure 27). Fractions 5-7 showed multiple bands, indicating the presence of αPDL1(scFv)-SNAP and BSA contaminant. Fractions 8-15 showed a single band each of an appropriate weight. Fraction 23 had no visible band. Fractions 8-12 (pool 1) and 13-15 (pool 2) were thus pooled and concentrated. Based on the data generated on GelAnalyzer, the protein yield was estimated to be 56.12%.

The concentration of αPDL1(scFv)-SNAP was then determined and these values were used to measure the volume of protein required for Western blot. Protein purity was determined, with all four samples falling will within the acceptable purity range (Table 11.1).

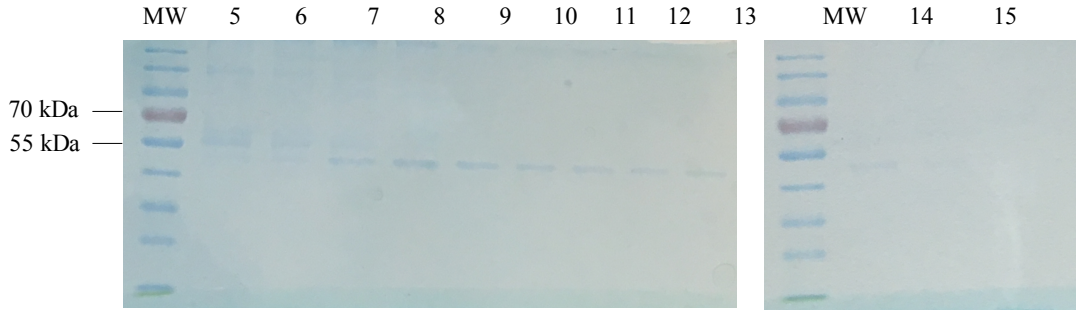

Figure 27: SDS-PAGE with coomassie blue stain to detect presence of protein. A protein ladder (MW) was used to evaluate the molecular weight of the protein in each band. The numbers correspond to the fraction represented in the chromatogram. This was used to determine the contents of each fraction in order to determine appropriate fraction pools.

Table 10.1: Quantification of purified αPDL1(scFv)-SNAP

Pool	Fractions	Conc. (mg/mL)	260/280	Vol. loaded (uL)
1	8-12	1.2505	0.62	1.622
2	13-15	1.2330	0.60	1.599

3.2.3.3 Protein confirmation

Following quantification, functional His_6-tag protein was validated by Western blot (Figure 28). An Anti-His_6-tag antibody conjugated to HRP was used for the chemiluminescent detection of functional protein. As predicted, pool 1 contain high quantities of αPDL1(scFv)-SNAP. Some was seen in pool 2, but no functional protein was detected in pool 3. Pool 1 was thus used for downstream experiments.

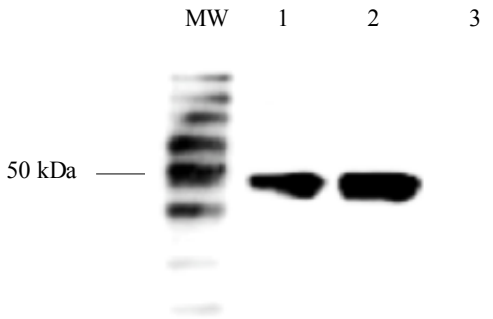

Figure 28: Visualization functional His_6-tag protein. A protein ladder (MW) was used to evaluate the molecular weight of the protein in each band. The numbers correspond to pools 1 and 2.

3.2.4 Immunoassays

3.2.4.1 Flow cytometry

αPDL1(scFv)-SNAP-Alexa488 conjugates were used to label cells and 1) confirm functional binding of the fusion protein and 2) investigate the prevalence of PD-L1 expression across the various cell lines. A375 is reported to be PD-L1-positive[161] and was used as a positive control. However, no binding was seen on this cell line (Figure 29B). SK-MEL-28, WM902 and UCT-MEL1 additionally showed no expression, and IGR-1 and IGR-39 show little expression (Figure 29C-E). The PD-L1-positive triple negative breast cancer cell line, HS578T, was thus used to confirm functional binding (Figure 29A). However, HS578T showed little binding in this assay. It is unclear whether these negative results are due to dysfunction of the protein, e.g. protein misfolding, or due to alterations in cellular receptor expression, e.g. loss of receptors when lifting cells. Overall, both aims of this experiment remain inconclusive. Table 12.1 shows the quantification gMFI for all cell lines when cells are unlabelled (background) compared to when they are labelled (signal). As is show, there is little change in gMFI across samples, with signal-to-background ratios of no higher than 2.76.

Table 11.1: Quantification of geometric mean fluorescence

Cell line	Unlabelled	Labelled
HS578T	2.34	6.45
A375	1.44	1.40
SK-MEL-28	2.93	3.00
WM902	1.80	1.96
UCT-Mel1	1.97	1.91
IGR-1	2.23	3.42
IGR-39	2.21	3.65

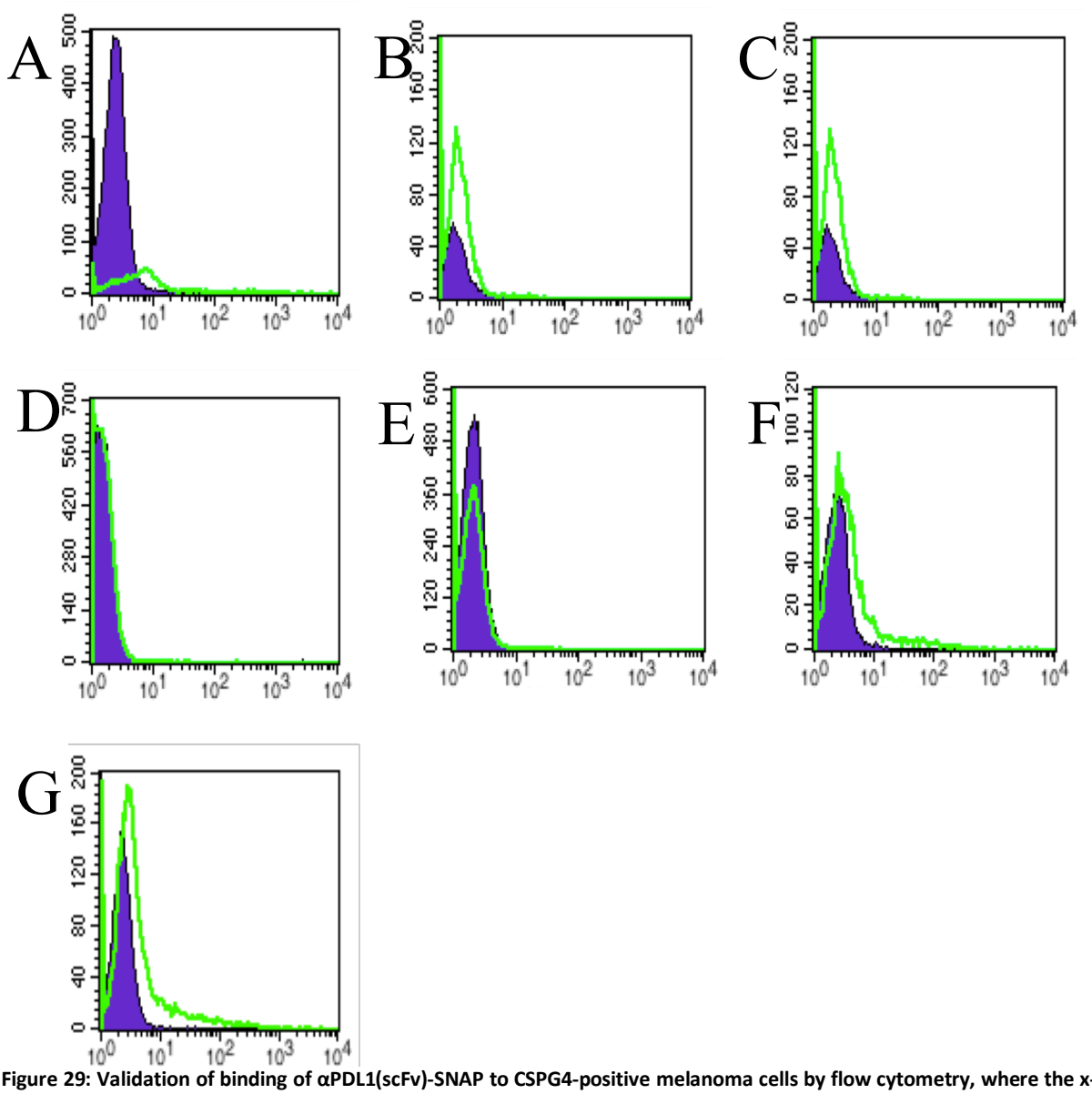

Figure 29: Validation of binding of αPDL1(scFv)-SNAP to CSPG4-positive melanoma cells by flow cytometry, where the x-axis represents the MFI and the y-axis represents the number of events. A) HS578T functional control. B) A375 positive control. C) SK-MEL-28. D) WM902. E) UCT-Mel1. F) IGR-1. G) IGR-39

3.2.4.2 Confocal microscopy

Confocal microscopy was performed to further investigate binding of αPDL1(scFv)-SNAP to cell surface PD-L1 in melanoma cells. Cells were labelled with αPDL1(scFv)-SNAP-549 for viewing. The staining patterns conformed to the data obtained by flow cytometry. Cytoplasmic staining was observed in some cell lines (Figure 30A-H), however; this is suspected to be noise, rather than true signal due to the fact that the gain used to collect these images was raised in an attempt to detect potentially weak signals. It is possible that expression was not changed due to lifting cells with trypsin but rather that prolonged culture

periods might be the cause of changes in receptor expression in the reportedly PD-L1-positive cell lines. More likely, there might be issues with the epitope-paratope interactions of this protein.

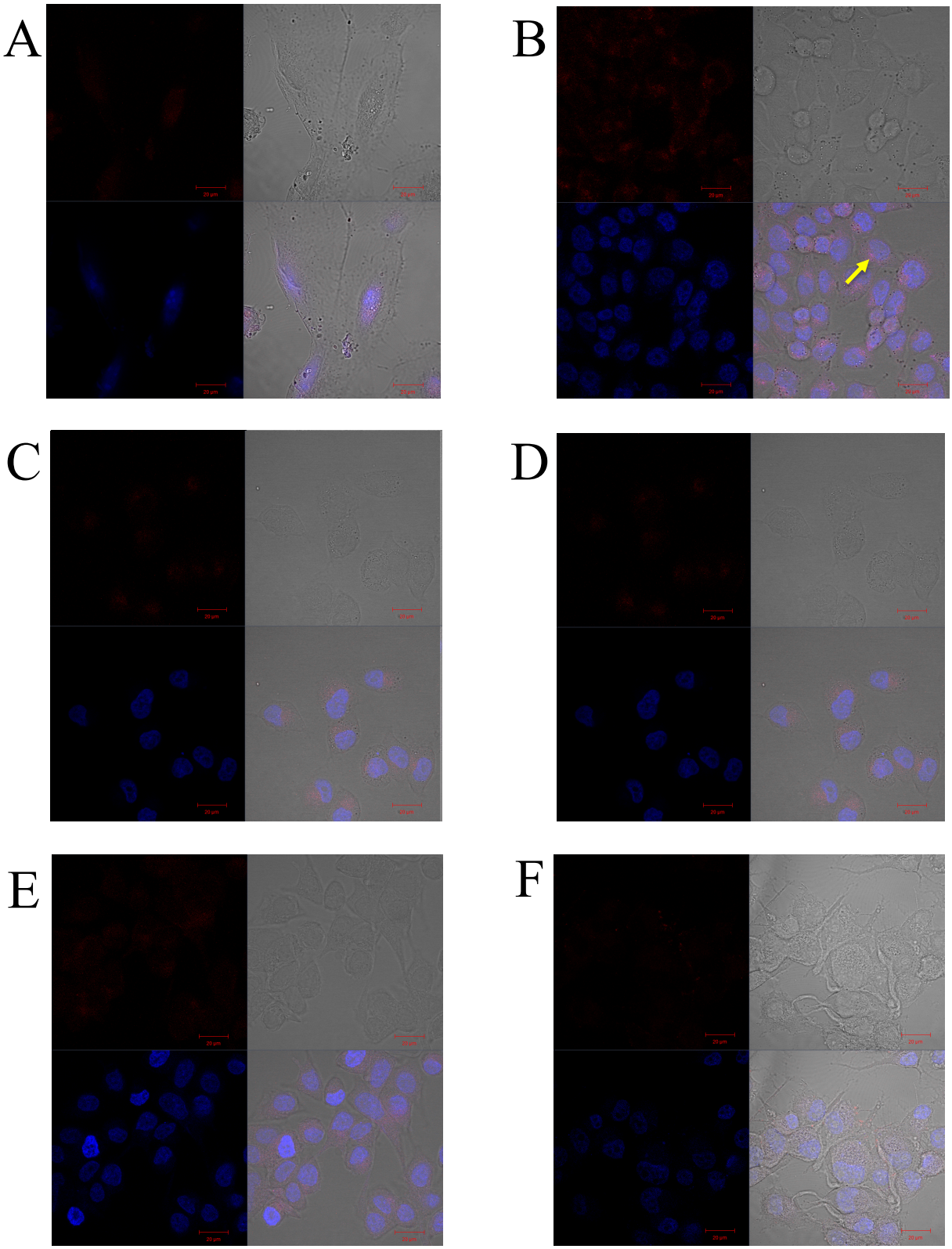

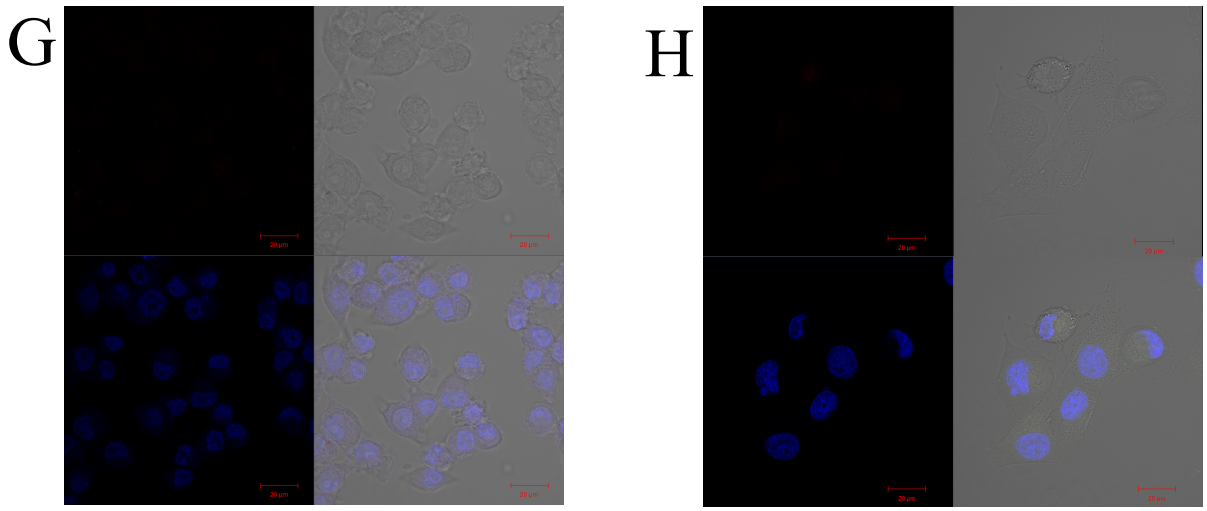

Figure 30: Confirmation of binding of αPDL1(scFv)-SNAP to melanoma cells by confocal microscopy. A) HS578T functional control. B) A375 positive control. Yellow arrow: cytoplasmic signal. C) SK-MEL-28. D) WM902. E) UCT-Mel1. F) IGR-1. G) IGR-39. H) Autofluorescence unstained control

3.2.5 Sequence generation

Binding studies with the αPDL1(scFv)-SNAP construct developed in this study were inadequate. Given the lack of convincing evidence, it is concluded that this antibody is not binding to the desired antigen, perhaps due to problems in the sequence used. A new antibody must therefore be generated, using a sequence that has confirmed binding data. The sequence of the anti-PD-L1 antibody 3G10 was thus obtained from publication.[162] All FRs and CDRs were identified and CDRs were subsequently aligned with the sequence (Figure 31). With the sequence confirmed, a pUC57 production vector containing the scFv was ordered for future work with this target.

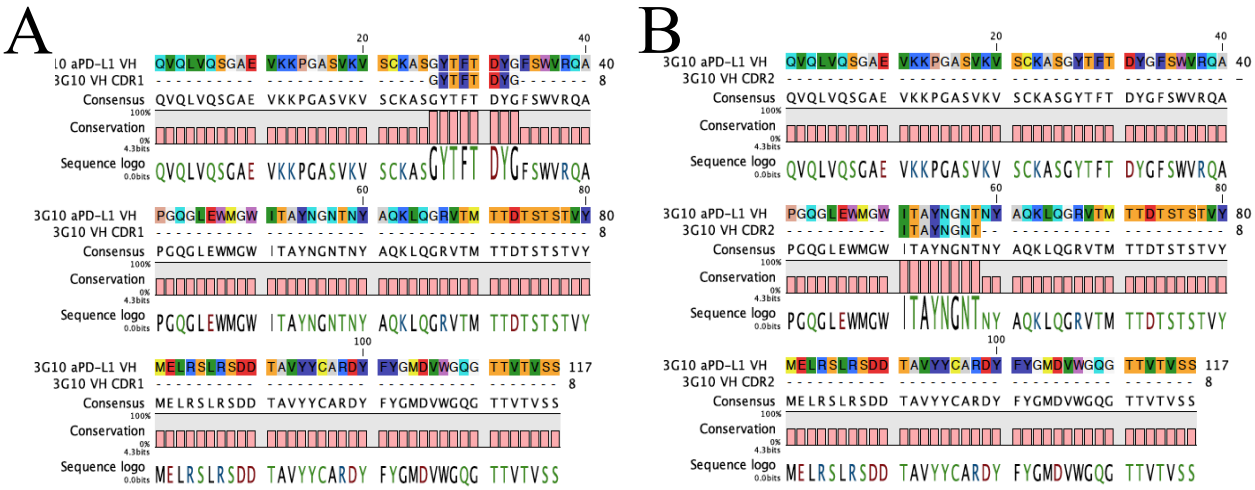

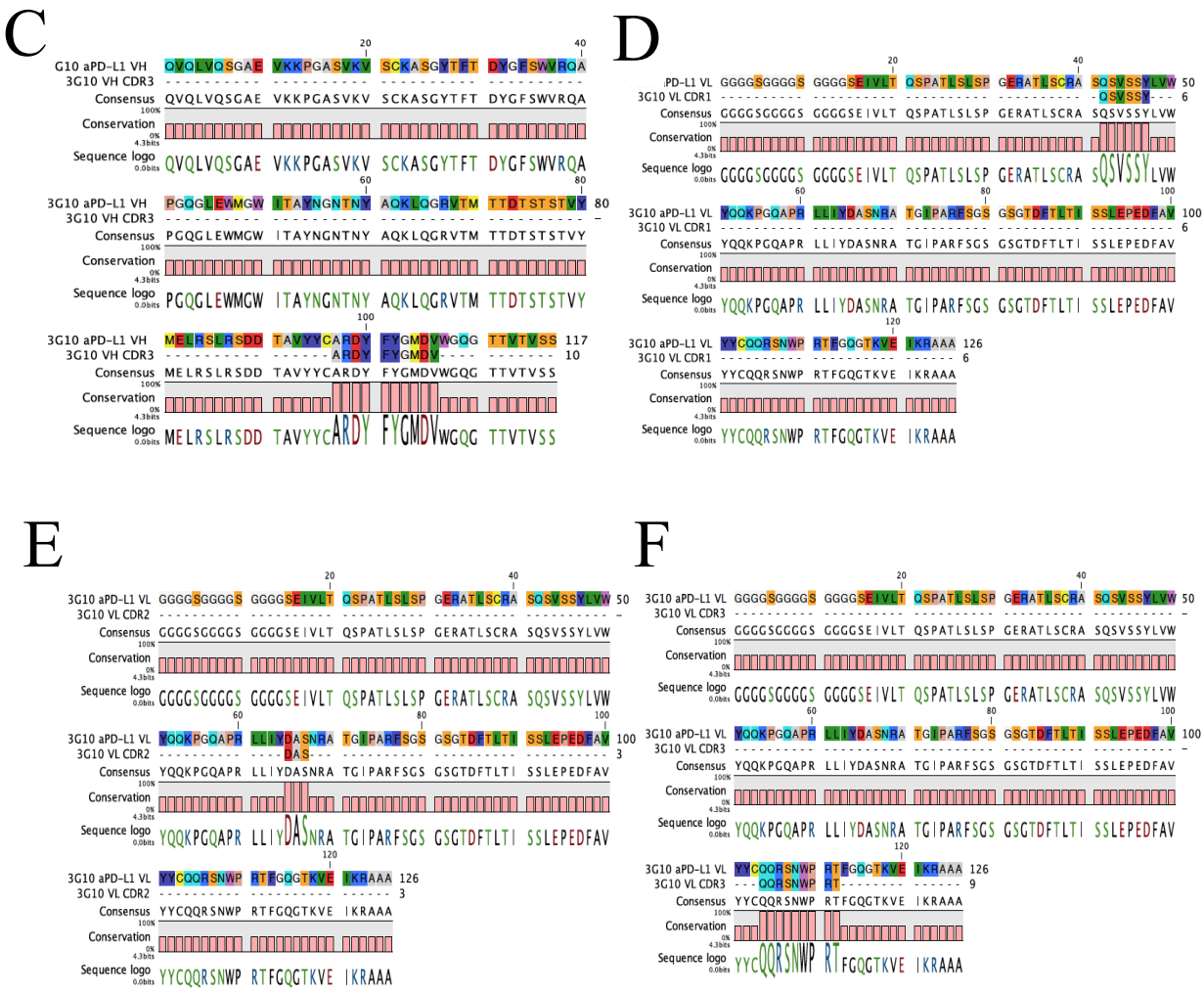

Figure 31: 3G10 anti-PD-L1 antibody CDR alignment. A) V_H CDR1. B) V_H CDR2. C) V_H CDR3. D) V_L CDR1. E) V_L CDR2. F) V_L CDR3.

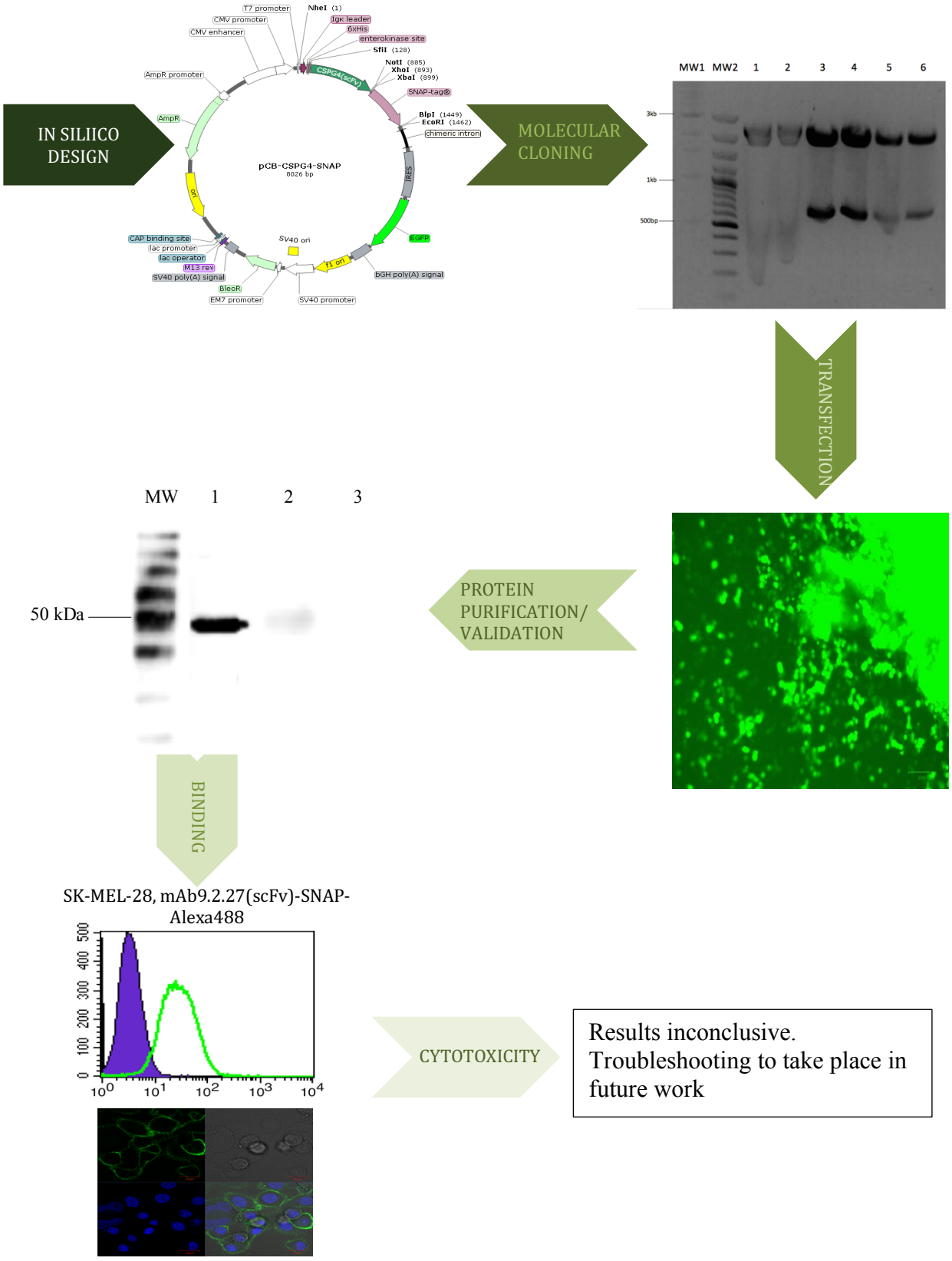

Figure 32: Summary figure. Step 1: in silico vector design using the pCB-SNAP mammalian expression vector. Step 2: molecular cloning of the mAb9.2.27(scFv) and PD-L1(scFv) inserts into the pCB-SNAP vector, confirmed through agarose gel electrophoresis. Step 3: successful transfection of ligated pCB- mAb9.2.27(scFv)-SNAP and PD-L1(scFv)-SNAP vectors into HEK293T cells, confirmed through eGFP expression. Step 4: purification of mAb9.2.27(scFv)-SNAP and PD-L1(scFv)-SNAP proteins, confirmed through SDS-PAGE and western blot analysis. Step 5: confirmation of binding of mAb9.2.27(scFv)-

SNAP-Alexa488 and PD-L1(scFv)-SNAP-Alexa48 proteins, confirmed through flow cytometry and confocal microscopy. Step 6: cytotoxicity of mAb9.2.27(scFv)-SNAP-IR700, confirmed through XXT assay.

4. Discussion

4.1 Melanoma

At present, the gold standard treatment for melanoma is surgical resection. However, while this strategy is effective at managing the disease when it is localized and in its early stages, those who are diagnosed at the late stages of the disease have very few options. According to the American Society of Clinical Oncology (2016), when patients are diagnosed early and undergo resection at the primary site the 5-year survival rate is 99%. If the cancer has invaded the lymph nodes 5-year survival rates drop to 63%. Once patients have reached the late metastatic stages survival rate drops further to 20%.[163] In South Africa, the unfortunate reality is that many patients present with late stage metastatic disease, as early diagnosis for is not always possible due to inadequate availability and access of diagnostic tools. [113] The low survival rates in late stage melanoma, as well as its inherent resistance to traditional chemotherapies and radiotherapies, have necessitated the need to develop alternative treatment strategies. These strategies include targeted therapies such as vemurafenib, which acts to inhibit mutated BRAF, and immunotherapies such as ipilimumab, which blocks the CTLA-4 immune checkpoint.[8, 9]

4.2 Immunotherapy

The ability to target cellular markers that are specific to various cancers has revolutionized our approach to treating this heterogenous disease. With so many phenotypical and genotypical differences between individual tumours (inter-tumour heterogeneity), and even between cell subpopulations within a single tumour (intra-tumour heterogeneity), it becomes necessary to consider that tumours with different morphologies, metabolisms, metastatic potentials and gene expression profiles might require different treatments. Heterogeneity affects drug resistance and patient outcome.[164, 165] So far, only thirteen mAbs have been FDA approved for use in cancer, three of which are used in detection only. Of the remaining ten, three are specific to melanoma. These are nivolumab and pembrolizumab, which target PD-1, and ipilimumab, which targets CTLA-4.[9, 131, 132] In addition to these mAbs, while there are currently 175 ADCs under investigation, only four are FDA approved. These are brentuximab vedotin, which treats relapsed/refractory Hodgkin lymphoma by targeting CD30; ado-trastuzumab entansine, which treats breast and lung cancer by targeting HER2; inotuzumab ozogamicin, which treats relapsed/refractory acute lymphoblastic leukemia by targeting

CD22; and gemtuzumab ozogamicin, which treats acute myeloid leukemia by targeting CD33.[166-170] While so much research is now being directed towards antibody-based therapies, the clinical approval rate is very low due to the limited efficacy of mAbs to induce cell death through inhibition of cell signalling, CDC or ADCC. [66, 75, 76] The success of mAbs is hindered by three problems: 1) they rely on the antibody-mediated response of a host immune system that is compromised and functioning sub-optimally, 2) they are working against cells that have developed advanced immune evasion mechanisms and are able to alter their microenvironment to induce immune tolerance, and 3) in response to repeated exposure to an mAb, cancer cells often adapt by downregulating the target receptor, thus causing resistance to the abrogated signal. [82, 171-173] It is for these reasons that ADCs have gained popularity.

Traditional cancer therapies rely on free toxins to kill aberrantly dividing cells, but their non-specificity contributes to systemic toxicity. Nausea, vomiting, hair loss, loss of appetite, decreased sexual life, dyspnoea, fatigue, pain and reduced ability to perform daily activities are just some of the side effects endured by patients on these toxic treatment regimes. Their overall quality of life is drastically reduced.[174, 175] By conjugating toxins to antibodies or antibody fragments, drugs are delivered directly to malignant cells with minimal or no effect on healthy cells. This specificity even allows for the use of drugs, such as Auristatin, that would otherwise be too toxic in the body. Furthermore, by using photosensitive compounds, the cytotoxic properties of the compound can be controlled through light activation. In the case that there is some anomalous off-target accumulation of the conjugate in tissues other than the tumour, it will have no effect at these sites, unless activated by light of a particular wavelength.[23] In addition to this, controlled drug release is provided by cleavable linkers. The polyethylene glycol (PEG) linker used here ensures that toxins are not released freely into the bloodstream but only detach from their antibodies once internalised into the target cells and exposed to the acidic environment of the endolysosome.[176, 177] Thus the photoimmunotherapy strategy used in the current study provides multiple levels of control to prevent unwanted cytotoxicity.

In the engineering of ADCs, a heterogenous population is produced, in which the configuration and stoichiometry of the conjugates is varied. This is a significant shortcoming

that negatively affects the probes' serum stability, creates challenges regarding their pharmacokinetics, and increases their risk of inducing immunogenicity. [11, 81, 87, 88, 178] The recombinant SNAP-tag scFv fusion proteins produced here have the advantages of 1) being a homogenous species with a 1:1 coupling at distinct site, 2) having a reduced size (±48-50 kDa), and thus increased tissue penetration compared to naked mAbs or ADCs, and 3) conferring minimal risk of induced immune response due to the human origin of the O^6-alkylguanine-DNA alkyltransferase enzyme from which SNAP-tag is engineered.

4.2.1 Chondroitin sulphate proteoglycan as target for melanoma

CSPG4 was first identified in melanoma and is known to be over-expressed in over 70% of primary tumour. It exhibits minimal expression in normal adult tissue but is highly expressed during foetal development.[134, 141-145] In this stage of life, cell motility is at its highest, as tissues undergo major reorganisation.[179, 180] CSPG4 expression has also been observed on pluripotent stem cell, as well as on CSCs. [133, 147-149] It has been suggested that CSPG4 plays an integral role in the motility and organisation of these cells. CSPG4 has furthermore been implicated in various stages of cancer, from its role in initiation to its role in metastasis. [139-142] Finally, CSPG4 expression has been identified in the pericytes and has shown to contribute to neoangiogenesis.[181] Pericytes are found within the basement membrane of the capillaries, where they play a crucial role in regulating proliferation of endothelial cells and subsequent growth of new capillaries.[182, 183]

CSPG4 has been identified as a tumour rejection antigen in a study showing that over 50% of mice immunized with a fragment of the antigen saw complete elimination of melanoma xenografts within 56 days.[181] Moreover, in another study, 60% of melanoma patients that underwent CSPG4 immunization exhibited prolonged survival and regression of metastases.[184] Preclinical studies have shown that xenograft bearing mice treated with an anti-CSPG4 full-length mAb have significantly reduced tumour growth, increased survival and inhibited metastasis. Additionally, mAb targeting of CSPG4 appears to decrease neoangiogenesis, with mice treated with anti-CSPG4 mAb having decreased vessel density in the tumour vasculature.[133]

In the current study, it has been shown through significant binding analysis that CSPG4 is a suitable target for the targeting of melanoma. Selective binding of fluorescently labelled mAb9.2.27(scFv)-SNAP to CSPG4-positive melanoma cells was validated by flow cytometry and confocal microscopy. These data strongly support CSPG4 as a target for melanoma. Using seven melanoma cell lines that are differentially representative of the various forms of the disease, it can be concluded that CSPG4 is expressed during all three growth phases of melanoma, in both its pigmented and unpigmented forms, and in chemoresistant cells. This data aligns with reports regarding the involvement of CSPG4 in various cellular functions relating to proliferation (radial growth phase); invasion (vertical growth phase) and migration and angiogenesis (metastatic growth phase.)[1]

4.2.2 Programmed death-ligand 1 as a target for melanoma

The immune system is heavily compromised in cancer. Not only do cancerous cells develop advance mechanisms to avoid recognition by the T cells but activated T cells are frequently inactivated through immune checkpoints occurring via the CTLA-4 and PD-1/PD-L1 pathways. This allows for more aggressive tumour growth with decreased immune surveillance in the subset of patients overexpressing PD-L1.[70, 185-187] Pembrolizumab, which targets PD-1, has shown to be more effective in hindering melanoma tumour growth and increasing survival than its predecessor, ipilimumab, which targets CTLA-4.[131]

In this study, PD-L1 targeting was inconclusive. While SDS-PAGE, GelAnalyzer and western blot indicate that functional His_6-tagged fusion protein was successfully expressed and purified, no clear binding was seen on any of the melanoma cell lines, including the melanoma A375 and the breast cancer HS578T positive control cell lines. Due to delayed delivery of the commercial anti-PD-L1 antibody, which was to serve as a positive control, it remains unconfirmed whether this was due to altered receptor expression in the cells or due to a problem with the binding ability of the protein. However, it is expected that the latter is the likely case and that the sequence originally provided for the antibody contained errors. Consequently, *in silico* sequence generation was performed in order to reclone this protein using a new sequence obtained from publication.

4.3 SNAP-tag as a therapeutic tool

4.3.1 Production of SNAP-tag fusion protein conjugates

In this study, SNAP-tag technology was investigated for is ability to produce homogeneous conjugate preparations by providing a distinct binding moiety for the coupling of the self-labelling enzyme with BG-modified substrates. Recombinant protein was engineered through the genetic fusion of the SNAP-tag cassette with the coding sequence of the anti-CSPG4 and anti-PD-L1 scFv. Endowed with SNAP-tag, any antibody can be autocatalytically labelled with any substrate that has been modified with a BG.

In silico cloning of the scFv-SNAP construct produced an in-frame sequence, free of any stop codons that would interfere with the transcription of the DNA. The resultant sequence was thus used to generate the relevant insert (ordered from Genscript). Molecular cloning was performed to extract the insert and ligate it into the pCB-SNAP backbone. Visualisation of the agarose gels confirmed the success of the restriction enzyme digests used during this process. The presence of bacterial colonies on LB agar plates, together with the absence of colonies on the bacteria only and vector only control plates, indicated the success of the ligation step, indicating 1) that all colonies contained the pCB-SNAP vector and 2) there was a very low rate of autoligation, making it unlikely to select an autoligated clone for downstream studies. This was further confirmed through restriction mapping, which demonstrated differential fragmentation of the ligated clones compared to the original vector. The final step in the cloning process was to confirm the validity of the plasmid through DNA sequencing. *In silico* alignment was performed using the sequence generated in SnapGene and the data showed no missense, nonsense or frameshift mutations.

After cloning, the vector was transfected in to HEK293T cells and expression was confirmed through visualization of GFP reporter gene expression. HEK293T cells allow for rapid expression and screening of recombinant proteins, and produce sufficiently a high yield for preclinical *in vitro* models (~5-15mg/L).[96, 188] Zeocin was used to select for positively transfected cells. Purification of the remaining supernatant was performed using IMAC, whereby SNAP fusion proteins were captured by their His_6-tag. SDS-PAGE and GelAnalyzer were used to confirm the presence of protein corresponding to the size of the construct and determine the yield, and Western blot was then used to confirm functional His_6-tag protein.

These protein validation assays further confirmed that the antigen binding of mAb9.2.27(scFv)-SNAP and the self-labelling activity of SNAP-tag were retained. Retention of the binding activity of the mAb9.2.27 scFv against CSPG4 is possible because SNAP-tag technology provides a distant conjugation, away from the paratope. By creating a spacer between the antibody and the effector molecule, the negative effects often associated with direct conjugation are avoided, such as altered structure, function and binding affinity. Moreover, functionality of the effector molecule, Alexa Fluor™ 488, was preserved in the conjugation process.

4.3.2 Targeted delivery of IR700 to tumour cells by SNAP-tag fusion protein

Currently, several photosensitizers, such as Photofrin and ALA, have been approved for clinical use, while others, such as Fotolon, have been approved for clinical trials.[189, 190] Unlike traditional cancer therapies, the cytotoxic effects of PDT are limited by their activation with harmless light. This has the advantage of significantly reducing systemic effects, such as necrosis of healthy tissue and photosensitivity. In the form of an antibody conjugate, these off-target effects are reduced even further compared to traditional PDT. This further allows for repeated treatment cycles, which facilitates tumour remission and decreases the risk of sub-curative treatment.[65, 66]

The photosensitizer used here, IR700, was chosen because it has maximal excitation in the NIR range. This offers an optimal balance between tissue penetration and photon efficiency, with 17-fold increase in the extinction coefficient of IR700 compared to hypericin.[52, 53, 191] In a clinical setting, deeper tissue penetration becomes imperative. IR700 modified with a BG-PEG_{24}-NH_2 linker was incubated at a 2-fold molar excess with mAb9.2.27(scFv)-SNAP. The conjugate was administered to previously mentioned cell lines and assessed for its ability to selectively kill those expressing CSPG4. These experiments were unfortunately unsuccessful. No phototoxicity was observed in the XTT cell viability assays. In light of the convincing binding analysis, it is concluded that inefficient solubilization of the lyophilized product resulted in inadequate conjugation of BG-IR700 with SNAP-tag. We were unable to confirm the conjugation of BG-IR700 to the fusion protein due to unavailability of an appropriate device able to detect the probe in the correct wavelength, i.e. 689 nm excitation and 700 nm

emission. None of the equipment available to us, the confocal microscope, flow cytometer and gel doc, had the appropriate filters for this purpose.

4.4 Outlook and future work

This study provides sufficient proof of concept for the use of CSPG4-specific SNAP-tag fusion protein in the selective targeting of melanoma. While several SNAP-tag fusion proteins have been developed to target other receptors, particularly EGFR, and other cancers, particularly breast cancer,[58, 108, 109, 192] no literature exists describing the use of this technology to target the CSPG4 antigen in melanoma. In existing *in vivo* studies, CSPG4-specifc SNAP-tag photoimmunoconjugates have not been investigated. Thus, once the issues encountered in this project, such as the unsuccessful conjugation of the BG-IR700 payload to the mAb9.2.27(scFv)-SNAP fusion protein, have been resolved, the logical continuation of this work is to progress with xenograft mouse models to evaluate the safety, biodistribution and biological activity of mAb9.2.27(scFv)-SNAP-IR700 as a novel cancer theranostic. Previous studies using anti-EGFR-SNAP recombinant proteins have shown that the protein exhibits high tumour accumulation and retention with simultaneous rapid renal filtration of unbound probe, creating a high tumour-to-background ratio 10 hours after administration of the probe,[57] allowing for efficient tumour imaging and minimizing the chance of off-target effects upon irradiation. In addition to its prominence in melanoma, CSPG4 is known to be overexpressed in several other cancers, including triple negative breast cancer and glioblastoma.[108, 135, 193] This photoimmunoconjugate might thus have potential use in the study, detect and treatment of these cancers.

One potential alteration that might be made to the photoimmunoconjugate is to increase the valency, i.e. increase the DAR in order to increase the phototoxicity. A second consideration is the routing of the probe. While free PSs tend to accumulate in different organelle within the cell, such as the melanosomes, mitochondria, golgi apparatus and endoplasmic reticulum, depending on their specific chemistry,[3, 194, 195] antibody conjugates such as those developed in this study, are internalised by receptor-mediated endocytosis. This manner of routing directs the antibody, carrying its payload, to the endosomes. Understanding the exact routing of the conjugate becomes critical for future work aimed at clinical application as it informs us where the drug is being delivered and hence how it will take effect. It also informs us which

linkers to use to ensure suitable drug release. Internalisation by receptor-mediated endocytosis also indicates that there will be no non-specific internalisation of unconjugated drug.[151, 196, 197] Receptor-mediated endocytosis, which here is the assumed method of internalisation, routes the antibody and its payload into the early endosome, which matures into late endosome, and, finally, fuses with the lysosome, where it undergoes lysosomal degradation.[151] There is, however, a risk of damaging and decreasing the efficiency of the effector molecule. Thus, the use of the lysine-aspartic acid-glutamic acid-leucine (KDEL) sequence should be considered. This sequence routes any protein containing this sequence at its C terminal to the endoplasmic reticulum.[198, 199] Alternatively, endosomal escape strategies that create pores in the endosome for the release of cargo could be considered. One example is photochemical internalisation, a technique in which an amphiphilic photosensitizer is co-administered and localises within the endosomal membrane. Upon light activation, the production of ROS causes local disruption to the membrane, allowing for the release of the cargo into the cytosol. Other techniques utilize pH buffering systems, peptides, viruses, bacteria or chemicals to facilitate pore formation.[200, 201]

In summary, we have been able to generate a next generation photoimmunotheranostic antibody fusion protein able to overcome several problems associated with traditional ADCs. Through the use of SNAP-tag technology, using a simple autocatalytic reaction that allows for a single step conjugation, we have produced a homogenous conjugate that shows retained function of both the mAb.9.2.27 scFv and the effector molecule. Efficient binding and dose dependent cytotoxicity are indicative of the future potential of this product in cancer therapy.

5. References

1. Bertolotto C. Melanoma: from melanocyte to genetic alterations and clinical options. Scientifica. 2013;2013.

2. Carlson JA, Ross JS, Slominski AJ. New techniques in dermatopathology that help to diagnose and prognosticate melanoma. Clinics in dermatology. 2009;27(1):75-102.

3. Davids L, Kleemann B. Combating melanoma: the use of photodynamic therapy as a novel, adjuvant therapeutic tool. Cancer treatment reviews. 2011;37(6):465-75.

4. Elliott AM, Al-Hajj MA. ABCB8 mediates doxorubicin resistance in melanoma cells by protecting the mitochondrial genome. Molecular Cancer Research. 2009;7(1):79-87.

5. Rutkowski P, Zdzienicki M, Nowecki ZI, Van Akkooi AC. Surgery of primary melanomas. Cancers. 2010;2(2):824-41.

6. Bergh J. Quo vadis with targeted drugs in the 21st century? : American Society of Clinical Oncology; 2009.

7. Fojo T, Grady C. How much is life worth: cetuximab, non–small cell lung cancer, and the $440 billion question. Journal of the National Cancer Institute. 2009;101(15):1044-8.

8. Chapman PB, Hauschild A, Robert C, Haanen JB, Ascierto P, Larkin J, et al. Improved survival with vemurafenib in melanoma with BRAF V600E mutation. n Engl J Med. 2011;2011(364):2507-16.

9. Hodi FS, O'day SJ, McDermott DF, Weber RW, Sosman JA, Haanen JB, et al. Improved survival with ipilimumab in patients with metastatic melanoma. N Engl j Med. 2010;2010(363):711-23.

10. Hampton T. Targeted Cancer Therapies Lagging. JAMA. 2006;296(16):1951-2.

11. Ducry L, Stump B. Antibody− drug conjugates: linking cytotoxic payloads to monoclonal antibodies. Bioconjugate chemistry. 2009;21(1):5-13.

12. Agostinis P, Berg K, Cengel KA, Foster TH, Girotti AW, Gollnick SO, et al. Photodynamic therapy of cancer: an update. CA: a cancer journal for clinicians. 2011;61(4):250-81.

13. T Hellwig C, Passante E, Rehm M. The molecular machinery regulating apoptosis signal transduction and its implication in human physiology and pathophysiologies. Current molecular medicine. 2011;11(1):31-47.

14. Chen KG, Valencia JC, Lai B, Zhang G, Paterson JK, Rouzaud F, et al. Melanosomal sequestration of cytotoxic drugs contributes to the intractability of malignant melanomas. Proceedings of the National Academy of Sciences. 2006;103(26):9903-7.

15. Jones P, George A. The ABC transporter structure and mechanism: perspectives on recent research. Cellular and Molecular Life Sciences. 2004;61(6):682-99.

16. Gottesman MM, Fojo T, Bates SE. Multidrug resistance in cancer: role of ATP–dependent transporters. Nature Reviews Cancer. 2002;2(1):48-58.

17. Wu C-P, Sim H-M, Huang Y-H, Liu Y-C, Hsiao S-H, Cheng H-W, et al. Overexpression of ATP-binding cassette transporter ABCG2 as a potential mechanism of acquired resistance to vemurafenib in BRAF (V600E) mutant cancer cells. Biochemical pharmacology. 2013;85(3):325-34.

18. Frank NY, Margaryan A, Huang Y, Schatton T, Waaga-Gasser AM, Gasser M, et al. ABCB5-mediated doxorubicin transport and chemoresistance in human malignant melanoma. Cancer research. 2005;65(10):4320-33.

19. Hadjur C, Richard MJ, Parat MO, Jardon P, Favier A. Photodynamic effects of hypericin on lipid peroxidation and antioxidant status in melanoma cells. Photochemistry and photobiology. 1996;64(2):375-81.

20. Davids LM, Kleemann B, Kacerovská D, Pizinger K, Kidson SH. Hypericin phototoxicity induces different modes of cell death in melanoma and human skin cells. Journal of Photochemistry and Photobiology B: Biology. 2008;91(2–3):67-76.

21. Hanahan D, Weinberg RA. Hallmarks of cancer: the next generation. cell. 2011;144(5):646-74.

22. Kleemann B, Loos B, Scriba TJ, Lang D, Davids LM. St John's Wort (Hypericum perforatum L.) photomedicine: Hypericin-photodynamic therapy induces metastatic melanoma cell death. PloS one. 2014;9(7):e103762.

23. Luksiene Z. Photodynamic therapy: mechanism of action and ways to improve the efficiency of treatment. Medicina (Kaunas, Lithuania). 2003;39(12):1137-50.

24. Gilaberte Y, Milla L, Salazar N, Vera-Alvarez J, Kourani O, Damian A, et al. Cellular intrinsic factors involved in the resistance of squamous cell carcinoma to photodynamic therapy. Journal of Investigative Dermatology. 2014;134(9):2428-37.

25. Calixto GMF, Bernegossi J, de Freitas LM, Fontana CR, Chorilli M. Nanotechnology-based drug delivery systems for photodynamic therapy of cancer: A review. Molecules. 2016;21(3):342.

26. Ogawa M, Tomita Y, Nakamura Y, Lee M-J, Lee S, Tomita S, et al. Immunogenic cancer cell death selectively induced by near infrared photoimmunotherapy initiates host tumor immunity. Oncotarget. 2017;8(6):10425.

27. Broussard L, Howland A, Ryu S, Song K, Norris D, Armstrong CA, et al. Melanoma Cell Death Mechanisms. Chonnam Med J. 2018;54(3):135-42.

28. Cheng Y, Ren X, Hait WN, Yang J-M. Therapeutic targeting of autophagy in disease: biology and pharmacology. Pharmacological reviews. 2013;65(4):1162-97.

29. Galluzzi L, Vitale I, Aaronson SA, Abrams JM, Adam D, Agostinis P, et al. Molecular mechanisms of cell death: recommendations of the Nomenclature Committee on Cell Death 2018. Cell Death & Differentiation. 2018;25(3):486-541.

30. Kessel D, Oleinick NL. Cell death pathways associated with photodynamic therapy: an update. Photochemistry and photobiology. 2018;94(2):213-8.

31. Kessel D, Reiners Jr JJ. Apoptosis and autophagy after mitochondrial or endoplasmic reticulum photodamage. Photochemistry and photobiology. 2007;83(5):1024-8.

32. Kessel DH, Price M, Reiners J, John J. ATG7 deficiency suppresses apoptosis and cell death induced by lysosomal photodamage. Autophagy. 2012;8(9):1333-41.

33. Wong RS. Apoptosis in cancer: from pathogenesis to treatment. Journal of experimental & clinical cancer research. 2011;30(1):87.

34. Caldarola G, Carbone A, Arena V, Pennacchia I, De CW, Vianale G, et al. Tumour necrosis factor-related apoptosis-inducing ligand (TRAIL): a possible pathogenic role in chronic plaque psoriasis. Giornale italiano di dermatologia e venereologia: organo ufficiale, Societa italiana di dermatologia e sifilografia. 2016;151(1):17-24.

35. Adewale OF, Basiru A, Olowoyeye A, Olayide I, Ojo O. Regulation of Apoptotic and Necroptotic Cell Death in Skin Cancer. Journal of Cancer Biology & Research. 2017.

36. Ouyang L, Shi Z, Zhao S, Wang FT, Zhou TT, Liu B, et al. Programmed cell death pathways in cancer: a review of apoptosis, autophagy and programmed necrosis. Cell proliferation. 2012;45(6):487-98.

37. Serrano-del Valle A, Anel A, Naval J, Marzo I. Immunogenic cell death and immunotherapy of multiple myeloma. Frontiers in Cell and Developmental Biology. 2019;7.

38. Chen DS, Mellman I. Oncology meets immunology: the cancer-immunity cycle. Immunity. 2013;39(1):1-10.

39. Apetoh L, Ghiringhelli F, Tesniere A, Obeid M, Ortiz C, Criollo A, et al. Toll-like receptor 4–dependent contribution of the immune system to anticancer chemotherapy and radiotherapy. Nature medicine. 2007;13(9):1050.

40. Michaud M, Martins I, Sukkurwala AQ, Adjemian S, Ma Y, Pellegatti P, et al. Autophagy-dependent anticancer immune responses induced by chemotherapeutic agents in mice. Science. 2011;334(6062):1573-7.

41. Shams M, Owczarczak B, Manderscheid-Kern P, Bellnier DA, Gollnick SO. Development of photodynamic therapy regimens that control primary tumor growth and inhibit secondary disease. Cancer Immunology, Immunotherapy. 2015;64(3):287-97.

42. Falk H. From the photosensitizer hypericin to the photoreceptor stentorin—the chemistry of phenanthroperylene quinones. Angewandte Chemie International Edition. 1999;38(21):3116-36.

43. Popovic A, Wiggins T, Davids L. Differential susceptibility of primary cultured human skin cells to hypericin PDT in an in vitro model. Journal of Photochemistry and Photobiology B: Biology. 2015;149:249-56.

44. Calzavara-Pinton P, Venturini M, Sala R. Photodynamic therapy: update 2006 Part 1: Photochemistry and photobiology. Journal of the European Academy of Dermatology and Venereology. 2007;21(3):293-302.

45. Horecker BL. The absorption spectra of hemoglobin and its derivatives in the visible and near infra-red regions. J biol Chem. 1943;148(1):173-83.

46. Faber DJ, Mik EG, Aalders MC, van Leeuwen TG. Light absorption of (oxy-) hemoglobin assessed by spectroscopic optical coherence tomography. Optics letters. 2003;28(16):1436-8.

47. Tsai C-L, Chen J-C, Wang W-J. Near-infrared absorption property of biological soft tissue constituents. Journal of Medical and Biological Engineering. 2001;21(1):7-14.

48. Mitsunaga M, Ogawa M, Kosaka N, Rosenblum LT, Choyke PL, Kobayashi H. Cancer Cell-Selective In Vivo Near Infrared Photoimmunotherapy Targeting Specific Membrane Molecules. Nature medicine. 2011;17(12):1685-91.

49. Gioux S, Choi HS, Frangioni JV. Image-guided surgery using invisible near-infrared light: fundamentals of clinical translation. Molecular imaging. 2010;9(5):237.

50. LI-COR. IRDye 700DX Infrared Dye: LI-COR, Inc.; 2018 [Available from: https://www.licor.com/bio/products/reagents/irdye/700dx/.

51. Halder M, Chowdhury P, Gordon M, Petrich J, Das K, Park J, et al. Hypericin and its perylene quinone analogs: probing structure, dynamics, and interactions with the environment. Adv Photochem. 2005;28:1-28.

52. Schmitt LA, Liu Y, Murphy PA, Petrich JW, Dixon PM, Birt DF. Reduction in hypericin-induced phototoxicity by Hypericum perforatum extracts and pure compounds. Journal of photochemistry and photobiology B, Biology. 2006;85(2):118-30.

53. Ruggiero E, Alonso-de Castro S, Habtemariam A, Salassa L. Upconverting nanoparticles for the near infrared photoactivation of transition metal complexes: new opportunities and challenges in medicinal inorganic photochemistry. Dalton Transactions. 2016;45(33):13012-20.

54. Wilson BC, Patterson MS. The determination of light fluence distributions in photodynamic therapy. Photodynamic therapy of neoplastic disease. 1990;1:129-44.

55. Mitsunaga M, Nakajima T, Sano K, Choyke PL, Kobayashi H. Near-infrared theranostic photoimmunotherapy (PIT): repeated exposure of light enhances the effect of immunoconjugate. Bioconjugate chemistry. 2012;23(3):604-9.

56. Ito K, Mitsunaga M, Nishimura T, Kobayashi H, Tajiri H. Combination photoimmunotherapy with monoclonal antibodies recognizing different epitopes of human epidermal growth factor receptor 2: an assessment of phototherapeutic effect based on fluorescence molecular imaging2016.

57. Pardo A, Stöcker M, Kampmeier F, Melmer G, Fischer R, Thepen T, et al. In vivo imaging of immunotoxin treatment using Katushka-transfected A-431 cells in a murine xenograft tumour model. Cancer Immunology, Immunotherapy. 2012;61(10):1617-26.

58. von Felbert V, Bauerschlag D, Maass N, Bräutigam K, Meinhold-Heerlein I, Woitok M, et al. A specific photoimmunotheranostics agent to detect and eliminate skin cancer cells expressing EGFR. Journal of cancer research and clinical oncology. 2016:1-9.

59. Nagaya T, Nakamura Y, Sato K, Harada T, Choyke PL, Hodge JW, et al. Near infrared photoimmunotherapy with avelumab, an anti-programmed death-ligand 1 (PD-L1) antibody. Oncotarget. 2017;8(5):8807.

60. Solban N, Pål SK, Alok SK, Sung CK, Hasan T. Mechanistic investigation and implications of photodynamic therapy induction of vascular endothelial growth factor in prostate cancer. Cancer research. 2006;66(11):5633-40.

61. Ferrario A, Von Tiehl KF, Rucker N, Schwarz MA, Gill PS, Gomer CJ. Antiangiogenic treatment enhances photodynamic therapy responsiveness in a mouse mammary carcinoma. Cancer research. 2000;60(15):4066-9.

62. Sitnik T, Hampton J, Henderson B. Reduction of tumour oxygenation during and after photodynamic therapy in vivo: effects of fluence rate. British journal of cancer. 1998;77(9):1386.

63. Fingar V, Kik P, Haydon P, Cerrito P, Tseng M, Abang E, et al. Analysis of acute vascular damage after photodynamic therapy using benzoporphyrin derivative (BPD). British journal of cancer. 1999;79(11-12):1702.

64. Kishimoto S, Bernardo M, Saito K, Koyasu S, Mitchell JB, Choyke PL, et al. Evaluation of oxygen dependence on in vitro and in vivo cytotoxicity of photoimmunotherapy using IR-700–antibody conjugates. Free Radical Biology and Medicine. 2015;85:24-32.

65. Saavedra R, Rocha LB, Dąbrowski JM, Arnaut LG. Modulation of biodistribution, pharmacokinetics, and photosensitivity with the delivery vehicle of a bacteriochlorin photosensitizer for photodynamic therapy. ChemMedChem. 2014;9(2):390-8.

66. Emens L. Breast cancer immunobiology driving immunotherapy: vaccines and immune checkpoint blockade. *Expert Review of Anticancer Therapy*. 2012;12(12):1597-611.

67. Lachiewicz AM, Berwick M, Wiggins CL, Thomas NE. Epidemiologic support for melanoma heterogeneity using the surveillance, epidemiology, and end results program. Journal of Investigative Dermatology. 2008;128(5):1340.

68. Piccart-Gebhart MJ, Procter M, Leyland-Jones B, Goldhirsch A, Untch M, Smith I, et al. Trastuzumab after Adjuvant Chemotherapy in HER2-Positive Breast Cancer. New England Journal of Medicine. 2005;353(16):1659-72.

69. Poncet B, Bachelot T, Colin C, Ganne C, Jaisson-Hot I, Orfeuvre H, et al. Use of the Monoclonal Antibody Anti-HER2 Trastuzumab in the Treatment of Metastatic Breast Cancer: A Cost-Effectiveness Analysis. American Journal of Clinical Oncology. 2008;31(4):363-8.

70. Topalian SL, Drake CG, Pardoll DM. Targeting the PD-1/B7-H1(PD-L1) pathway to activate anti-tumor immunity. Current Opinion in Immunology. 2012;24(2):207-12.

71. Malas S, Harrasser M, Lacy KE, Karagiannis SN. Antibody therapies for melanoma: new and emerging opportunities to activate immunity. Oncology reports. 2014;32(3):875-86.

72. Salven P, Heikkilä P, Joensuu H. Enhanced expression of vascular endothelial growth factor in metastatic melanoma. British journal of cancer. 1997;76(7):930.

73. Curran MA, Montalvo W, Yagita H, Allison JP. PD-1 and CTLA-4 combination blockade expands infiltrating T cells and reduces regulatory T and myeloid cells within B16 melanoma tumors. Proceedings of the National Academy of Sciences. 2010;107(9):4275-80.

74. Powell DJ, Felipe-Silva A, Merino MJ, Ahmadzadeh M, Allen T, Levy C, et al. Administration of a CD25-directed immunotoxin, LMB-2, to patients with metastatic melanoma induces a selective partial reduction in regulatory T cells in vivo. The Journal of Immunology. 2007;179(7):4919-28.

75. Clynes RA, Towers TL, Presta LG, Ravetch JV. Inhibitory Fc receptors modulate in vivo cytoxicity against tumor targets. Nature medicine. 2000;6(4):443-6.

76. Zangemeister-Wittke U. Antibodies for targeted cancer therapy–technical aspects and clinical perspectives. Pathobiology. 2005;72(6):279-86.

77. Fitting J, Blume T, ten Haaf A, Blau W, Gattenlöhner S, Tur MK, et al., editors. Phage display-based generation of novel internalizing antibody fragments for immunotoxin-based treatment of acute myeloid leukemia. MAbs; 2015: Taylor & Francis.

78. Bösmüller H, Fischer A, Pham DL, Fehm T, Capper D, von Deimling A, et al. Detection of the BRAF V600E mutation in serous ovarian tumors: a comparative analysis of immunohistochemistry with a mutation-specific monoclonal antibody and allele-specific PCR. Human Pathology. 2013;44(3):329-35.

79. Gong H, Olive DM, Kovar JL, Sampath L. Targeting EGFR and HER2 for Molecular Imaging of Cancer: INTECH Open Access Publisher; 2012.

80. Axup JY, Bajjuri KM, Ritland M, Hutchins BM, Kim CH, Kazane SA, et al. Synthesis of site-specific antibody-drug conjugates using unnatural amino acids. Proceedings of the National Academy of Sciences. 2012;109(40):16101-6.

81. Young BC, T. Antibody Drug Conjugates: Structure, Safety & Stability: Health and Medicine; 2015 [Available from: https://www.slideshare.net/bathasu/antibody-drug-conjugates-structure-safety-stability.

82. Thery J-C, Spano J-P, Azria D, Raymond E, Penault Llorca F. Resistance to human epidermal growth factor receptor type 2-targeted therapies. European Journal of Cancer. 2014;50(5):892-901.

83. Dai X, Li T, Bai Z, Yang Y, Liu X, Zhan J, et al. Breast cancer intrinsic subtype classification, clinical use and future trends. American journal of cancer research. 2015;5(10):2929-43.

84. ACTIP. Monoclonal Antibodies Approved by the EMA and FDA for Therapeutic Use (status 2017): Animal Cell Technology Industrial Platform; 2017 [cited 2018. Available from: http://www.actip.org/products/monoclonal-antibodies-approved-by-the-ema-and-fda-for-therapeutic-use/.

85. AIM. FDA Approved Drugs for Melanoma: AIM at Melanoma Foundation; 2014 [Available from: https://www.aimatmelanoma.org/melanoma-treatment-options/fda-approved-drugs-for-melanoma/.

86. FDA. 2017 New Drug Therapy Approvals: U.S. Food and Drug Administration; 2017 [cited 2017. Available from: https://www.fda.gov/downloads/aboutfda/centersoffices/officeofmedicalproductsandtobacco/cder/reportsbudgets/ucm591976.pdf.

87. Hamblett KJ, Senter PD, Chace DF, Sun MMC, Lenox J, Cerveny CG, et al. Effects of Drug Loading on the Antitumor Activity of a Monoclonal Antibody Drug Conjugate. American Association for Cancer Research. 2004;10(20):7063-70.

88. Axup JY, Bajjuri KM, Ritland M, Hutchins BM, Kim CH, Kazane SA, et al. Synthesis of site-specific antibody-drug conjugates using unnatural amino acids. Proceedings of the National Academy of Sciences. 2012;109(40):16101-6.

89. Oliveira S, van Dongen GAMS, Walsum MS-v, Roovers RC, Stam JC, Mali W, et al. Rapid Visualization of Human Tumor Xenografts through Optical Imaging with a Near-infrared Fluorescent Anti--Epidermal Growth Factor Receptor Nanobody. Molecular Imaging. 2012;11(1):33-46.

90. Dolan ME, Moschel RC, Pegg AE. Depletion of mammalian O6-alkylguanine-DNA alkyltransferase activity by O6-benzylguanine provides a means to evaluate the role of this protein in protection against carcinogenic and therapeutic alkylating agents. Proceedings of the National Academy of Sciences. 1990;87(14):5368-72.

91. Juillerat A, Gronemeyer T, Keppler A, Gendreizig S, Pick H, Vogel H, et al. Directed Evolution of O6-Alkylguanine-DNA Alkyltransferase for Efficient Labeling of Fusion Proteins with Small Molecules In Vivo. Chemistry & Biology. 2003;10(4):313-7.

92. Keppler A, Kindermann M, Gendreizig S, Pick H, Vogel H, Johnsson K. Labeling of fusion proteins of O6-alkylguanine-DNA alkyltransferase with small molecules in vivo and in vitro. Methods. 2004;32(4):437-44.

93. Strop P, Liu S-H, Dorywalska M, Delaria K, Dushin Russell G, Tran T-T, et al. Location Matters: Site of Conjugation Modulates Stability and Pharmacokinetics of Antibody Drug Conjugates. Chemistry & Biology. 2013;20(2):161-7.

94. Pegg AE, Dolan ME, Moschel RC. Structure, function, and inhibition of O6-alkylguanine-DNA alkyltransferase. Progress in nucleic acid research and molecular biology. 1995;51:167-223.

95. Keppler A, Gendreizig S, Gronemeyer T, Pick H, Vogel H, Johnsson K. A general method for the covalent labeling of fusion proteins with small molecules in vivo. Nat Biotech. 2003;21(1):86-9.

96. Kampmeier F, Ribbert M, Nachreiner T, Dembski S, Beaufils F, Brecht A, et al. Site-specific, covalent labeling of recombinant antibody fragments via fusion to an engineered version of 6-O-alkylguanine DNA alkyltransferase. Bioconjugate chemistry. 2009;20(5):1010-5.

97. Johnsson K. SNAP-tag Technologies: Novel Tools to Study Protein Function: NEB Expressions; 2008 [updated 2018. Available from: https://www.neb.com/tools-and-resources/feature-articles/snap-tag-technologies-novel-tools-to-study-protein-function.

98. Gronemeyer T, Chidley C, Juillerat A, Heinis C, Johnsson K. Directed evolution of O6-alkylguanine-DNA alkyltransferase for applications in protein labeling. Protein Engineering Design and Selection. 2006;19(7):309-16.

99. Juillerat A, Heinis C, Barnikow J, Jaccard H, Kunz B, Terskikh A, et al. Engineering Substrate Specificity of O6-Alkylguanine-DNA Alkyltransferase for Specific Protein Labeling in Living Cells. ChemBioChem. 2005;6(7):1263-9.

100. Harding FA, Stickler MM, Razo J, DuBridge R, editors. The immunogenicity of humanized and fully human antibodies: residual immunogenicity resides in the CDR regions. MAbs; 2010: Taylor & Francis.

101. Holliger P, Hudson PJ. Engineered antibody fragments and the rise of single domains. Nature biotechnology. 2005;23(9):1126-36.

102. Kijanka M, Warnders F-J, El Khattabi M, Lub-de Hooge M, van Dam GM, Ntziachristos V, et al. Rapid optical imaging of human breast tumour xenografts using anti-HER2 VHHs site-directly conjugated to IRDye 800CW for image-guided surgery. European Journal of Nuclear Medicine and Molecular Imaging. 2013;40(11):1718-29.

103. Puettmann C, Kolberg K, Hagen S, Schmies S, Fischer R, Naehring J, et al. A monoclonal antibody for the detection of SNAP/CLIP-tagged proteins. *Immunology Letters*. 2013;150(1–2):69-74.

104. ADL. Cloning of Single-Chain Fv Fragments San Diego, CA: Antibody Design Labs; 2014 [Available from: http://www.abdesignlabs.com/technical-resources/scfv-cloning/.

105. Kampmeier F, Niesen J, Koers A, Ribbert M, Brecht A, Fischer R, et al. Rapid optical imaging of EGF receptor expression with a single-chain antibody SNAP-tag fusion protein. European Journal of Nuclear Medicine and Molecular Imaging. 2010;37(10):1926-34.

106. Bojkowska K, Santoni de Sio F, Barde I, Offner S, Verp S, Heinis C, et al. Measuring In Vivo Protein Half-Life. Chemistry & Biology. 2011;18(6):805-15.

107. Gong H, Kovar JL, Baker B, Zhang A, Cheung L, Draney DR, et al. Near-Infrared Fluorescence Imaging of Mammalian Cells and Xenograft Tumors with SNAP-Tag. PLoS ONE. 2012;7(3):e34003.

108. Amoury M, Bauerschlag D, Zeppernick F, von Felbert V, Berges N, Di Fiore S, et al. Photoimmunotheranostic agents for triple-negative breast cancer diagnosis and therapy that can be activated on demand. Oncotarget. 2016;7(34):54925-36.

109. Hussain AF, Kampmeier F, von Felbert V, Merk H-F, Tur MK, Barth S. SNAP-Tag Technology Mediates Site Specific Conjugation of Antibody Fragments with a Photosensitizer and Improves Target Specific Phototoxicity in Tumor Cells. Bioconjugate Chemistry. 2011;22(12):2487-95.

110. Richmond A, Su Y. Mouse xenograft models vs GEM models for human cancer therapeutics. Disease Models and Mechanisms. 2008;1(2-3):78-82.

111. Leong ASY, Zhuang Z. The Changing Role of Pathology in Breast Cancer Diagnosis and Treatment. Pathobiology. 2011;78(2):99-114.

112. Alford R, Ogawa M, Choyke PL, Kobayashi H. Molecular probes for the in vivo imaging of cancer. Molecular BioSystems. 2009;5(11):1279-91.

113. Panieri E. Breast cancer screening in developing countries. Best practice & research Clinical obstetrics & gynaecology. 2012;26(2):283-90.

114. Coates A, Abraham S, Kaye SB, Sowerbutts T, Frewin C, Fox R, et al. On the receiving end—patient perception of the side-effects of cancer chemotherapy. European Journal of Cancer and Clinical Oncology. 1983;19(2):203-8.

115. Alatrash G MJ. Tumour-associated Antigens. Immune Biology of Allogeneic Hematopoietic Stem Cell Transplantation: Elsevier Inc.; 2013. p. 143-64.

116. Kaneko K, Ishigami S, Kijima Y, Funasako Y, Hirata M, Okumura H, et al. Clinical implication of HLA class I expression in breast cancer. BMC Cancer. 2011;11(1):1-6.

117. Boon T, Coulie PG, Van den Eynde B. Tumor antigens recognized by T cells. Immunology today. 1997;18(6):267-8.

118. Koziol JA, Imai H, Dai L, Zhang J-Y, Tan EM. Early detection of hepatocellular carcinoma using autoantibody profiles from a panel of tumor-associated antigens. Cancer Immunology, Immunotherapy. 2018;67(5):835-41.

119. Liu W, De La Torre IG, Gutiérrez-Rivera MC, Wang B, Liu Y, Dai L, et al. Detection of autoantibodies to multiple tumor-associated antigens (TAAs) in the immunodiagnosis of breast cancer. Tumor Biology. 2015;36(2):1307-12.

120. Li J, Huang M, Luo M, Dai L, Xie W, Qin X, et al. Detection of autoantibodies against tumor-associated antigens (TAAs) improving immunodiagnosis in human osteosarcoma by serological proteome analysis. AACR; 2017.

121. Shi J-X, Qin J-J, Ye H, Wang P, Wang K-J, Zhang J-Y. Tumor associated antigens or anti-TAA autoantibodies as biomarkers in the diagnosis of ovarian cancer: a systematic review with meta-analysis. Expert review of molecular diagnostics. 2015;15(6):829-52.

122. Krupnick AS, Gelman AE, Barchet W, Richardson S, Kreisel FH, Turka LA, et al. Cutting edge: murine vascular endothelium activates and induces the generation of allogeneic CD4+ 25+ Foxp3+ regulatory T cells. The Journal of Immunology. 2005;175(10):6265-70.

123. Sakaguchi S, Yamaguchi T, Nomura T, Ono M. Regulatory T cells and immune tolerance. Cell. 2008;133(5):775-87.

124. Keir ME, Butte MJ, Freeman GJ, Sharpe AH. PD-1 and its ligands in tolerance and immunity. Annu Rev Immunol. 2008;26:677-704.

125. Francisco LM, Salinas VH, Brown KE, Vanguri VK, Freeman GJ, Kuchroo VK, et al. PD-L1 regulates the development, maintenance, and function of induced regulatory T cells. Journal of Experimental Medicine. 2009;206(13):3015-29.

126. Keir ME, Liang SC, Guleria I, Latchman YE, Qipo A, Albacker LA, et al. Tissue expression of PD-L1 mediates peripheral T cell tolerance. Journal of Experimental Medicine. 2006;203(4):883-95.

127. Zitvogel L, Kroemer G. Targeting PD-1/PD-L1 interactions for cancer immunotherapy. Oncoimmunology. 2012;1(8):1223-5.

128. Muenst S, Schaerli A, Gao F, Däster S, Trella E, Droeser R, et al. Expression of programmed death ligand 1 (PD-L1) is associated with poor prognosis in human breast cancer. Breast cancer research and treatment. 2014;146(1):15-24.

129. Zhou J, Mahoney KM, Giobbie-Hurder A, Zhao F, Lee S, Liao X, et al. Soluble PD-L1 as a Biomarker in Malignant Melanoma Treated with Checkpoint Blockade. Cancer Immunology Research. 2017;5(6):480-92.

130. Gadiot J, Hooijkaas AI, Kaiser AD, van Tinteren H, van Boven H, Blank C. Overall survival and PD-L1 expression in metastasized malignant melanoma. Cancer. 2011;117(10):2192-201.

131. Robert C, Schachter J, Long GV, Arance A, Grob JJ, Mortier L, et al. Pembrolizumab versus ipilimumab in advanced melanoma. 2015;372(26):2521-32.

132. Robert C, Long GV, Brady B, Dutriaux C, Maio M, Mortier L, et al. Nivolumab in previously untreated melanoma without BRAF mutation. 2015;372(4):320-30.

133. Wang X, Wang Y, Yu L, Sakakura K, Visus C, Schwab J, et al. CSPG4 in cancer: multiple roles. Current molecular medicine. 2010;10(4):419-29.

134. Price MA, Wanshura LEC, Yang J, Carlson J, Xiang B, Li G, et al. CSPG4, a potential therapeutic target, facilitates malignant progression of melanoma. Pigment cell & melanoma research. 2011;24(6):1148-57.

135. Svendsen A, Verhoeff JJC, Immervoll H, Brøgger JC, Kmiecik J, Poli A, et al. Expression of the progenitor marker NG2/CSPG4 predicts poor survival and resistance to ionising radiation in glioblastoma. Acta Neuropathologica. 2011;122(4):495.

136. Tang F, Lord MS, Stallcup WB, Whitelock JM. Cell surface chondroitin sulphate proteoglycan 4 (CSPG4) binds to the basement membrane heparan sulphate proteoglycan, perlecan, and is involved in cell adhesion. J Biochem. 2018;1:14.

137. Jordaan S, Chetty S, Mungra N, Koopmans I, van Bommel PE, Helfrich W, et al. CSPG4: A Target for Selective Delivery of Human Cytolytic Fusion Proteins and TRAIL. Biomedicines. 2017;5(3):37.

138. Asher RA, Morgenstern DA, Properzi F, Nishiyama A, Levine JM, Fawcett JW. Two separate metalloproteinase activities are responsible for the shedding and processing of the NG2 proteoglycan in vitro. Molecular and Cellular Neuroscience. 2005;29(1):82-96.

139. Wang X, Osada T, Wang Y, Miyazato P, Thorne S, DeLeo A, et al. Antibody-based immunotherapy: targeting CSPG4 on human basal breast cancer stem cells. AACR; 2009.

140. Yang J, Price MA, Neudauer CL, Wilson C, Ferrone S, Xia H, et al. Melanoma chondroitin sulfate proteoglycan enhances FAK and ERK activation by distinct mechanisms. The Journal of cell biology. 2004;165(6):881-91.

141. Nicolosi PA, Dallatomasina A, Perris R. Theranostic impact of NG2/CSPG4 proteoglycan in cancer. Theranostics. 2015;5(5):530.

142. Yang J, Price MA, Li GY, Bar-Eli M, Salgia R, Jagedeeswaran R, et al. Melanoma proteoglycan modifies gene expression to stimulate tumor cell motility, growth, and epithelial-to-mesenchymal transition. Cancer research. 2009;69(19):7538-47.

143. Natali P, Bigotti A, Cavalieri R, Wakabayaski S, Taniguchi M, Ferrone S. Distribution of a cross-species melanoma-associated antigen in normal and neoplastic human tissues. Journal of investigative dermatology. 1985;85(4):340-6.

144. Wen Y, Makagiansar IT, Fukushi J-i, Liu F-T, Fukuda MN, Stallcup WB. Molecular basis of interaction between NG2 proteoglycan and galectin-3. Journal of Cellular Biochemistry. 2006;98(1):115-27.

145. Goretzki L, Burg MA, Grako KA, Stallcup WB. High-affinity Binding of Basic Fibroblast Growth Factor and Platelet-derived Growth Factor-AA to the Core Protein of the NG2 Proteoglycan. Journal of Biological Chemistry. 1999;274(24):16831-7.

146. Harper J, Reisfeld R. Inhibition of anchorage-independent growth of human melanoma cells by a monoclonal antibody to a chondroitin sulfate proteoglycan. Journal of the National Cancer Institute. 1983;71(2):225-.

147. Jordan CT, Guzman ML, Noble M. Cancer stem cells. New England Journal of Medicine. 2006;355(12):1253-61.

148. Soltysova A, Altanerova V, Altaner C. Cancer stem cells. Neoplasma. 2005;52(6):435.

149. Reya T, Morrison SJ, Clarke MF, Weissman IL. Stem cells, cancer, and cancer stem cells. nature. 2001;414(6859):105.

150. Legg J, Jensen UB, Broad S, Leigh I, Watt FM. Role of melanoma chondroitin sulphate proteoglycan in patterning stem cells in human interfollicular epidermis. Development. 2003;130(24):6049-63.

151. Ritchie M, Tchistiakova L, Scott N. Implications of receptor-mediated endocytosis and intracellular trafficking dynamics in the development of antibody drug conjugates. mAbs. 2013;5(1):13-21.

152. Wang J, Svendsen A, Kmiecik J, Immervoll H, Skaftnesmo KO, Planagumà J, et al. Targeting the NG2/CSPG4 Proteoglycan Retards Tumour Growth and Angiogenesis in Preclinical Models of GBM and Melanoma. PLOS ONE. 2011;6(7):e23062.

153. Schulz G, Bumol TF, Reisfeld RA. Monoclonal antibody-directed effector cells selectively lyse human melanoma cells in vitro and in vivo. Proceedings of the National Academy of Sciences. 1983;80(17):5407-11.

154. Jamil NS, Azfer A, Worrell H, Salter DM. Functional roles of CSPG4/NG2 in chondrosarcoma. International journal of experimental pathology. 2016;97(2):178-86.

155. Wang X, Osada T, Wang Y, Yu L, Sakakura K, Katayama A, et al. CSPG4 protein as a new target for the antibody-based immunotherapy of triple-negative breast cancer. Journal of the National Cancer Institute. 2010;102(19):1496-512.

156. Invitrogen. pSecTag2 A, B, and C Carlsbad, CA USA: Life Technologies Corporation; 2012 [Available from: https://tools.thermofisher.com/content/sfs/manuals/psectag2_man.pdf.

157. Sigma-Aldrich. M13 Reverse Primer Set Darmstadt, Germany: Merck; 2018 [Available from: https://www.sigmaaldrich.com/catalog/product/sigma/p3223?lang=en&region=ZA&gclid=CjwKCAjwwbHWBRBWEiwAMIV7E_0iJHU8SGiGdWyVrguUDzJxBjc8kvsY40Blvvyy_BsAidr4xuGhXxoCs6IQAvD_BwE.

158. Pearson. Concept 3:The lac Operator: Pearson Education, Inc; [Available from: http://www.phschool.com/science/biology_place/biocoach/lacoperon/operator.html.

159. Busby S, Ebright RH. Transcription activation by catabolite activator protein (CAP). Journal of molecular biology. 1999;293(2):199-213.

160. Matlock B. Assessment of Nucleic Acid Purity Wilmington, MA, USA: Thermo Fisher Scientific; 2015 [cited 2018. Technical notes]. Available from: https://tools.thermofisher.com/content/sfs/brochures/TN52646-E-0215M-NucleicAcid.pdf.

161. Kleffel S, Posch C, Barthel SR, Mueller H, Schlapbach C, Guenova E, et al. Melanoma cell-intrinsic PD-1 receptor functions promote tumor growth. 2015;162(6):1242-56.

162. Koopmans I, Hendriks D, Samplonius DF, van Ginkel RJ, Heskamp S, Wierstra PJ, et al. A novel bispecific antibody for EGFR-directed blockade of the PD-1/PD-L1 immune checkpoint. 2018:e1466016.

163. ASCO. Melanoma: Statistics: ASCO; 2016 [Available from: https://www.cancer.net/cancer-types/melanoma/statistics.

164. Fisher R, Pusztai L, Swanton CJBjoc. Cancer heterogeneity: implications for targeted therapeutics. 2013;108(3):479.

165. Liu J, Dang H, Wang XWJE, medicine m. The significance of intertumor and intratumor heterogeneity in liver cancer. 2018;50(1):e416.

166. Li BT, Shen R, Buonocore D, Olah ZT, Ni A, Ginsberg MS, et al. Ado-trastuzumab emtansine in patients with HER2 mutant lung cancers: Results from a phase II basket trial. 2017;35(15_suppl):8510-.

167. Pavone V, Mele A, Carlino D, Specchia G, Gaudio F, Perrone T, et al. Brentuximab vedotin as salvage treatment in Hodgkin lymphoma naïve transplant patients or failing ASCT: the real life experience of Rete Ematologica Pugliese (REP). 2018;97(10):1817-24.

168. Khan N, Hills RK, Virgo P, Couzens S, Clark N, Gilkes A, et al. Expression of CD33 is a predictive factor for effect of gemtuzumab ozogamicin at different doses in adult acute myeloid leukaemia. 2017;31(5):1059.

169. Kantarjian HM, DeAngelo DJ, Stelljes M, Liedtke M, Stock W, Goekbuget N, et al. Inotuzumab Ozogamicin (InO) Vs Standard of Care (SC) in Patients with Relapsed/Refractory (R/R) Acute Lymphoblastic Leukemia (ALL): Long-Term Results of the Phase 3 INO-VATE Study. Am Soc Hematology; 2017.

170. Reichert JM, Valge-Archer VEJNRDD. Development trends for monoclonal antibody cancer therapeutics. 2007;6(5):349.

171. Chen DS, Mellman IJN. Elements of cancer immunity and the cancer–immune set point. 2017;541(7637):321.

172. Galluzzi L, Buqué A, Kepp O, Zitvogel L, Kroemer G. Immunogenic cell death in cancer and infectious disease. Nature Reviews Immunology. 2016;17:97.

173. Juneja VR, McGuire KA, Manguso RT, LaFleur MW, Collins N, Haining WN, et al. PD-L1 on tumor cells is sufficient for immune evasion in immunogenic tumors and inhibits CD8 T cell cytotoxicity. 2017;214(4):895-904.

174. Lorusso D, Bria E, Costantini A, Di Maio M, Rosti G, Mancuso AJEjocc. Patients' perception of chemotherapy side effects: Expectations, doctor–patient communication and impact on quality of life–An Italian survey. 2017;26(2):e12618.

175. Pearce A, Haas M, Viney R, Pearson S-A, Haywood P, Brown C, et al. Incidence and severity of self-reported chemotherapy side effects in routine care: A prospective cohort study. 2017;12(10):e0184360.

176. Alley SC, Okeley NM, Senter PD. Antibody–drug conjugates: targeted drug delivery for cancer. Current opinion in chemical biology. 2010;14(4):529-37.

177. Pohlit H, Bellinghausen I, Schömer M, Heydenreich Br, Saloga J, Frey HJB. Biodegradable pH-sensitive poly (ethylene glycol) nanocarriers for allergen encapsulation and controlled release. 2015;16(10):3103-11.

178. Firer MA, Gellerman GJJoh, oncology. Targeted drug delivery for cancer therapy: the other side of antibodies. 2012;5(1):70.

179. Scarpa E, Mayor RJJCB. Collective cell migration in development. 2016;212(2):143-55.

180. McShane SG, Molè MA, Savery D, Greene ND, Tam PP, Copp AJJDb. Cellular basis of neuroepithelial bending during mouse spinal neural tube closure. 2015;404(2):113-24.

181. Maciag PC, Seavey MM, Pan Z-K, Ferrone S, Paterson YJCr. Cancer immunotherapy targeting the high molecular weight melanoma-associated antigen protein results in a broad antitumor response and reduction of pericytes in the tumor vasculature. 2008;68(19):8066-75.

182. Ribatti D, Nico B, Crivellato EJIJoDB. The role of pericytes in angiogenesis. 2011;55(3):261-8.

183. Gerhardt H, Betsholtz CJC, research t. Endothelial-pericyte interactions in angiogenesis. 2003;314(1):15-23.

184. Mittelman A, Chen ZJ, Yang H, Wong GY, Ferrone S. Human high molecular weight melanoma-associated antigen (HMW-MAA) mimicry by mouse anti-idiotypic monoclonal antibody MK2-23: induction of humoral anti-HMW-MAA immunity and prolongation of survival in patients with stage IV melanoma. Proceedings of the National Academy of Sciences. 1992;89(2):466-70.

185. Audrito V, Serra S, Stingi A, Orso F, Gaudino F, Bologna C, et al. PD-L1 up-regulation in melanoma increases disease aggressiveness and is mediated through miR-17-5p. Oncotarget. 2017;8(9):15894-911.

186. Massi D, Brusa D, Merelli B, Ciano M, Audrito V, Serra S, et al. PD-L1 marks a subset of melanomas with a shorter overall survival and distinct genetic and morphological characteristics. Annals of oncology. 2014;25(12):2433-42.

187. Knol AC, Nguyen JM, Pandolfino MC, Denis MG, Khammari A, Dréno B. PD-L1 expression by tumor cell-lines: a predictive marker in melanoma. Experimental dermatology. 2018.

188. Ooi A, Wong A, Esau L, Lemtiri-Chlieh F, Gehring CJFip. A guide to transient expression of membrane proteins in HEK-293 cells for functional characterization. 2016;7:300.

189. Zhang J, Jiang C, Longo JPF, Azevedo RB, Zhang H, Muehlmann LAJApsB. An updated overview on the development of new photosensitizers for anticancer photodynamic therapy. 2017.

190. Firczuk M WM, Muchowicz A, Wachowska M, Januszewska M, Bojarczuk K, Salwa P, Nowis D. Approaches to improve photodynamic therapy of cancer. Frontiers in bioscience : a journal and virtual library. 2011;16.

191. Douillard S, Olivier D, Patrice TJP, Sciences P. In vitro and in vivo evaluation of Radachlorin® sensitizer for photodynamic therapy. 2009;8(3):405-13.

192. Hussain AF, Krüger HR, Kampmeier F, Weissbach T, Licha K, Kratz F, et al. Targeted delivery of dendritic polyglycerol–doxorubicin conjugates by scFv-SNAP fusion protein suppresses EGFR+ cancer cell growth. Biomacromolecules. 2013;14(8):2510-20.

193. Poli A, Wang J, Domingues O, Planagumà J, Yan T, Rygh CB, et al. Targeting glioblastoma with NK cells and mAb against NG2/CSPG4 prolongs animal survival. 2013;4(9):1527.

194. Buytaert E, Callewaert G, Hendrickx N, Scorrano L, Hartmann D, Missiaen L, et al. Role of endoplasmic reticulum depletion and multidomain proapoptotic BAX and BAK proteins in shaping cell death after hypericin-mediated photodynamic therapy. 2006;20(6):756-8.

195. Ritz R, Roser F, Radomski N, Strauss WS, Tatagiba M, Gharabaghi AJAr. Subcellular colocalization of hypericin with respect to endoplasmic reticulum and Golgi apparatus in glioblastoma cells. 2008;28(4B):2033-8.

196. Erickson HK, Phillips GDL, Leipold DD, Provenzano CA, Mai E, Johnson HA, et al. The effect of different linkers on target cell catabolism and pharmacokinetics/pharmacodynamics of trastuzumab maytansinoid conjugates. 2012:molcanther. 0727.2011.

197. Sharman WM, van Lier JE, Allen CMJAddr. Targeted photodynamic therapy via receptor mediated delivery systems. 2004;56(1):53-76.

198. Reithmeier RA. Assembly of proteins into membranes. New Comprehensive Biochemistry. 20: Elsevier; 1991. p. 525-78.

199. Capitani M, Sallese MJFl. The KDEL receptor: new functions for an old protein. 2009;583(23):3863-71.

200. Haug M, Brede G, Håkerud M, Nedberg AG, Gederaas OA, Flo TH, et al. Photochemical internalization of Peptide antigens Provides a novel strategy to realize Therapeutic cancer Vaccination. 2018;9:650.

201. Varkouhi AK, Scholte M, Storm G, Haisma HJJJoCR. Endosomal escape pathways for delivery of biologicals. 2011;151(3):220-8.

6 Appendices

6.1 INDEX OF FIGURES AND TABLES

6.1.1 Figures

6.1.2 Tables

6.2 SEQUENCING ALIGNMENT

6.2.1 mAb9.2.27(scFv)-SNAP sequence alignment

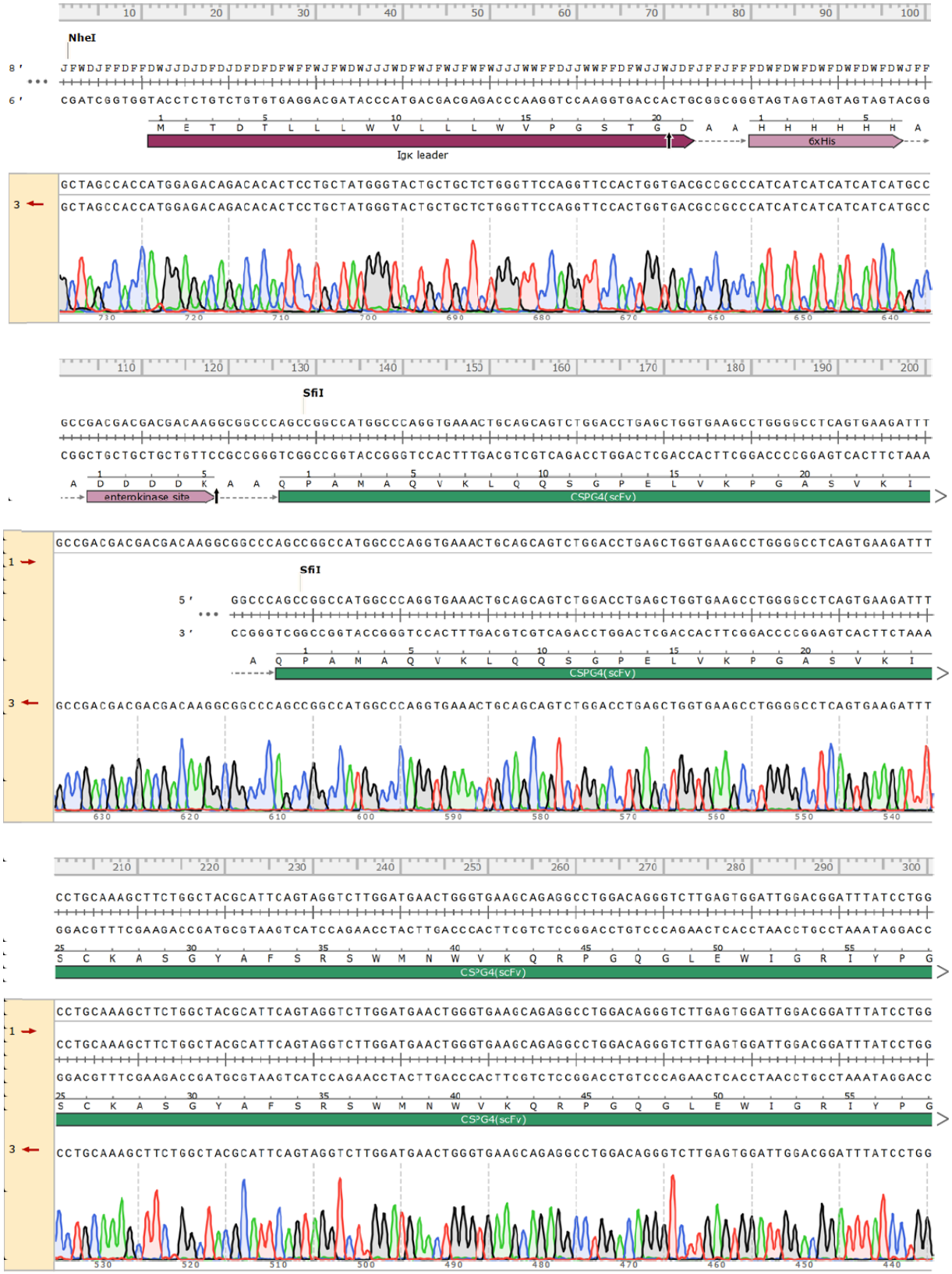


CSPG4(scFv)
CSPG4(scFv)
CSPG4(scFv)
CSPG4(scFv)

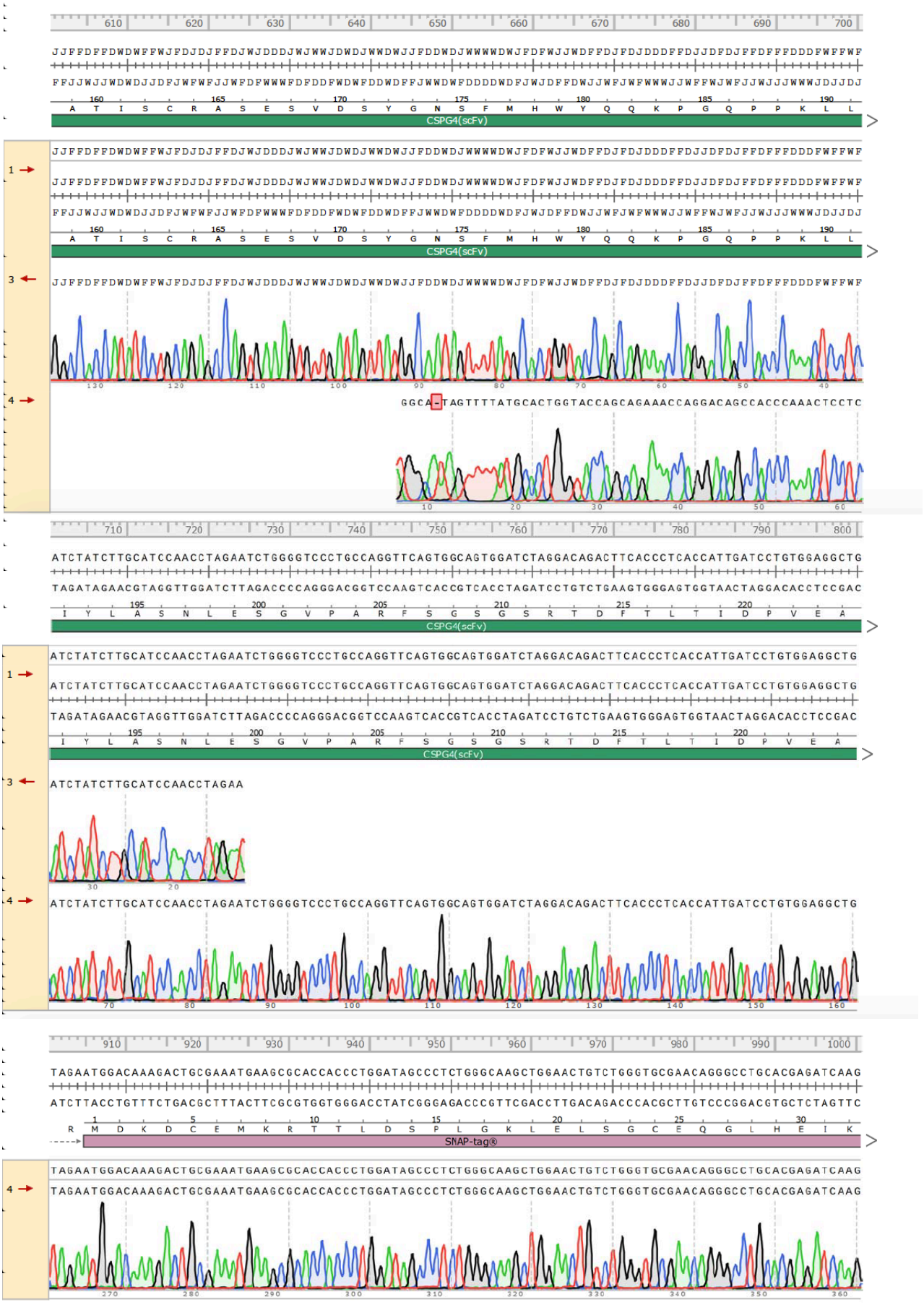
CSPG4(scFv)
CSPG4(scFv)
GGCA-TAGTTTTATGCACTGGTACCAGCAGAAACCAGGACAGCCACCCAAACTCCTC
CSPG4(scFv)
CSPG4(scFv)
ATCTATCTTGCATCCAACCTAGAA
SNAP-tag®

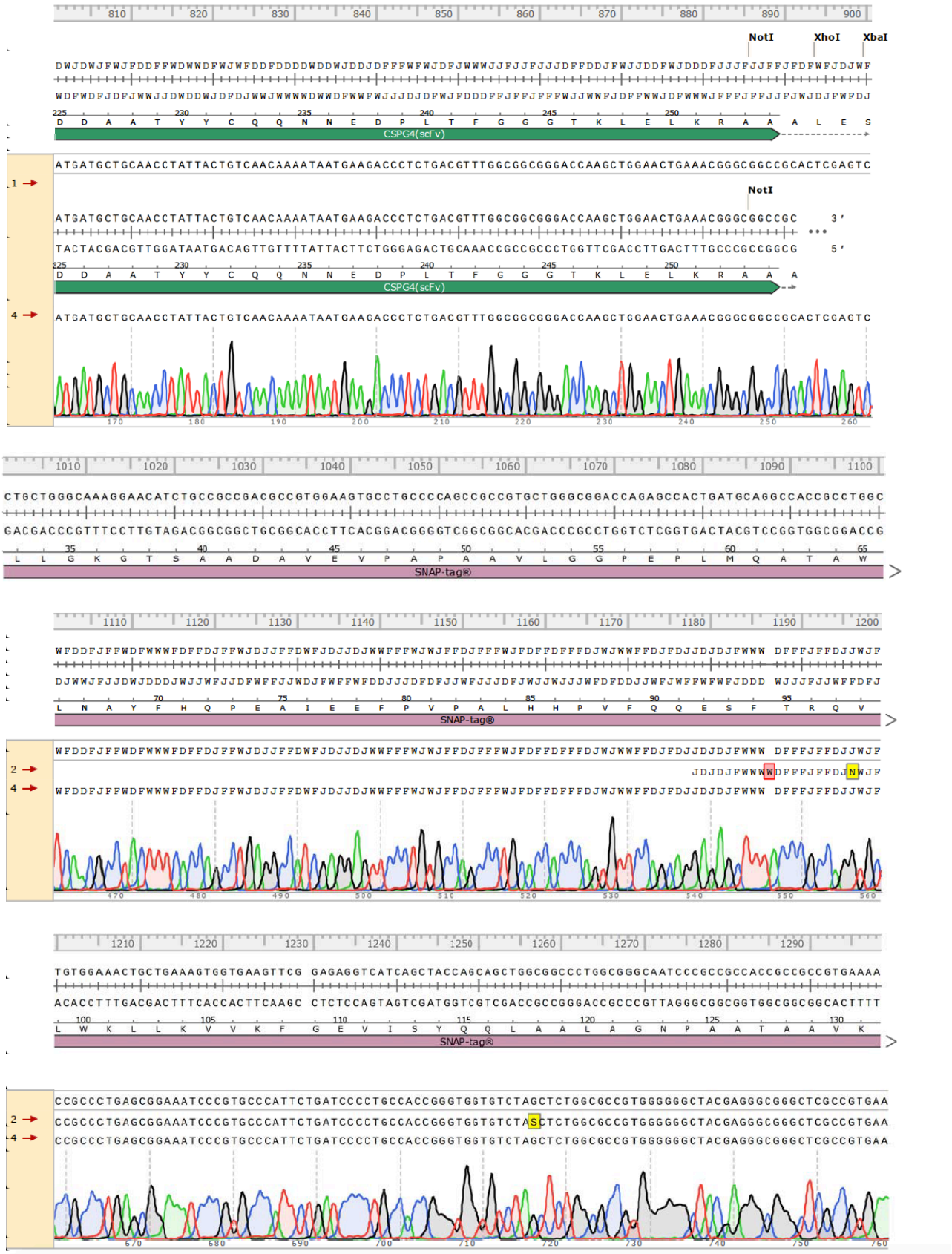
NotI
XhoI
XbaI
CSPG4(scFv)
SNAP-tag®

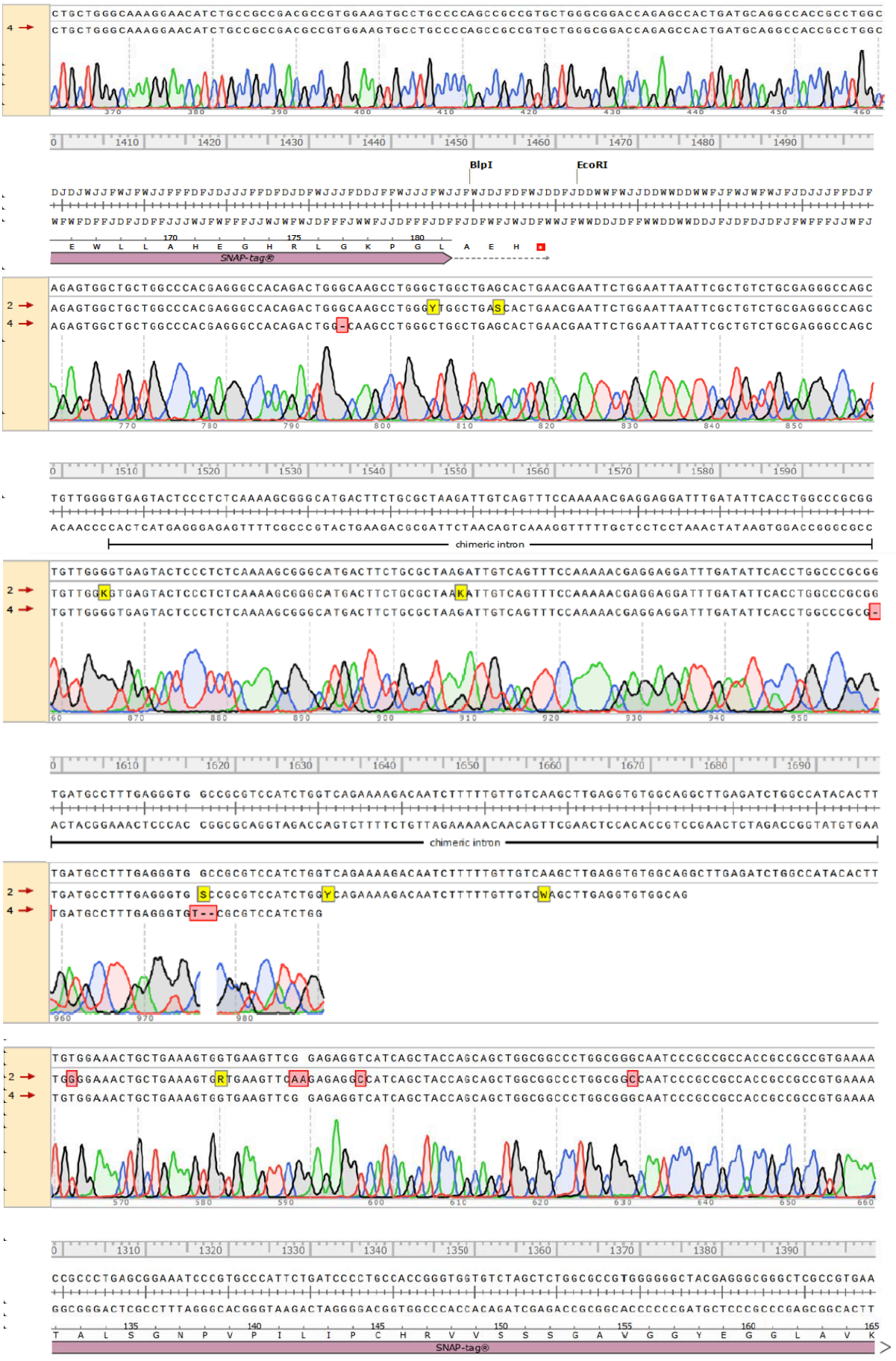
BlpI
EcoRI
SNAP-tag®
chimeric intron
chimeric intron
SNAP-tag®

6.2.2 αPDL1(scFv)-SNAP sequence alignment

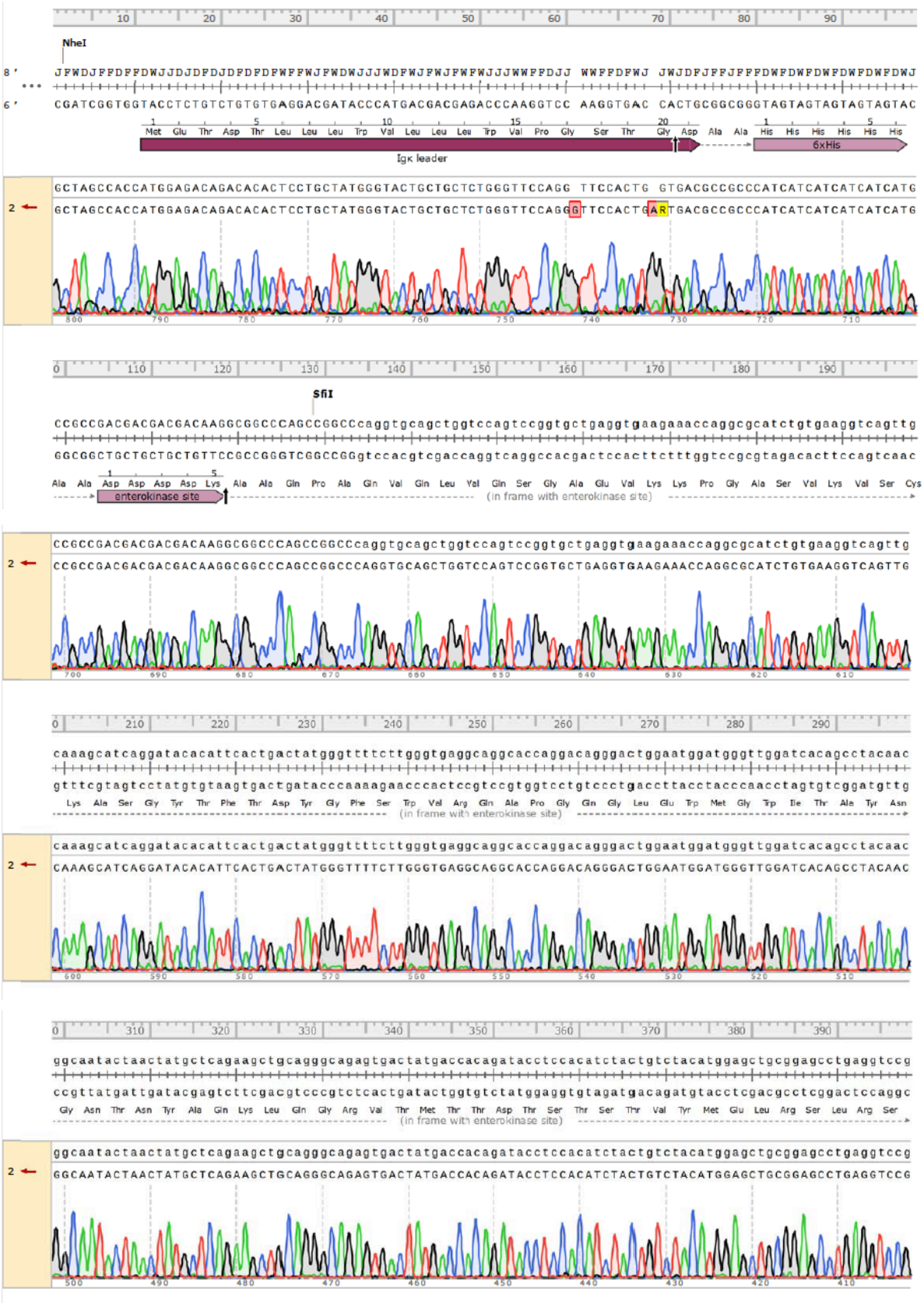

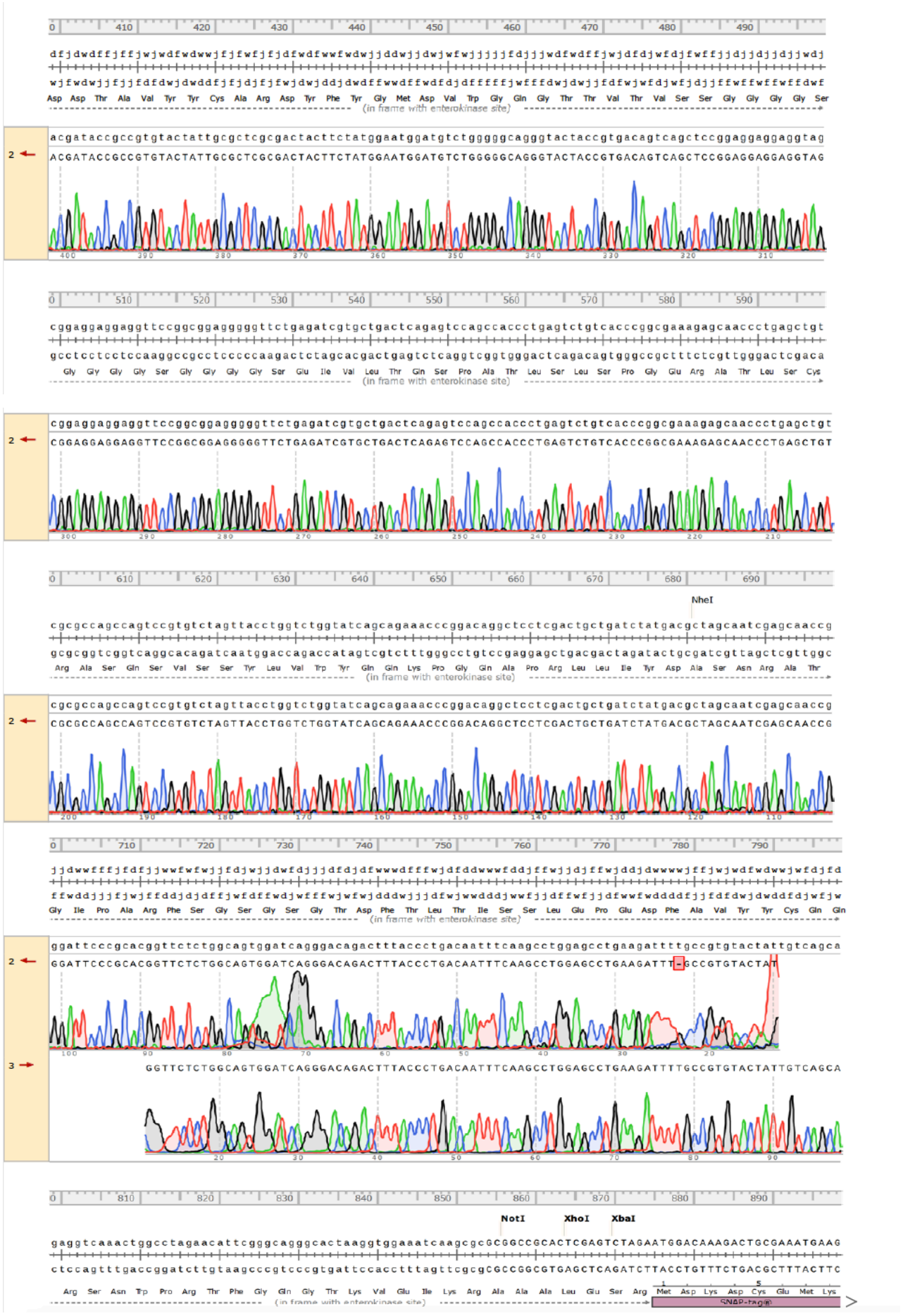
(in frame with enterokinase site)
NheI
NotI
XhoI
XbaI
SNAP-tag®

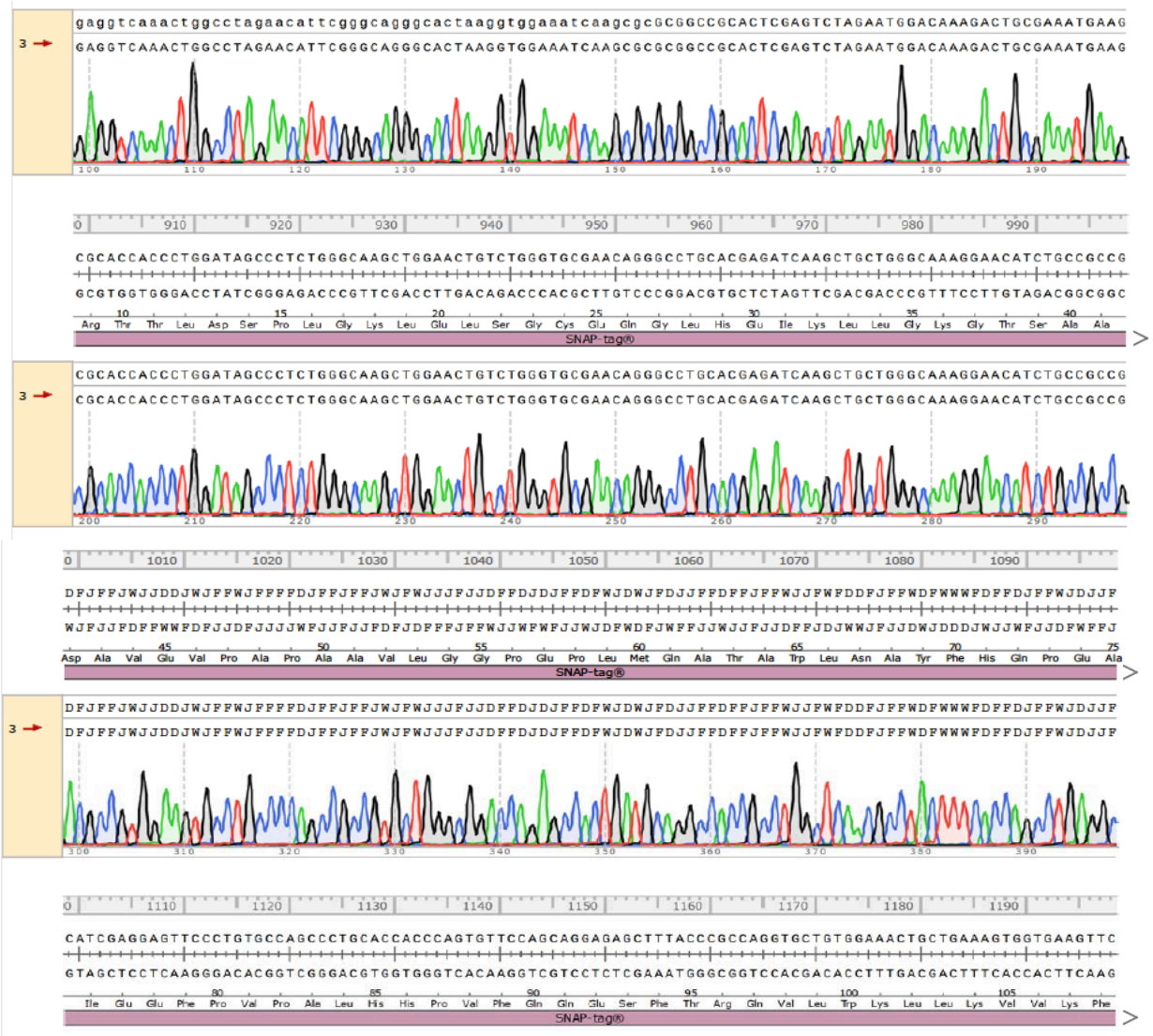
gaggtcaaactggcctagaacattcgggcagggcactaaggtggaaatcaagcgcGCGGCCGCACTCGAGTCTAGAATGGACAAAGACTGCGAAATGAAG
GAGGTCAAACTGGCCTAGAACATTCGGGCAGGGCACTAAGGTGGAAATCAAGCGCGCGGCCGCACTCGAGTCTAGAATGGACAAAGACTGCGAAATGAAG
CGCACCACCCTGGATAGCCCTCTGGGCAAGCTGGAACTGTCTGGGTGCGAACAGGGCCTGCACGAGATCAAGCTGCTGGGCAAAGGAACATCTGCCGCCG
GCGTGGTGGGACCTATCGGGAGACCCGTTCGACCTTGACAGACCCACGCTTGTCCCGGACGTGCTCTAGTTCGACGACCCGTTTCCTTGTAGACGGCGGC
Arg Thr Thr Leu Asp Ser Pro Leu Gly Lys Leu Glu Leu Ser Gly Cys Glu Gln Gly Leu His Glu Ile Lys Leu Leu Gly Lys Gly Thr Ser Ala Ala
SNAP-tag®
CGCACCACCCTGGATAGCCCTCTGGGCAAGCTGGAACTGTCTGGGTGCGAACAGGGCCTGCACGAGATCAAGCTGCTGGGCAAAGGAACATCTGCCGCCG
DFJFFJWJJDDJWJFFWJFFFFDJFFJFFJWJFWJJJFJJDFFDJDJFFDFWJDWJFDJJFFDFFJFFWJJFWFDDFJFFWDFWWWFDFFDJFFWJDJJF
WJFJJFDFFWWFDFJJDFJJJJWFJJFJJFDFJDFFFJFFWJJWFWFJJWJDFWDFJWFFJJWJJFJJDFFJDJWWJFJJDWJDDDJWJJWFJJDFWFFJ
Asp Ala Val Glu Val Pro Ala Pro Ala Ala Val Leu Gly Gly Pro Glu Pro Leu Met Gln Ala Thr Ala Trp Leu Asn Ala Tyr Phe His Gln Pro Glu Ala
SNAP-tag®
DFJFFJWJJDDJWJFFWJFFFFDJFFJFFJWJFWJJJFJJDFFDJDJFFDFWJDWJFDJJFFDFFJFFWJJFWFDDFJFFWDFWWWFDFFDJFFWJDJJF
DFJFFJWJJDDJWJFFWJFFFFDJFFJFFJWJFWJJJFJJDFFDJDJFFDFWJDWJFDJJFFDFFJFFWJJFWFDDFJFFWDFWWWFDFFDJFFWJDJJF
CATCGAGGAGTTCCCTGTGCCAGCCCTGCACCACCCAGTGTTCCAGCAGGAGAGCTTTACCCGCCAGGTGCTGTGGAAACTGCTGAAAGTGGTGAAGTTC
GTAGCTCCTCAAGGGACACGGTCGGGACGTGGTGGGTCACAAGGTCGTCCTCTCGAAATGGGCGGTCCACGACACCTTTGACGACTTTCACCACTTCAAG
Ile Glu Glu Phe Pro Val Pro Ala Leu His His Pro Val Phe Gln Gln Glu Ser Phe Thr Arg Gln Val Leu Trp Lys Leu Leu Lys Val Val Lys Phe
SNAP-tag®

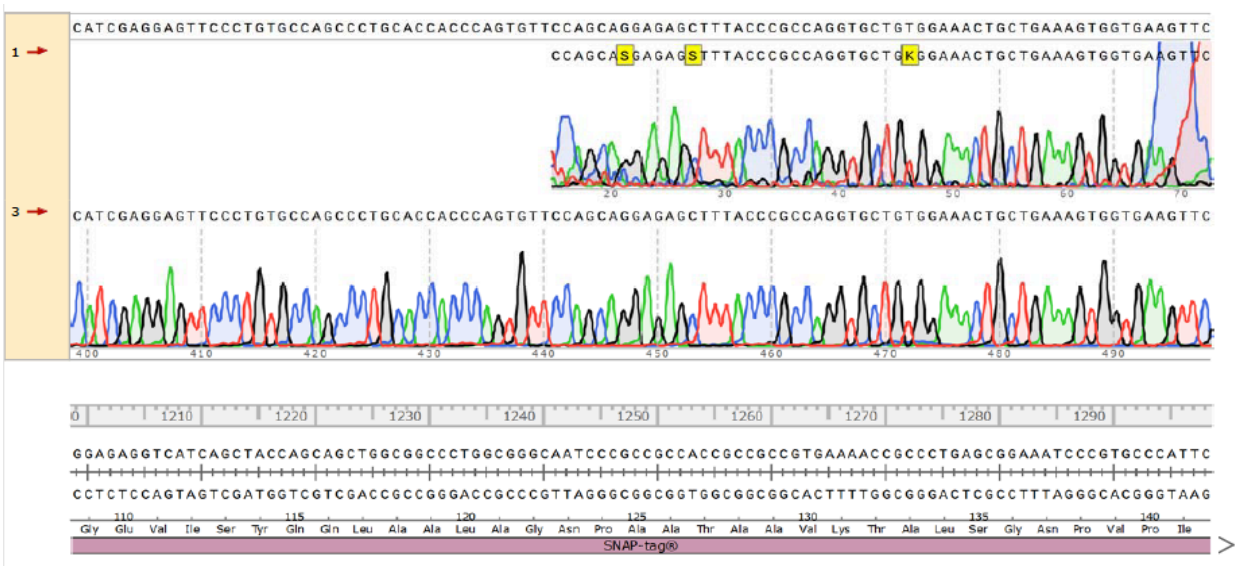
1
3
SNAP-tag®

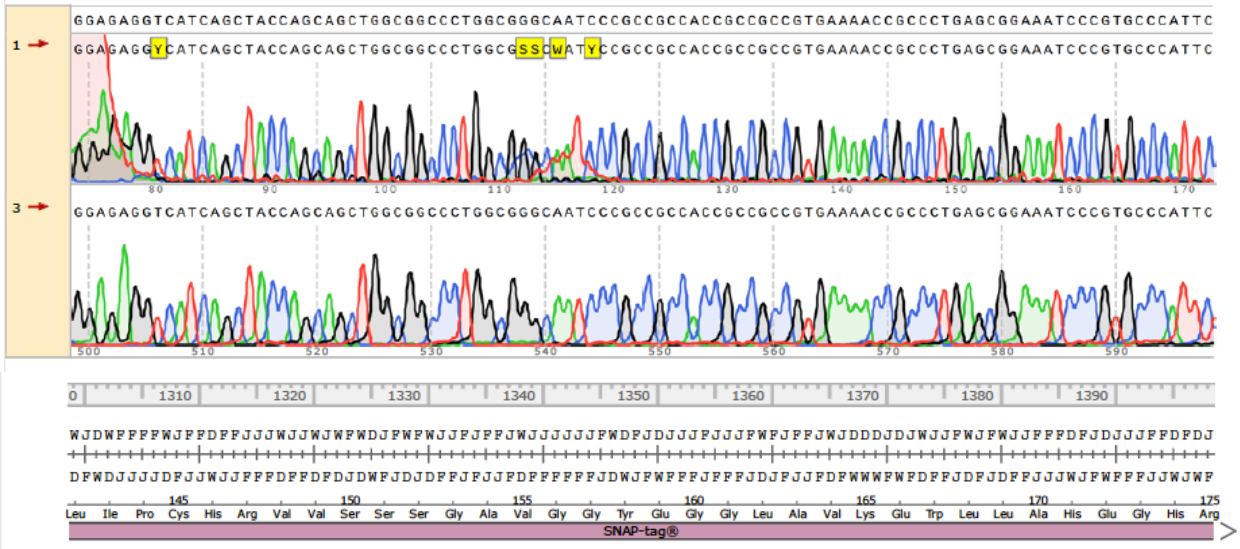
1
3
SNAP-tag®

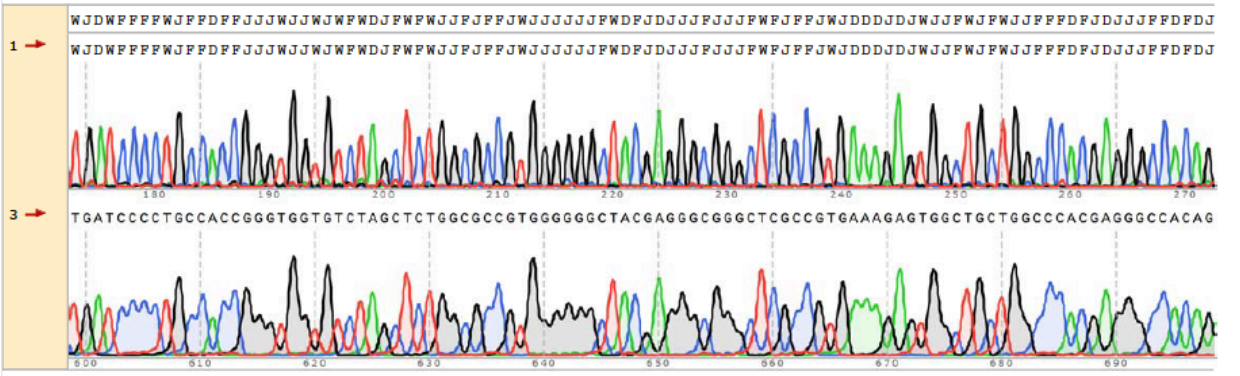
1
3


BlpI
SNAP-tag®
HindIII

6.3 ABBREVIATIONS

$^1O_2$	Singlet oxygen
αCSPG4	Anti-CSPG4
ABC transporter	ATP-Binding Cassette Transporter Protein
ADC	Antibody-Drug Conjugate
ADCC	Antibody-Dependent Cellular Cytotoxicity
Alexa488	Alexa Fluor™ 488
AMP	Ampicillin
AMP^R	Ampicillin Resistance
APC	Antibody-Photoabsorber Conjugate
BG	Benzylguanine
BRAF	Proto-oncogene B-Raf
CANSA	Cancer Association of South Africa
CAP	Catabolite Activator Protein
CCSN	Cell Culture Supernatant
CDC	Complement-Dependent Cytotoxicity
Ce6	Chlorin e6
CSC	Cancer Stem Cell
CSPG4	Chondroitin Sulphate Proteoglycan 4
CTL	Cytotoxic T Lymphocytes
Cys145	Cysteine Residue 145
DAR	Drug-to-Antibody Ratio
DMEM	Dulbecco's Modified Eagle's Medium
DMSO	Dimethyl Sulphoxide
DTHe	Dimethyl Tetrahydroxyhelianthrone
E. coli	*Escherichia coli*
eGFP	Enhanced Green Fluorescent Protein
EKR	Extracellular Signal-Regulating Kinase
EMT	Epithelial-to-Mesenchyal Transition
ER	Oestrogen Receptor
FACS	Fluorescence-Activated Cell Sorting
FAK	Focal Adhesion Kinase
FBS	Foetal Bovine Serum
Fc	Fragment Crystallizable
FDA	United States Food and Drug Administration
FRET	Fluorescence Resonance Energy Transfer
GFP	Green Fluorescent Protein
gMFI	Geometric Mean Fluorescent Intensity
hAGT	Human Alkylguanine-DNA Alkyltransferase
HER2	Human Epidermal Growth Factor Receptor 2
HMW MAA	High Molecular Weight Melanoma-Associated Antigen
HRP	Horse Radish Peroxidase
IMAC	Immobilized Metal Affinity Chromatography
LB	Luria Bertani Broth
mAb	Monoclonal Antibody
MAP-K	Mitogen-Activated Protein Kinase
MBI	Medical Biotechnology and Immunotherapy Research Group
MCSP	Melanoma-Associated Chondroitin-Sulphate Proteoglycan

MFI	Mean Fluorescent Intensity
nfH_20	Nuclease-Free (Molecule Biology Grade) Water
NIR	Near Infrared Radiation
ORF	Open Reading Frame
PBS	Phosphate
PD-1	Programmed Death Protein 1
PD-L1	Programmed Death Ligand 1
PDT	Photodynamic Therapy
PIT	Photoimmunotheranostic
PR	Progesterone Receptor
PS	Photosensitizer
RE	Restriction Enzyme
RGP	Radial Growth Phase
ROS	Reactive Oxygen Species
sdH_2O	Sterile Deionized (Molecular Biology Grade) Water
SDS	Sodium Dodecylsulphate
SDS-PAGE	Sodium Dodecylsulphate Polyacrylamide Gel Electrophoresis
scFv	Single Chain Variable Fragment
SOC	Super Optimal Broth with Catabolite repression
TAA	Tumour-Associated Antigen
T cell	T-Lymphocyte Cell
TCR	T Cell Receptor
TIL	tumour infiltrating lymphocytes
TNBC	Triple Negative Breast Cancer
TSA	Tumour-Specific Antigen
UVR	Ultraviolet Radiation
VEGF	Vascular Epithelial Growth Factor
VGP	Vertical Growth Phase
w/v	Weight per Volume
XXT	Tetrazolium Dye Cell Proliferation Assay

6.4 Recipes

6.4.1 1.2% (w/v) Agarose Gel Preparation

Recipe (100mL)

1.2g agarose powder
Top up to 100mL 1X TAE Buffer
10µL SYBRsafe

Protocol

1. Weigh agarose into a flask
2. Top up to 100mL with 1X TAE Buffer
3. Microwave at top voltage for 45 seconds (or until bubbles are seen)
4. Allow to cool to touching temperature
5. Add SYBRsafe
6. Place comb and pour gel into tray
7. Allow to set in a dark space (SYBRsafe is degraded by UV light)
8. Once solidified, carefully remove comb
9. Place in tank, fully submerged in 1X TAE Buffer
10. Load samples with pipette as required

6.4.2 Gel Electrophoresis

4x Laemmli Loading Dye (5mL)

0.151375g Tris (pH6.8)
0.3g SDS
0.00025g Bromophenol Blue
2mL Glycerol
0.5ml β-mercaptoethanol

1M Tris (1L)

121.1g Tris
Top up to 800mL with dH_2O
Adjust to appropriate pH with HCl and NaOH
Top up to 1000mL with dH_2O

5M NaOH (100mL)

20g NaOH
Top up to 100mL with dH_2O

5M HCl (100mL)

8.239g HCl
Top up to 100mL with dH_2O

0.5M EDTA (1L)

146.12g EDTA pH8.0 (1L)
Top up to 1000mL with dH_2O

10X TAE (1L)
48.4g Trizma Base
20mL 0.5M EDTA pH8.0
11.44mL glacial acetic acid
Top up to 1000mL with dH_2O

1X TAE (1L)
100mL 10X TAE
900mL dH_2O

10X TE Buffer (1L)
100mL 1M Tris-HCl pH7.5
20mL 0.5M EDTA
880mL dH_2O

6.4.3 LB Agar Plate Preparation

Recipe (1L)
35g LB agar powder (Sigma)
Top up to 1000mL with dH_2O
Add AMP to 200ng/µl (stock at 100µg/ml)

Protocol

1. Place 35g LB agar powder in a flask
2. Top up to 1L with dH_20, stir to dissolve
3. Autoclave for 15min at 121°C
4. Cool to ~50°C (to be able to touch, but not to solidify)
5. Pour negative plates
6. Add AMP at correct ratio (e.g. 100µL AMP per 50mL LB)
7. Pour plates
8. Allow plates to cool and solidify

6.4.4 Purification buffers

4x Incubation buffer (pH 8.0)

	Conc.	Mr	Mass(g)
NaH_2PO_4	200mM	119.98	24.00
NaCl	1.2M	58.44	70.13
Imidazole	40mM	68.08	2.72
ddH_2O			fill to **1000ml**

Equilibration buffer (pH 8.0)

	Conc.	Mr	Mass(g)
NaH_2PO_4	50mM	119.98	6.00
NaCl	300mM	58.44	17.53
ddH_2O			fill to **1000ml**

Elution buffer (pH 8.0)

	Conc.	Mr	Mass(g)
NaH_2PO_4	50mM	119.98	6.00
NaCl	300mM	58.44	17.53
Imidazole	250mM	68.08	17.02
ddH_2O			fill to **1000ml**